THE SIGNIFICANCE OF MAGMA MINGLING AND MIXING DURING THE FORMATION OF THE HOST-ROCK SUCCESSIONS OF ARCHEAN MASSIVE SULFIDE DEPOSITS IN THE NORANDA CAMP, ABITIBI SUBPROVINCE, QUEBEC

by

Olivia Oseguera

A thesis submitted to the Faculty and Board of Trustees of the Colorado School of Mines in partial fulfillment of the requirements for the degree of Master of Science (Geology).

Golden, Colorado

Date _____

Signed: _____

Olivia Oseguera

Signed: _____

Dr. Thomas Monecke

Thesis Advisor

Golden, Colorado

Date _____

Signed: _____

Dr. Paul Santi

Professor and Head

Department of Geology and Geological Engineering

ABSTRACT

The Noranda mining district contains some of the most important volcanic-hosted massive sulfide deposits of the Neoarchean Abitibi subprovince of northern Ontario and Quebec. With a historic production of 54.3 Mt of ore grading 2.2% Cu and 6.1 g/t Au, the Horne deposit was the largest base and precious metal producer within the district. The Quemont deposit, located just north of the Horne mine, was the second largest producer with a historic production of 13.9 Mt of ore grading 1.31% Cu and 5.38g/t Au.

The Horne mine is hosted by a felsic-dominated volcanic succession that is crosscut by mafic dikes feeding into a conformably overlying mafic volcanic package. One of the best exposed and preserved sections of Horne stratigraphy is located in the Horne West area. In this area, a large flow-banded rhyolite cryptodome containing abundant mafic xenoliths is exposed. To characterize the occurrence of the mafic xenoliths, the shape, trend, size, and contact relationships were recorded for each xenolith. Volcanic facies analysis showed that tabular xenoliths are abundantly present in the lower portion of the cryptodome and become increasingly sparse, blocky, and irregularly distributed and shaped up-stratigraphy. Flow banding around the xenoliths is well developed in the lower portion of the rhyolite. The contacts between the mafic xenoliths and the surrounding rhyolite are commonly scalloped. The facies relationships suggest that incorporation of the mafic xenoliths into the rhyolite cryptodome is best explained by a process of magma mingling. Mingling presumably occurred through synchronous emplacement of the felsic feeder of the cryptodome and a mafic dike along a synvolcanic fault.

The host rock succession of the Quemont deposit primarily comprises coherent rhyolite and felsic volcaniclastic units. The succession is cut by a dike-in-dike complex containing both mafic and felsic intrusions. Magma mingling and mixing are observed along the contacts between a mafic dike and a quartz- and feldspar-phyric rhyolite dike. The style of mingling and mixing is heterogeneous along the contact. Common textural relationships include the presence of elongate mafic xenoliths along the margin of the rhyolite dike, centimeter-sized inclusions of mafic material in a matrix of intermediate composition, centimeter-sized mafic inclusions and wispy xenoliths within a rhyolite matrix, and areas characterized by mixed rhyolite and basalt, resulting in an intrusion of andesitic composition. The intricate contact relationships observed

suggest that the dike-in-dike complex at Quemont Hill formed through synchronous emplacement of felsic and mafic melts along a major synvolcanic structure.

The results of the volcanic facies analysis lend support to models assuming that the Horne and Quemont deposits, which represent some of the largest synvolcanic gold enrichments world-wide, formed in a volcanic setting characterized by synvolcanic faulting caused by crustal extension. Widespread mingling and mixing of magmas of significantly different compositions likely resulted from the upwelling of mantle-derived melts into the crust, promoted by an extensional setting. As magma mingling and mixing indicate bimodal volcanism, a hallmark of crustal extension, it is proposed here that volcanic textures produced by these processes can be used to identify areas in volcanic belts that are favorable for volcanic-hosted massive sulfides.

TABLE OF CONTENTS

LIST OF FIGURES

LIST OF TABLES

LIST OF ABBREVIATIONS

General:

ID – TIMS	Isotope dilution-thermal ionization mass spectrometry
PPL	Plane polarized light
REE	Rare earth element
RSD	Relative standard deviation
VHMS	Volcanic-hosted massive sulfide
XPL	Crossed-polarized light

Units:

cm	Centimeter
Ga	Billion years
g/t	Gram per (metric) ton
km	Kilometer
m	Meter
µm	Micrometer
Ma	Million years
Mt	Million (metric) tons
t	(Metric) ton
%	Percent

ACKNOWLEDGMENTS

I am grateful to my advisor Dr. Thomas Monecke for the unique and exciting opportunity to complete this project. Thank you for your constant cheerful support and encouragement from project start to finish. I appreciate the continued guidance and discussion from my committee members Drs. Yvette Kuiper and Elizabeth Holley throughout the process of this thesis. I also highly value the helpful input I received from Drs. Richard Wendlandt and Nigel Kelly. Thanks to Ben Frieman for being a great friend and field partner while completing my research in Rouyn-Noranda.

This research would not have been possible without the financial support provided by the Stewart R. Wallace Endowment in Economic Geology at Colorado School of Mines. I am also grateful for a Society of Economic Geologist's Graduate Student Fellowship and a KGHM International Scholarship.

Lastly I would like to thank those who have supported me with love and friendship throughout my graduate career including my encouraging and loving parents, Oscar and Melodie, my determined sister Amanda, my other half, Tynan Conner, and my colleagues at the Colorado School of Mines, Helen Thomas and Jena Long. Your support and kindness throughout this project has made it a wonderful experience.

CHAPTER 1
INTRODUCTION

1.1. Volcanic-Hosted Massive Sulfide Deposits

Volcanic-hosted massive sulfide (VHMS) deposits represent predominantly strata-bound sulfide accumulations and related cross-cutting stringer zones or massive replacement pipes that formed from hydrothermal fluids on or immediately below the ancient seafloor (Franklin et al., 2005). The deposits are hosted by coherent volcanic rocks or volcaniclastic deposits formed or emplaced in a submarine setting (Gibson et al., 1999). VHMS deposits represent a significant source of copper, zinc, and lead. Some deposits contain economic grades of silver, gold and elements such as Co, Sn, Cd, In, Bi, and Ga, and can be recovered as co- or byproducts (Franklin et al., 2005). The deposits formed throughout Earth's history with the oldest examples recognized in pre-3.7 Ga old volcanic rocks at Isua, Greenland (Appel, 1979). Massive sulfide formation still occurs today at venting hydrothermal sites on the modern seafloor (Hannington et al., 2005).

1.2. Bimodal Volcanic Successions

Massive sulfide deposits form in volcanically active settings. Most significant VHMS districts have been formed near convergent plate margins settings characterized by major crustal extension (Allen et al., 2002; Franklin et al., 2005) and many of the world's most important deposits are hosted by bimodal volcanic successions (Barrie and Hannington, 1999; Barrett and McLean, 1999; Franklin et al., 2005; Piercey, 2011). Approximately 22% of the total tonnage of massive sulfides worldwide is hosted by host rock successions dominated by mafic rocks. These deposits and are thought to represent volcanic successions formed during rifting of primitive volcanic arcs. An additional 20% of the world's total tonnage of massive sulfides is contained in felsic-dominated bimodal successions. These deposits probably formed in compositionally more mature rifted volcanic arcs (Barrie and Hannington, 1999;).

Bimodal volcanism is a result of the coeval venting of mantle-derived mafic melts and felsic material produced by crustal melting or differentiation of the mafic melts. Bimodal volcanism is common in extensional environments which are characterized by high heat flow from the mantle such as rifts and back-arc basins developing in continental margin arcs, transitional arcs, and intraoceanic arcs (Fryer et al., 1990; Hochstaedter et al., 1990; Gill et al., 1994; Clift, 1995; Stolz, 1995; Shinjo and Kato, 2000; Piercey, 2011).

The synchronous emplacement of bimodal volcanic suites may result in the mingling or mixing of magmas of contrasting compositions. Magma mingling and magma mixing are differentiated by the extent to which physical magma interaction has occurred. Magma mixing typically results in the formation of a homogeneous or "hybrid" composition due to the close interaction of two magmas of contrasting compositions. Magma mingling refers to magma interaction that has resulted in physically distinct magmas with heterogeneous compositions (Johnson and Barnes, 2006). The process and extent of mixing and mingling are generally controlled by the density and viscosity of the end member magmas, which are also a function of the respective temperature and water content (Neves and Vauchez, 1995).

It is the aim of the present study to test whether magma mingling and mixing are common processes occurring during the formation of VHMS deposits within bimodal volcanic host rocks. In addition, the study presents whether volcanic textures produced by these processes can be used to identify favorable exploration locations within volcanic belts that likely underwent significant extension to allow contemporaneous emplacement of mafic and felsic melts. The study was conducted in the Neoarchean Noranda camp in Quebec, Canada, which is host to two of the world's largest gold-rich VHMS deposits.

1.3. Noranda District, Abitibi Subprovince

The Noranda district near Rouyn-Noranda in Quebec arguably represents one of the best studied VHMS districts in the world. The Neoarchean volcanic rocks in the district are exceptionally well preserved (Gibson and Galley, 2007). Regional metamorphism has occurred at prehnite-pumpellyite to lower greenschist facies conditions (Powell et al., 1995) and penetrative fabric development is only locally pronounced (Gibson and Galley, 2007). Research conducted on the massive sulfide deposits and their host-rock successions has significantly

contributed the understanding of VHMS deposits and the development of genetic and exploration models for this deposit type (Gibson and Galley, 2007).

The massive sulfide deposits of the Noranda camp are hosted by volcanic rocks belonging to the Blake River assemblage, which represents the youngest (2704-2695 Ma) assemblage of submarine volcanic rocks in the Neoarchean Abitibi subprovince (Fig. 1-1) (Thurston et al., 2008; McNicoll et al., 2014). The Noranda district is host to 25 massive sulfide deposits and a number of uneconomic occurrences (Kerr and Gibson, 1993; Gibson and Galley, 2007; Mercier-Langevin et al., 2011a). Most of the deposits mined in the district are hosted by the mafic-dominated bimodal volcanic succession of the Noranda Main Camp. The deposits largely formed at the ancient seafloor as classical mound-style massive sulfides. In general, these deposits are small in size (<5 Mt) and base-metal-rich, but have comparably low precious metal grades (<2 g/t Au).

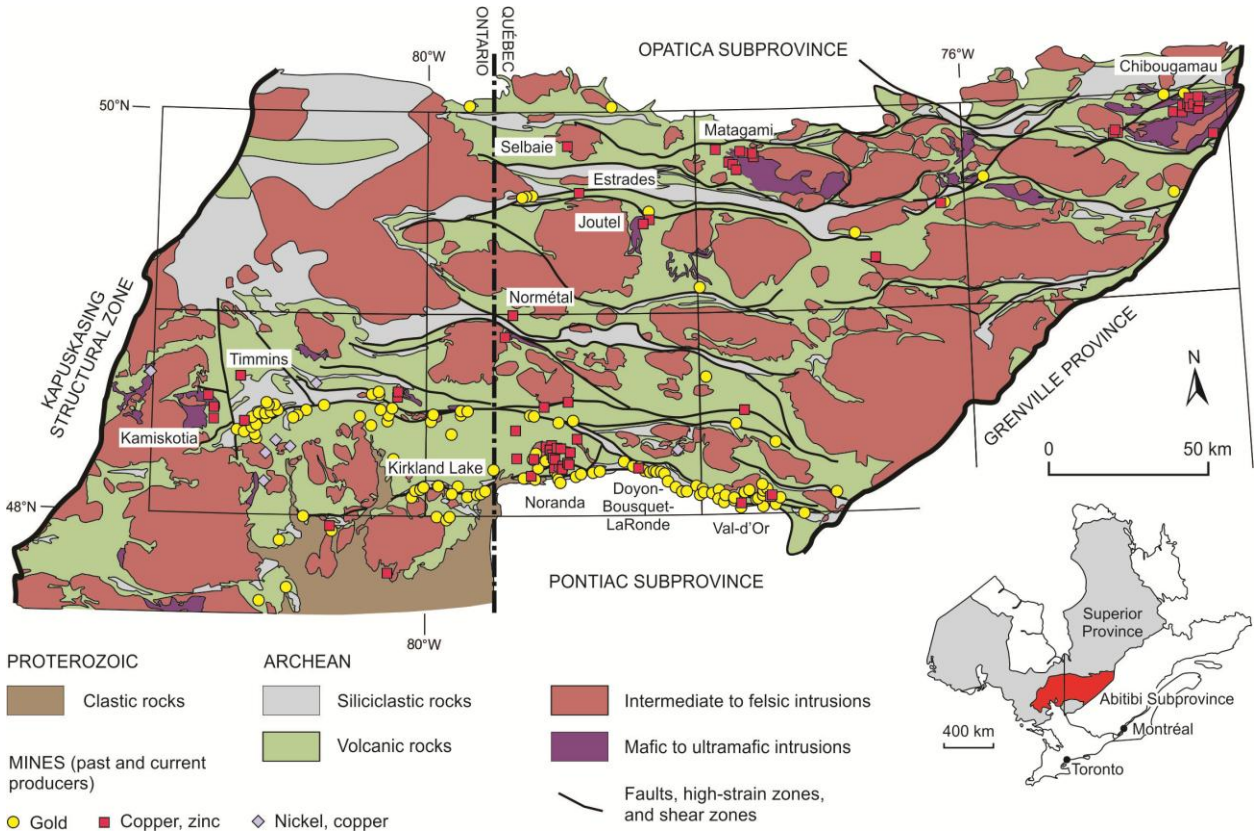

Fig. 1-1: Geological map of the Abitibi greenstone belt of northern Ontario and Quebec (modified after Thurston et al., 2008).

In contrast to the VHMS deposits of the Noranda Main Camp, the Horne and Quemont deposits are located within felsic-dominated bimodal volcanic successions that primarily comprise volcaniclastic rocks (Kerr and Gibson, 1993;Gibson and Galley, 2007; Mercier-Langevin et al., 2011a). The Horne deposit is the largest Au-rich massive sulfide deposits within the Noranda district with a total past production of 54.3 Mt of ore grading 2.2% Cu and 6.1 g/t Au (Gibson and Galley, 2007). The Quemont deposit yielded 16.65 Mt of ore at 1.2% Cu and 5.5g/t Au (Gibson and Galley, 2007). The unusual size of these two deposits may, at least in part, be explained by the fact that the Horne and Quemont deposits formed largely by subseafloor sulfide infiltration and replacement.

Recent high-precision U-Pb age dating has demonstrated that the Horne and Quemont deposits are hosted by felsic volcanic rocks that are 2,702 ± 0.9 Ma and 2,702 ± 0.8 Ma in age, respectively (McNicoll et al., 2014). The host rock successions of the two gold-rich deposits are consequently about 1-2 Ma older than the deposits in the Noranda Main Camp. This may suggest that the Horne and Quemont deposits not only formed in a different volcanic setting than the deposits of the Noranda Main Camp, but that regional-scale processes such as the geodynamic setting may have exerted important control on deposit formation and metal endowment (Mercier-Langevin et al., 2011b; McNicoll et al., 2014).The present study will provide new critical information on the regional setting of the Horne and Quemont deposits.

1.4. Research Approach

The present study aims to identify and characterize magma mingling and mixing textures in surface outcrops of the host rock successions of the Horne and Quemont deposits. Based on detailed textural observations, the volcanic processes that are responsible for the observed textures are reconstructed, providing critical information on the volcanological and geodynamic setting of both deposits.

At Horne, a well-exposed rhyolite cryptodome containing abundant mafic xenoliths (Monecke et al., 2008) was chosen to study processes of magma mingling between felsic and mafic melts. The research involved the detailed mapping of the rhyolite cryptodome and each of the xenoliths; the description and analyses of the composition, contacts and textural characteristics of mafic xenoliths within the rhyolite cryptodome; contouring the xenoliths based

on size, shape, trend, and abundance in order to understand outcrop scale trends; and comparison of the xenolith textures with other known magma mingling occurrences.

Within the Quemont area, detailed volcanic facies analyses were conducted at a dike-in-dike complex at Quemont Hill (Huthmann, 2009; Monecke et al., 2011). The research included extensive mapping over a comparably large field area and detailed mapping of the magma mingling and mixing features within the dike-in-dike complex; geochemical and petrographic analyses of the volcanic lithofacies present within the dike swarm to observe large scale compositional variations; and comparison of the magma mingling and mixing features across the outcrop to assess the processes of their emplacement.

The research at Horne and Quemont addressed the following specific questions:

1) What are the characteristics of volcanic features within the Horne area that formed through mingling of felsic and mafic magmas and how can they be quantified across the surficial outcrops?
2) What are the volcanic processes responsible for the formation of these textures and what do the interpreted volcanic processes suggest about the synchronous emplacement of felsic and mafic magma?
3) What are the magma mingling and mixing textures present at Quemont and how are they spatially distributed throughout the bimodal dike-in-dike complex near the Quemont massive sulfide deposit?
4) How does the occurrence of magma mingling and mixing relate to the volcanic environment in which the Horne and Quemont deposit formed?

In addition to these key questions, the present study will compare the textural evidence for magma mingling and mixing observed in the host rock successions at Horne and Quemont with those textures described in the literature for other settings.

1.5. Thesis Outline

The thesis is structured into four chapters. The first chapter provides an introduction to the subject matter and outlines the goal of the research. The research results are presented in separate chapters that are written as manuscripts and will be submitted to the international peer-reviewed journals *Precambrian Research* and *Journal of Volcanology and Geothermal*

Research. Chapter 2 focuses on the occurrence of magma mingling during the formation of the volcanic host rock succession of the giant Horne deposit. The chapter derives a model for the incorporation of mafic xenoliths into the rhyolite cryptodome at Horne West. Chapter 3 focuses on the research conducted at Quemont Hill, which forms part of the host rock succession of the Quemont deposit. It is demonstrated that magma mingling and mixing occurred during the emplacement of a dike-in-dike complex that is composed of rhyolite and basalt intrusions. Chapter 4 provides a summary of the research findings and a comparison between the case studies at Horne and Quemont. Implications to exploration for volcanic-hosted massive sulfides are discussed.

CHAPTER 2

THE SIGNIFICANCE OF MAGMA MINGLING DURING THE FORMATION OF THE VOLCANIC HOST-ROCK SUCCESSION OF THE GIANT HORNE MASSIVE SULFIDE DEPOSIT, ROUYN-NORANDA, QUEBEC

Manuscript to be submitted to Precambrian Research

Keywords: Archean, Abitibi subprovince, Blake River assemblage, Horne deposit, magma mingling, rhyolite cryptodomes, volcanic facies mapping

2.1. Abstract

The Noranda mining camp represents one of the most important hosts of volcanic-hosted massive sulfide deposits in the Neoarchean Blake River assemblage of the Abitibi subprovince of northern Canada. With a past production of 1.13 Mt of Cu and 260 t of Au, the Horne mine, located near Rouyn-Noranda in Quebec, was the largest base and precious metal producer within the district. The host-rock succession of the giant Horne deposit primarily comprises a succession of felsic volcanic rocks that is crosscut by a dike complex feeding into a conformably overlying package of mafic volcanic rocks.

Detailed mapping showed that a flow-banded rhyolite cryptodome exposed in the footwall of the deposit contains abundant mafic xenoliths. The characteristics of the mafic xenoliths, including their shapes, sizes, trends, and contact relationships, were recorded using a one by one meter surface grid. Based on contour maps, it was possible to identify several systematic changes in the xenolith characteristics across the rhyolite cryptodome. Abundant tabular xenoliths are present in the stratigraphically lower part of the outcrop. The xenoliths become increasingly sparse, blocky, and irregular towards the top of the rhyolite unit. Distinct flow-banding in the southernmost outcrops are indicative for an E-W flow of the rhyolite around the xenoliths. Scalloped margins on the xenoliths suggest that rapid quenching of the mafic xenoliths occurred upon emplacement. The observed relationships between the flow-banded rhyolite and the mafic xenoliths are indicative of magma mingling, suggesting that the felsic melt producing the rhyolite cryptodome and the mafic melt forming the xenoliths were emplaced

synchronously. It is likely that both melts erupted at the same time along a synvolcanic fault, resulting in mingling along the feeder dike and transport of the xenoliths into the effusive portion of the cryptodome.

The present study demonstrates that magma mingling of felsic and mafic melts indicates bimodal volcanism during the formation of the host stratigraphy of the Horne deposit. As bimodal volcanism is a hallmark of extensional suprasubduction settings, it is proposed here that the Horne deposit formed in a geodynamic setting similar to rifts forming in modern volcanic arc environments.

2.2. Introduction

The Horne volcanic-hosted massive sulfide deposit in the Neoarchean Abitibi subprovince of northern Ontario and Quebec represents one of the largest synvolcanic base and precious metal deposits in the world. Between 1927 and 1976, the deposit produced approximately 1.13 Mt of Cu and 260 t of Au from 53.7 Mt of ore that graded 2.22% Cu, 6.1 g/t Au, and 13 g/t Ag (Gibson et. al., 2000). Despite its economic significance, little research on the volcanic succession has been conducted at Horne, constraining the volcanological environment and general tectonic setting in which this giant deposit formed.

Previous research indicated that the host rock succession of the Horne deposit is distinctly bimodal in character. The massive sulfide lenses of the Horne deposit are hosted by coherent rhyolite, associated volcaniclastic rocks interpreted to have formed by autobrecciation and quench fragmentation, and pyroclastic material delivered from felsic explosive sources (Sinclair, 1971; Kerr and Mason, 1990; Gibson et al., 2000; Monecke et al., 2008). The felsic host rock succession, including the ore lenses that formed through processes of subseafloor infiltration and replacement of the volcaniclastic units (Kerr and Mason, 1990; Gibson et al., 2000; Monecke et al., 2008), is crosscut by a basalt dike complex. The basalt intrusions commonly have chilled margins and interfinger irregularly with volcaniclastic rocks (Monecke et al., 2008). Although mapping of the limited surface outcrops (Monecke and Gibson, 2013) has not revealed conclusive evidence for the occurrence of peperitic contact relationships, some of the basaltic intrusions have been affected by hydrothermal alteration, suggesting that emplacement of the dike complex was initiated during the waning stages of the hydrothermal

activity. Historic mine plans suggest that the basaltic dike complex feeds a thick succession of mafic rocks that overlies the felsic host rock succession of the Horne deposit (Kerr and Mason, 1990; Monecke et al., 2008).

The present paper provides new constraints on the relationships between the felsic and mafic volcanic rocks forming the host rock succession of the Horne deposit. The well-exposed outcrop area to the west of the deposit that was studied in detail is characterized by the occurrence of abundant mafic xenoliths within a flow-banded rhyolite cryptodome. Volcanic facies analysis of the outcrop area included detailed mapping and the documentation of the distribution, size, abundance, and trend of the mafic xenoliths present within the coherent rhyolite unit. Based on the mapping results and the study of textural relationships, it is concluded that the mafic xenoliths were incorporated into the flow-banded rhyolite cryptodome through mingling of the mafic and felsic magmas. The occurrence of magma mingling demonstrates conclusively that bimodal volcanism was contemporaneous to the formation of the world-class Horne massive sulfide deposit. It is proposed that magma mingling of mantle-derived mafic melts and crustal felsic magmas is a direct consequence of the extensional suprasubduction setting in which the Horne massive sulfide deposit formed.

2.3. Geological Setting

The host rocks of the Horne deposit belong to the 2704-2695 Ma Blake River assemblage, which represents the youngest package of submarine volcanic rocks within the Abitibi subprovince of the Superior Province (Fig. 1-1). The bimodal tholeiitic to calc-alkaline volcanic rocks of the Blake River assemblage form a distinct east-west trending belt that is approximately 50 km wide and stretches for about 140 km from eastern Ontario into western Quebec (Dimroth et al., 1982, Goodwin, 1982). This belt of submarine volcanic rocks is bounded to the north by the Porcupine-Destor deformation zone and to the south by the Larder Lake-Cadillac deformation zone (Thurston et al., 2008).

The Noranda mining district, located east of the provincial border between Ontario and Quebec comprises over 25 massive sulfide deposits that are hosted by the volcanic rocks of the Blake River assemblage (Kerr and Gibson, 1993; Gibson and Galley, 2007; Mercier-Langevin et al., 2011a). Most of these deposits are hosted within the Noranda Main Camp (Fig. 2-1), which is

composed of a thick volcanic succession comprising alternating packages of coherent basalt or andesite and rhyolite. Mafic volcanic rocks form predominantly pillowed and massive flows while rhyolite lavas were largely emplaced as tabular flows and low relief domes (Spence and de Rosen-Spence, 1975; Kerr and Gibson, 1993). Intercalated volcaniclastic rocks are volumetrically only of minor importance (Gibson, 1990; Spence, 1976). High-precision U-Pb (ID – TIMS) zircon dating indicates that the onset of bimodal volcanism of the Noranda Main Camp occurred just prior to 2,700.7 ± 0.6 Ma (McNicoll et al., 2014), with much of the stratigraphy having formed by 2,698.3 ± 1.2/-1.0 Ma (David et al., 2006, 2010).

The volcanic succession of the Noranda Main Camp is crosscut by a large number of synvolcanic diorite and gabbro dikes and sills. In addition, the large synvolcanic Flavrian and Powell plutons are located within the Noranda Main Camp (Fig. 2-1), which are composed of sill-like intrusions characterized by generally conformable contacts with the overlying volcanic strata. The Lac Dufault pluton, located to the east, is a younger, post-volcanic intrusion (Mortensen, 1993) that is surrounded by a pronounced contact metamorphic aureole (de Rosen-Spence, 1969; Beaty and Taylor, 1982).

Several major faults and their extrapolations divide the volcanic succession of the Noranda district into distinct fault blocks (Spence, 1976; Péloquin et al., 1990). The Hunter Creek fault is located at the northern boundary of the Flavrian block, with the Beauchastel fault forming the southern boundary. The Flavrian block hosts the massive sulfide deposits of the Noranda Main Camp. The Beauchastel and Horne Creek faults to the south enclose the Powell block. The area between the Horne Creek fault and Andesite fault makes up the Horne block. The Rouyn-Pelletier block occurs to the south between the Andesite fault and the Larder Lake-Cadillac deformation zone (Fig. 2-1).

The giant Horne deposit is located within the Horne block that is bound by the Horne Creek and Andesite faults. Both faults dip steeply toward each other and converge approximately 2.2 km to the west of the deposit (Kerr and Mason, 1990; Péloquin et al., 1990; Gibson et al., 2000). The approximately 900 m thick, fault-bounded package of volcanic rocks hosting the Horne deposit face to the north, strike approximately west-northwest, and dip steeply to the north (Wilson, 1941; Hodge, 1967; Sinclair, 1971; Kerr and Mason, 1990; Kerr and Gibson, 1993; Gibson et al., 2000; Monecke et al., 2008; Monecke and Gibson, 2013). Recent high-precision U-Pb zircon dating has demonstrated that a rhyolite sill occurring in the mineralized stratigraphic

footwall of the deposit formed at 2,702.2 ± 0.9 Ma (McNicoll et al., 2014), suggesting that the volcanic package hosting the Horne deposit is older than the bimodal volcanic succession of the Noranda Main Camp (Mercier-Langevin et al., 2011a; McNicoll et al., 2014).

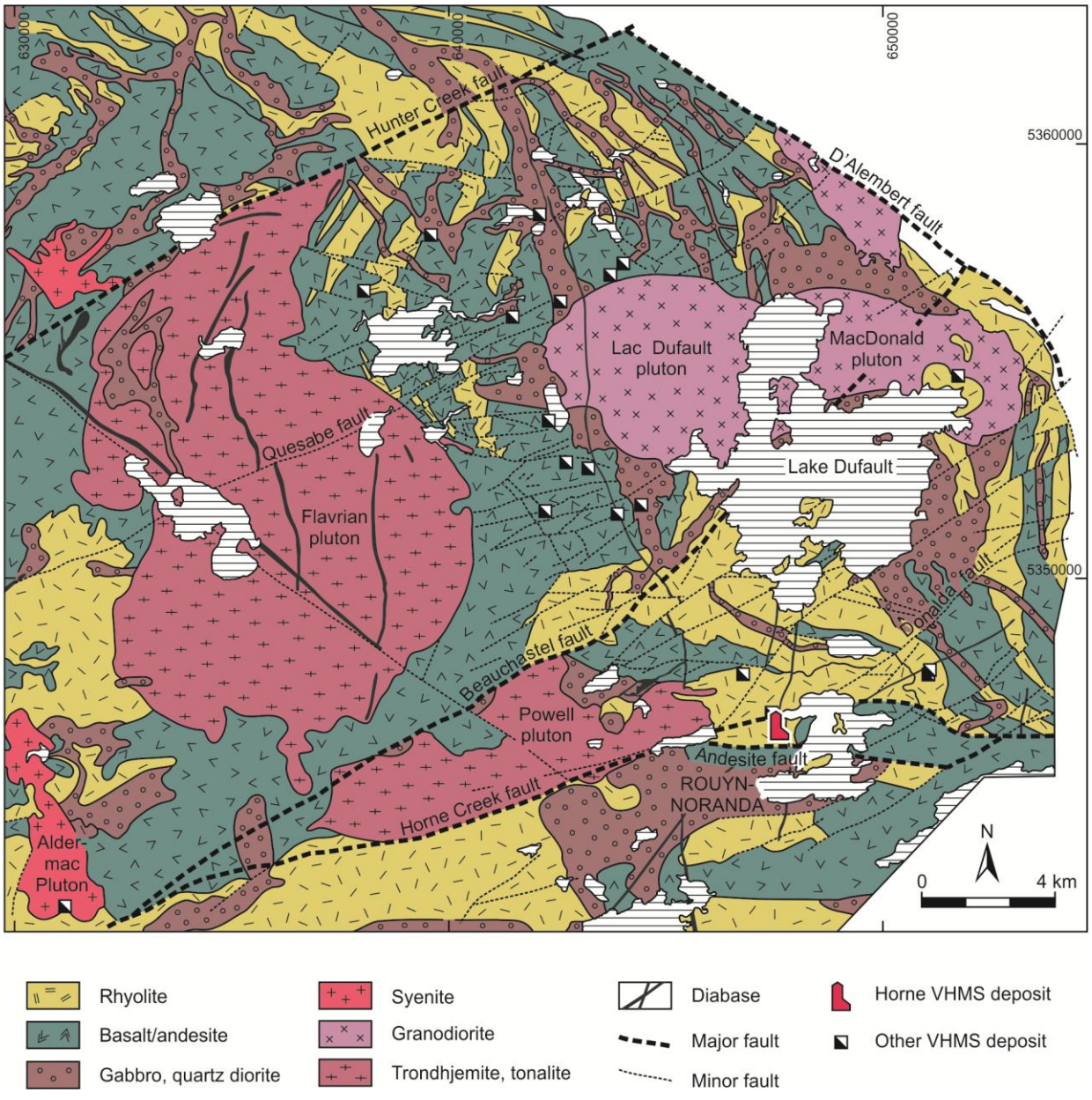

Fig. 2-1: Geological map of the Noranda volcanic complex, illustrating the distribution of major volcanic and intrusive rock units. The location of the field area near the Horne deposit is highlighted (modified from Santaguida, 1999).

The dominantly felsic volcanic succession hosting the Horne deposit consists mainly of coherent rhyolite and associated breccia facies, interpreted to represent subaqueous lava flows, cryptodomes and shallow intrusions, redeposited syn-eruptive volcaniclastic deposits, and possible primary pyroclastic deposits (Kerr and Mason, 1990; Kerr and Gibson, 1993; Gibson et al., 2000; Monecke et al., 2008). Mining was focused on two main orebodies, known as the Upper H and Lower H orebodies. Nearly all historic production from the Horne deposit came from the Upper H ore body, which extended from surface to a mine depth of 395 m, and the Lower H ore body, located at a mine depth of 365 to 945m (Price, 1934; Hodge, 1967; Gibson et al., 2000). The Lower H ore body is stratigraphically overlain by a tabular zone of massive to semi-massive sulfides, referred to as the No. 5 Zone (Sinclair, 1971). This ore zone extends for a strike length of more than 1,000 m to a depth of at least 2,650 m and ranges from approximately 30 to 140 m in thickness (Sinclair, 1971; Fisher, 1974; Gibson et al., 2000). Due to low metal grades, this zone has not been mined extensively (Gibson et al., 2000).

The sulfide zones of the Horne deposit are crosscut by numerous basaltic dikes. Historic mine plans suggest that the mafic intrusions extend towards a package of mafic rocks located to the northeast of the Horne deposit (Kerr and Mason, 1990). This package thickens towards the east, separating the ore bodies from the Horne Creek fault. The succession of mafic rocks appears to conformably overlie the felsic volcanic rocks, which would imply that the mafic rocks were emplaced as flows or sills. However, the mafic volcanic rocks are poorly exposed and have previously been variably interpreted as being intrusive or extrusive in nature (Monecke et al., 2008).

The present study focuses on the Horne West outcrop area, which represents one of the best exposed sections of Horne stratigraphy. Stratigraphically, the volcanic rocks at Horne West are thought to be located several hundred meters below the Upper H and Lower H orebodies (Kerr and Gibson, 1993). The outcrop is located immediately to the north of the Andesite fault and approximately 1 km west of the main Horne deposit.

The volcanic succession at Horne West is dominated by coherent rhyolite and associated juvenile breccia facies that formed through autobrecciation and quench fragmentation. In addition, various mass-flow-derived coarse volcaniclastic facies have been recognized. Some of the volcaniclastic deposits show a high abundance of formerly glassy particles that may represent pyroclasts produced by explosive felsic volcanism (Monecke et al., 2008). The outcrop area at

the Horne West occurrence has been previously mapped at a scale of 1:200 (Monecke et al., 2008; Monecke and Gibson, 2013). Mapping revealed the presence of a large rhyolite cryptodome at the northern end of the outcrop area (Monecke et al., 2008). The coherent facies of the rhyolite dome exhibits well-defined flow-foliation as well as columnar jointing. The rhyolite contains abundant mafic xenoliths of varying sizes (Fig. 2-2).

Figure 2-2: Photograph of surficial rhyolite outcrops at Horne West. Mafic xenoliths are observed in the in the front of the outcrop. The xenoliths range from 10 cm to 1 m in length.

2.4. Materials and Methods

As part of the present investigations, the coherent rhyolite cryptodome located at the northern end of the Horne West occurrence has been remapped in detail at a scale of 1:50. Mapping of the outcrop covering an area that is approximately 30 by 30 m in size was supported by the use of a Magellan ProMark 3 differential GPS system that comprises a stationary and kinematic rover GPS pair. The rover GPS unit was used to produce an accurate map of outcrop outlines and important contact relationships.

A 1 by 1m surface grid was established across all six rhyolite outcrops. The corners of each grid square were georeferenced with the differential GPS system to accurately plot the grid on the outcrop map. All important textural characteristics of the coherent rhyolite were recorded. In particular, the prominent flow banding was mapped across the outcrops using the established

surface grid. The trend of the flow banding was measured in representative locations. Where columnar jointing was observed, the trends and column morphologies were recorded in addition to column size and spacing.

The surface grid was also used to determine the total number of clasts in each grid square. Within each square meter, the long axis, short axis, and trend of each xenolith were measured. In addition, the contact relationships between the xenoliths and the surrounding rhyolite were recorded and the general morphology of the xenoliths described. To visualize the data, contour maps were constructed. For this, the central point of each square meter was assigned a value for the number of clasts per square meter, the percent surface area of xenoliths, the average long axis, and the average aspect ratio of the xenoliths.

Selected samples of the coherent rhyolite and mafic xenoliths were collected from surface outcrop to characterize both volcanic rock types petrographically and to determine their geochemical characteristics. Several contacts between the rhyolite and mafic xenoliths were sampled at surface to study the textural relationships between both rock types in thin section.

Whole-rock geochemical analysis of the samples collected was conducted at Actlabs in Ancaster, Ontario to determine major and trace element concentrations. Following crushing and milling of the samples at the Colorado School of Mines, the major element compositions of the rocks were determined by X-ray fluorescence analysis using standard fused disks. To minimize matrix effects, the heavy absorber fusion technique described by Norrish and Hutton (1969) was employed. The loss of ignition of the samples was determined by gravimetry following roasting of the sample powders at 1,050°C for 2 hours. The total carbon and sulfur contents were determined by the Leco method, which involves combustion of the samples, followed by measurement of the carbon dioxide and total sulfur content by infrared absorption. Trace element analysis was conducted by inductively coupled plasma-mass spectrometry following closed vessel digestion of the samples using a combination of hydrofluoric, hydrochloric, nitric, and perchloric acids.

Repeated analyses of sample materials and in-house and international georeference materials showed that the precision of the major and trace element analyses was typically <5% RSD. Element abundances measured on international georeference materials were in close agreement with the recommended values. The deviations of the analytical results from the recommended values were found to be in the order of ±10% or below for all elements occurring

at concentration levels significantly above the respective detection limits, indicating that the major and trace element analysis was also highly accurate.

2.5. Characteristics of Rhyolite Cryptodome

At the surface, the rhyolite cryptodome is exposed in six relatively large, glacially polished, smooth outcrops. The outcrops permit essentially continuous mapping of the eastern portion of the cryptodome from its bottom contact to the top. The six outcrops were consecutively labeled to facilitate description (Fig. 2-3).

The rhyolite is aphanitic and aphyric in nature and weathers from white-buff to yellow-white. The westernmost outcrop area of the rhyolite is distinctly green in color, as the rhyolite has been affected by chlorite alteration. In weathered surfaces, the rhyolite has a granular texture at the millimeter scale. The rock contains approximately 1-5% disseminated pyrite grains. Locally occurring pyrite veinlets are surrounded by pale yellow sericitic envelopes that are up to 2 cm wide.

The contacts between the coherent rhyolite and the enclosing volcaniclastic rocks are sharp and locally marked by the presence of in-situ polyhedral blocky-clast rhyolite breccia and non-stratified polyhedral blocky-clast and slabby-clast rhyolite breccia (Monecke et al., 2008). Along the lower contact, the rhyolite has intruded into a stratified chlorite-wisp-bearing lithic sandstone facies. Locally, classical perlite defined by distinctly arcuate and concentrically arranged cracks can be recognized in coherent rhyolite close to the bottom contact, suggesting that the rhyolite was initially, at least in part, glassy.

At the surface, the upper contact of the rhyolite with a stratified sulfide-clast-bearing lithic sandstone and breccia facies is passive. Logging of historic exploration drill core has shown, however, that the stratigraphic position of the upper rhyolite contact varies along strike and down-dip, suggesting that the rhyolite intruded into a succession of stratified volcaniclastic debris. Several meters above the upper rhyolite contact, two large xenolith-bearing clasts (150 by 100 cm and 65 by 33 cm, respectively) of the rhyolite are observed in outcrop. They are located within a stratified sulfide-clast-bearing quartz-phyric rhyolite breccia facies. Incorporation of these clasts into a mass-flow emplaced volcaniclastic unit suggests that the rhyolite locally

emerged at the ancient seafloor. The rhyolite cyptodome must have breached the seafloor during emplacement or, alternatively, became exposed at the seafloor because of synvolcanic faulting.

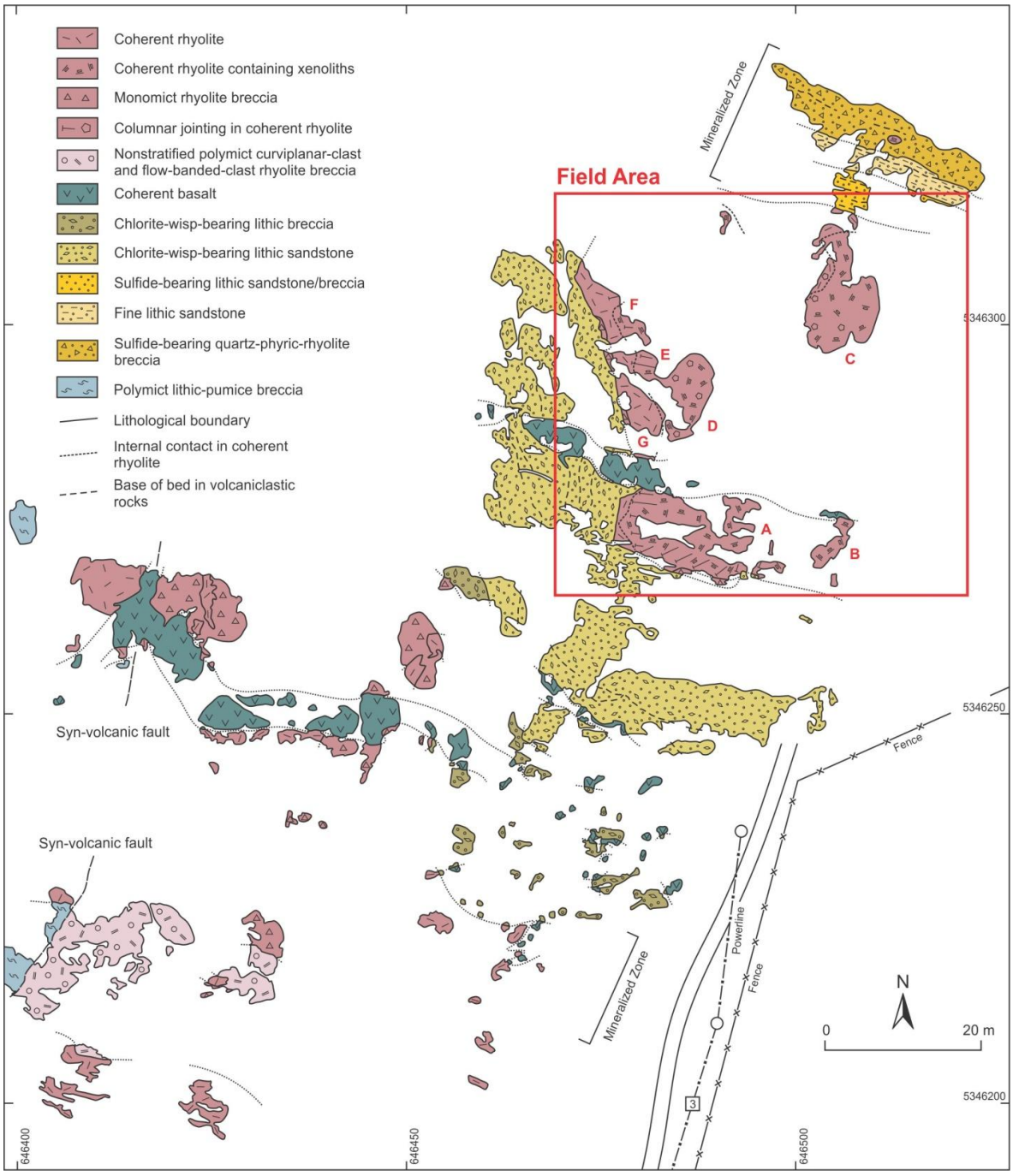

Fig. 2-3: Map of the Horne West outcrop that shows the distribution of coherent and volcaniclastic facies. The location of the rhyolite cryptodome studied in the present study is outlined in red (modified from Monecke et al., 2008; Monecke and Gibson, 2013).

2.5.1. Flow-Banding

The rhyolite cryptodome exhibits distinct flow foliation that is characterized by millimeter-to several centimeter wide bands of slightly different colors. The flow foliation varies from subparallel flow bands to bands that are strongly deformed and contorted, especially around the mafic xenoliths (Fig. 2-4).

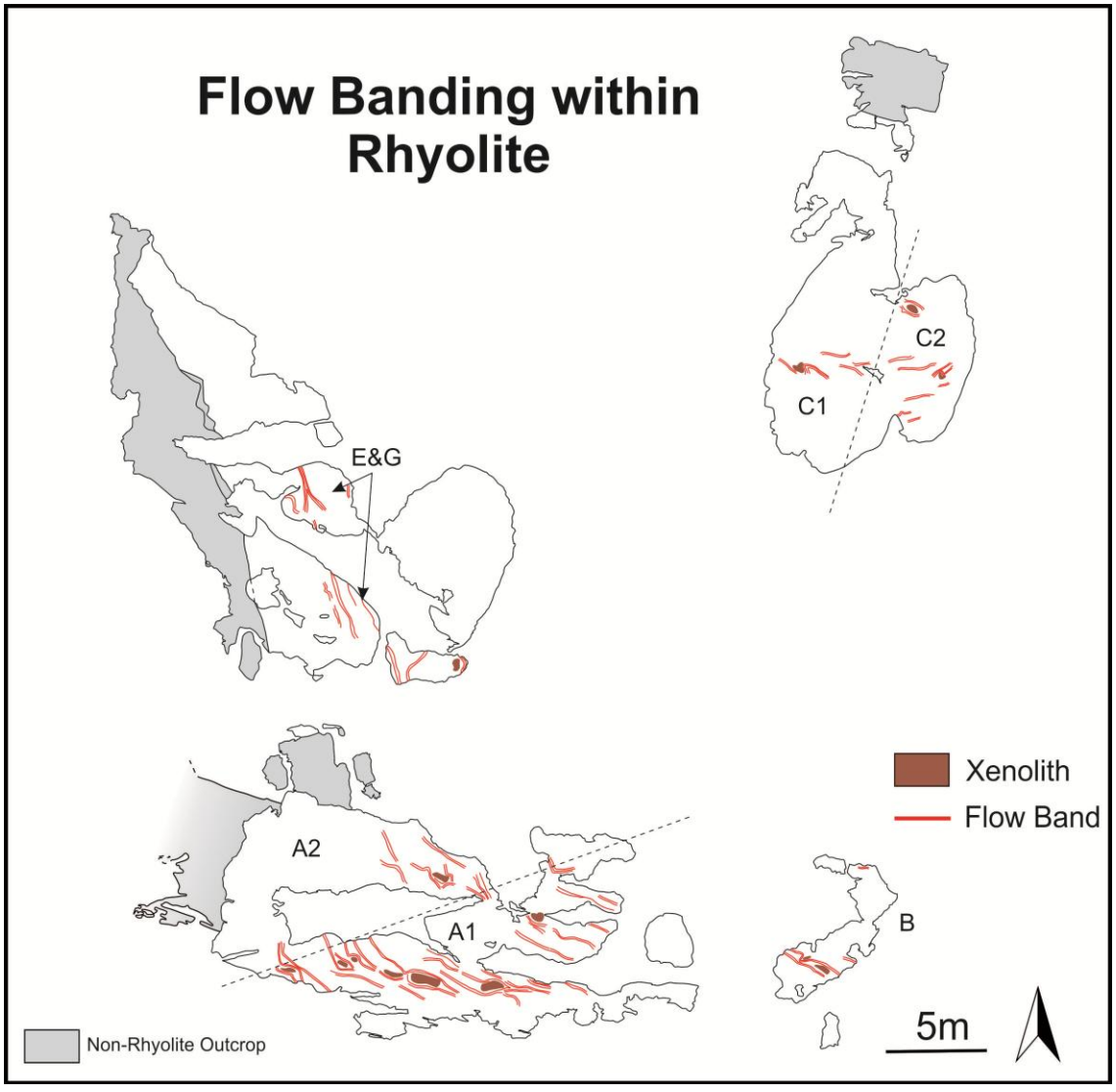

Fig. 2-4: Detailed map of the six outcrops of the rhyolite cryptodome. The map also shows the distribution of flow-banding and large mafic xenoliths. Flow-banding domains were defined by broad changes in the trend of the flow banding.

Flow banding is most easily recognizable in outcrop A. Based on the trend of the flow-banding, two different domains can be distinguished in outcrop. The flow-banding trends E-W in outcrop A1 and has a SE-NW trend in outcrop A2. Based on the map pattern, the trend of flow-banding appears to change across a NE-trending axis. Flow banding within outcrop C also varies in trend. The western half of the outcrop, referred to as outcrop C_1, is characterized by flow banding that has an average trend of 291°. The eastern portion of the outcrop, referred to as outcrop C_2, is characterized by banding that has an average trend of 265°.

Contortion of flow banding around the mafic xenoliths is typically pronounced, especially for the larger xenoliths (Fig. 2-5A). The flow bands asymmetrically wrap around the xenoliths. Separation of flow bands occurs largely on the eastern margins of the xenoliths. Widened parallel flow bands occur of the western margins. A crescent-shaped xenolith within outcrop C demonstrates flow banding directed into the concave down region of the xenolith and deflection of the flow banding around the western margin (Fig. 2-5B). Truncation of the flow bands against the xenoliths is rare.

2.5.2. Columnar Jointing

The southernmost outcrops of the rhyolite cryptodome are characterized by sets of regularly spaced joints that are interpreted to represent columnar joints viewed from the side (Fig. 2-5C). The trend of the joints ranges from 252° to 288° in outcrops A and B, with an average trend of 267°. The columns are spaced approximately 5 to 10 cm apart. Joints in outcrop F are more difficult to delineate due to the gossanous nature of the outcrop. The joints have a slightly more irregular spacing and are 10 to 20 cm apart. The joints have an average trend of 293°. In all three outcrops, the trend of the joints is at high angle to the contact between the rhyolite and the hosting chlorite-wisp-bearing lithic sandstone. In outcrops C and D, the columns occur in cross-section are defined by easily recognizable hexagonal or polygonal joint patterns (Fig. 2-5D). In outcrop C, the columns increase in size and decrease in abundance from east to west. They range from 5 to 10 cm in diameter in the east and reach sizes exceeding 10 cm in the west. The trend of the columns in outcrops C and D suggests that the morphology of the rhyolite cryptodome is quite irregular and the cooling surface in these locations must have been approximately parallel to surface.

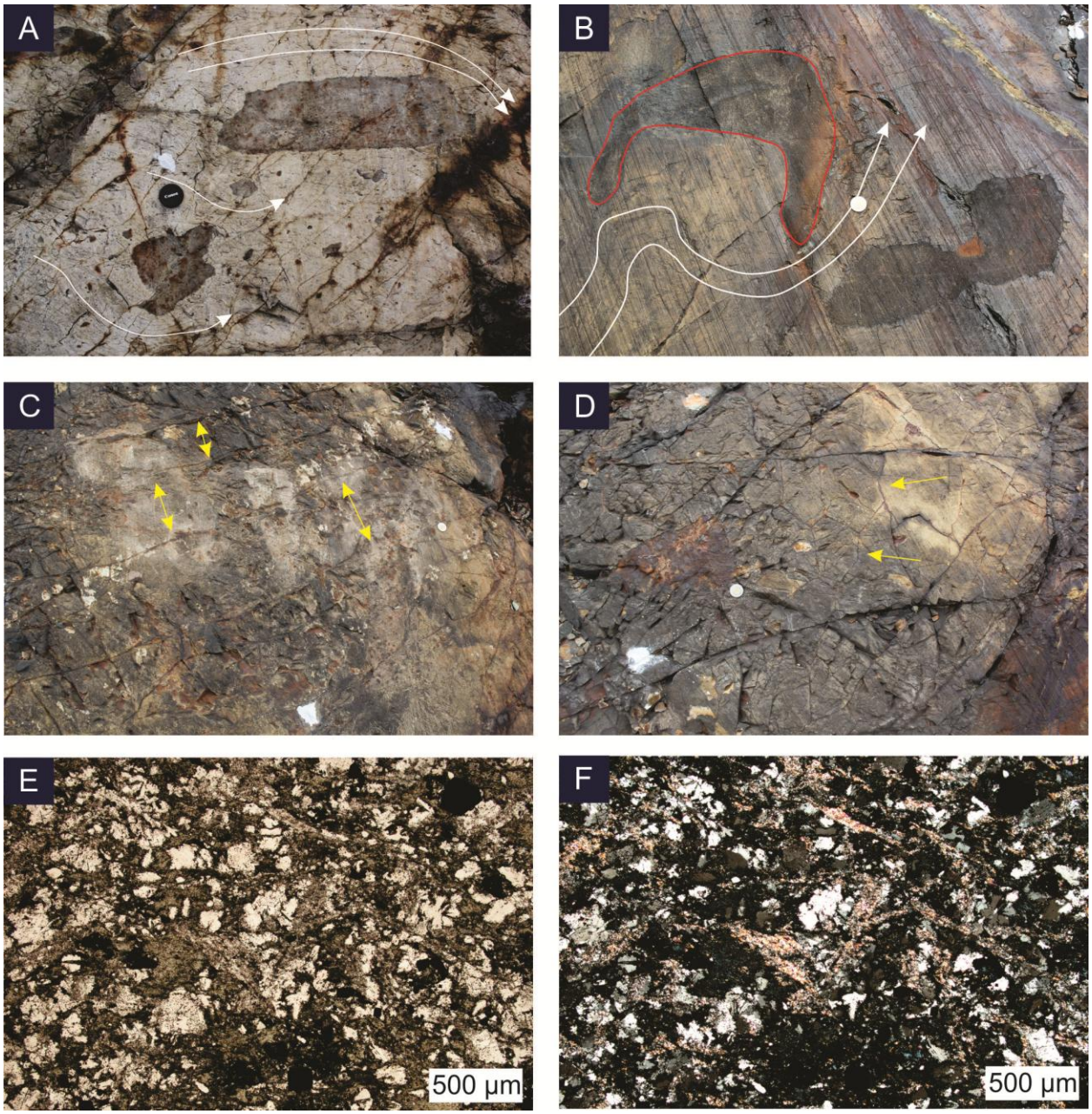

Fig. 2-5: Photographs of felsic host rock features in outcrop and photomicrographs of textures in felsic rocks. A. Asymmetric flow banding interacting with large and small xenoliths. B. A crescent-shaped xenolith adjacent to a large peanut-shaped xenolith with prominent flow-banding interaction. Flow banding appears directed into the concave-down part of the xenolith and flows around its western margin. C. Side view of several parallel columnar joints with 5-15 cm spacing between them oriented approximately E-W. D. Hexagonal and polygonal columnar joints contained between two larger fractures oriented E-W. E. Representative photo of the rhyolite in PPL. F. XPL photo of the same area showing micas replacing aligned feldspars as well as quartz and feldspar phenocrysts. Coin is 2.8 cm in diameter and camera lens is 6 cm.

2.5.3. Petrographic Characteristics

The coherent rhyolite is aphyric and aphanitic. In thin section, the rhyolite is composed of a fine-grained groundmass of interlocking quartz and feldspar (Fig. 2-5E and F). Quartz grains are subhedral and typically form grains that are approximately 200 µm in diameter. Feldspar in the groundmass is typically pervasively altered and largely replaced by white mica. The feldspar grains are similar in size to the quartz grains. White mica flakes in the groundmass range in size from 100 to 250 µm. In addition, chlorite is present throughout the groundmass. The occurrence of small disseminated pyrite grains, clusters of pyrite, and small pyrite veins is interpreted to be related to the hydrothermal alteration of the rhyolite.

2.5.4. Geochemical Characteristics

Five coherent rhyolite samples were geochemically analyzed in order to refine the rhyolite composition. Major and trace element analyses are reported in Table 2-1. SiO_2 contents of the samples range from 70-75 wt. %. Immobile element ratios were used to determine the geochemical composition in comparison to the composition determined in the field (cf. Floyd and Winchester, 1978). The Zr/TiO_2 versus Nb/Y and Pr/Zr versus Ti/Zr discrimination diagrams put forth by Winchester and Floyd (1977) and Stolz (1995) show consistent clustering of samples within the rhyodacite-dacite to high-silica dacite fields (Fig. 2-6 and 2-7). The coherent volcanic host rocks are geochemically classified as rhyodacite.

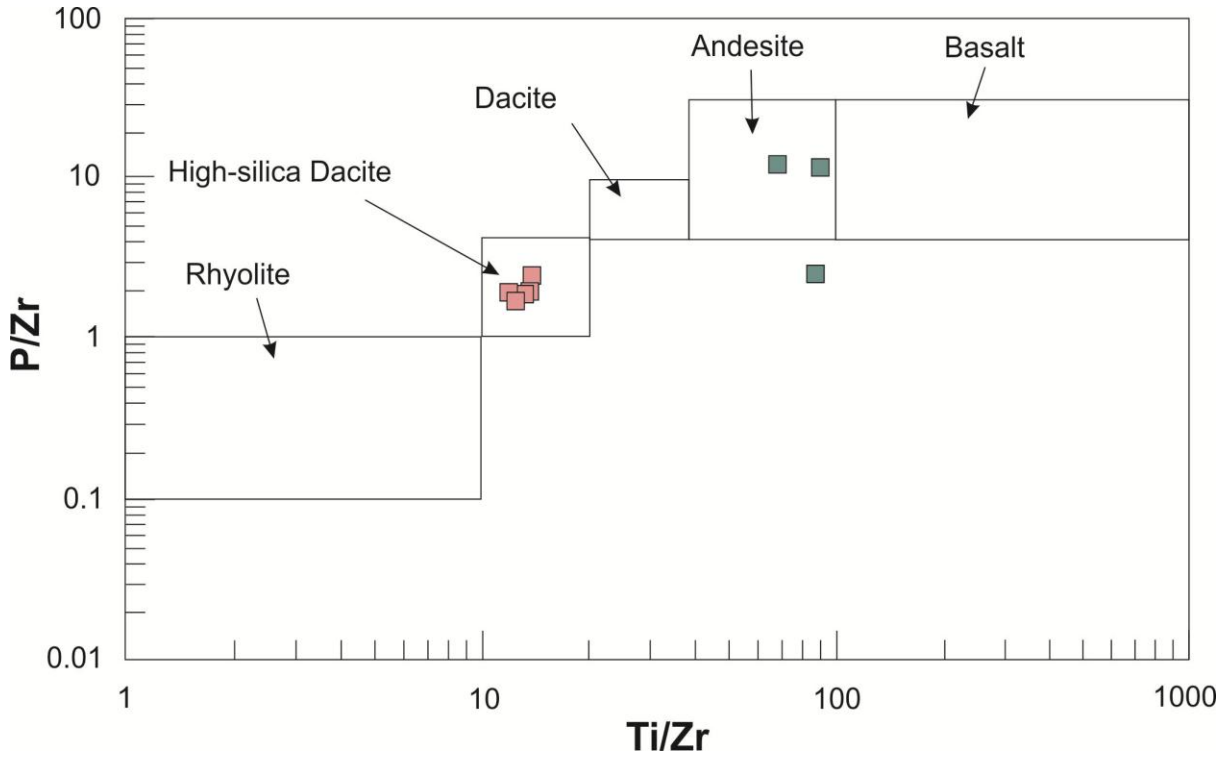

Fig. 2-6: Plot of P/Zr vs. Ti/Zr used to discriminate the composition of the mafic xenoliths (teal) and felsic host rocks (pink) present at Horne West. Sample HWZ009 was omitted from analysis due to P_2O_5 levels below detection. Felsic host rocks are geochemically classified as rhyodacite according to this diagram and the mafic xenoliths are classified as basalt-andesite (diagram from Stolz, 1995)

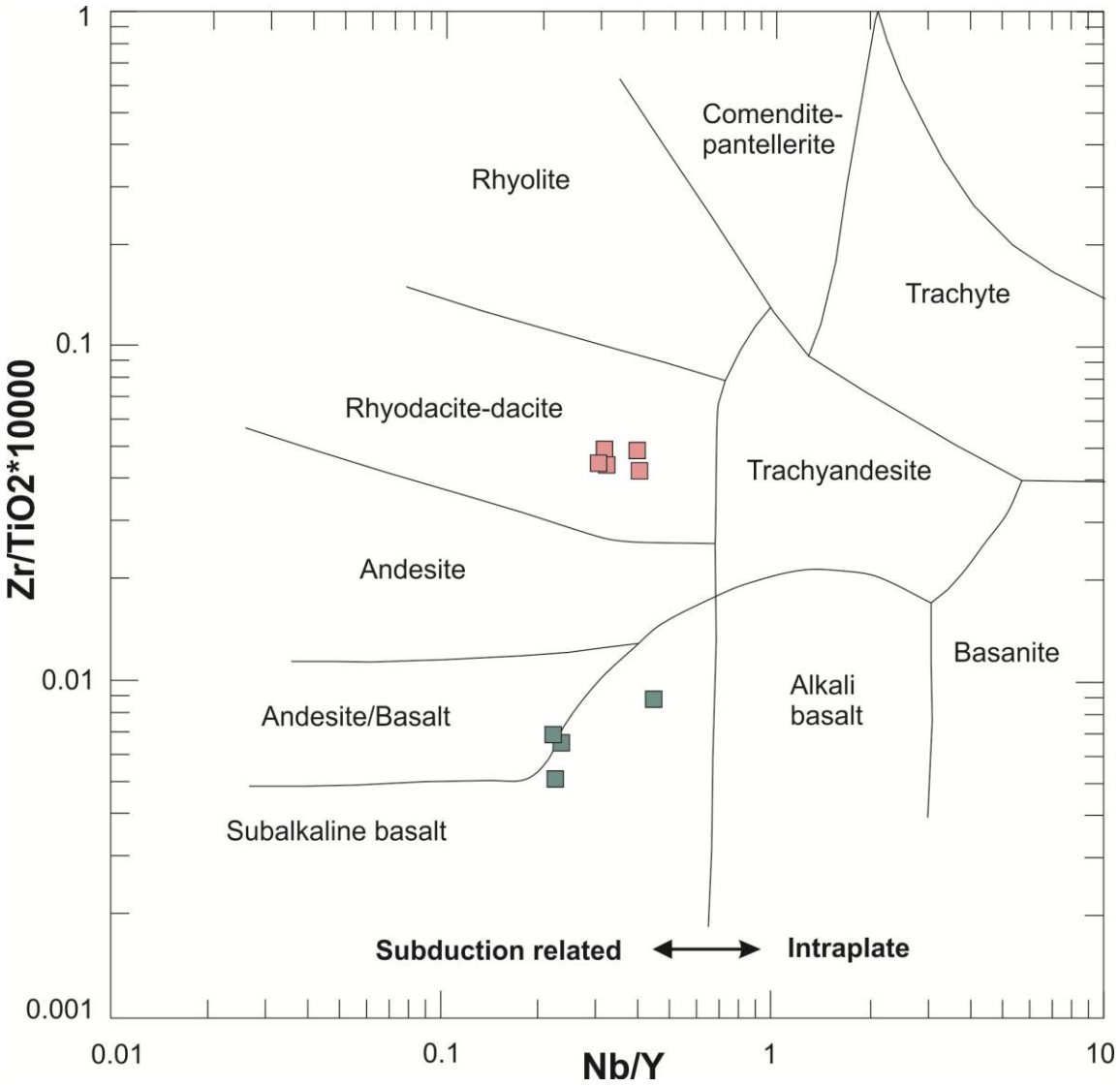

Fig. 2-7: Plot of Zr/TiO_2 vs. Nb/Y used to classify the xenoliths (teal) and host rock (pink) at Horne West. Xenoliths demonstrate a subalkaline affinity and are compositionally classified as basalt to andesite/basalt and the host rock is geochemically defined as a rhyodacite (diagram from Winchester and Floyd, 1977).

Table 2-1: Major (wt.%) and trace element (ppm) contents of volcanic rocks from Horne West

	Xenolith				Rhyolite				
Sample	HWZ01	HWZ03	HWZ05	HWZ09	HWZ02	HWZ04	HWZ07	HWZ08	HWZ10
SiO_2	55.87	56.13	66.18	50.72	70.91	71	71.68	74.53	72
Al_2O_3	15.71	16.2	16.59	16.39	12.77	12.86	12.35	12.59	12.92
Fe_2O_3(T)	14.62	13.58	6.71	19.14	7.24	8.52	8.03	5.24	6.21
MnO	0.237	0.315	0.14	0.813	0.098	0.1	0.241	0.325	0.233
MgO	2.23	2.18	1.45	2.43	1.09	2	1.03	0.59	0.99
CaO	1.26	0.58	0.27	0.91	0.67	0.12	0.12	0.67	0.79
Na_2O	0.56	0.42	0.22	0.17	1.92	0.12	0.18	0.28	2.22
K_2O	2.67	2.88	4.06	2.02	2.02	2.4	2.5	2.89	1.72
TiO_2	1.002	0.971	0.913	1.118	0.359	0.37	0.353	0.339	0.356
P_2O_5	0.04	0.17	0.22	< 0.01	0.07	0.09	0.07	0.07	0.07
LOI	6.14	5.5	3.55	5.82	3.01	3.02	3.17	2.67	2.4
Total	100.33	98.92	100.30	99.53	100.15	100.60	99.72	100.19	99.90
CO_2	0.35	< 0.01	< 0.01	< 0.01	< 0.01	0.1	< 0.01	0.26	0.02
Total S	3.39	2.99	0.67	3.16	1.29	0.05	0.89	0.25	0.55
Ag	< 1	< 1	< 1	1	< 1	< 1	< 1	< 1	< 1
As	0.9	1.6	4.1	2.6	0.5	< 0.5	0.8	< 0.5	< 0.5
Au (ppb)	50	35	21	37	22	< 5	12	9	16
B	16	16	19	10	13	16	16	21	19
Ba	791	687	894	271	698	767	506	449	319
Be	1	1	< 1	1	< 1	< 1	< 1	< 1	< 1
Bi	0.3	0.2	< 0.1	0.1	0.2	< 0.1	< 0.1	< 0.1	< 0.1
Cd	< 0.2	4.9	< 0.2	36.8	< 0.2	< 0.2	17.9	0.7	8.8
Co	17.4	18.5	15.1	28.4	18.4	8.9	16.2	15.8	20.6
Cr	2	< 1	1	2	1	1	2	1	< 1
Cs	0.9	1	1.4	1.2	0.7	0.8	0.9	1.1	0.6
Cu	170	269	16.2	57.1	115	11.6	42	27.7	71.9
Ga	22	23	29	23	18	20	17	18	18
Ge	1.2	1.4	1.2	1.8	1	1.3	1	1	1.3
Hf	1.8	1.8	2.1	1.6	4.1	3.9	4.1	4.4	4.4
Hg	< 5	12	< 5	104	< 5	< 5	27	< 5	20
Li	23	22	11	48	11	20	13	10	13
Mn	1810	2600	1140	6640	805	874	1990	2320	1890

Table 2-1: cont'd

Sample	HWZ01	HWZ03	HWZ05	HWZ09	HWZ02	HWZ04	HWZ07	HWZ08	HWZ10
Ni	< 1	1	< 1	2	< 1	< 1	< 1	< 1	< 1
Pb	4	4	3	16	5	< 2	3	14	3
Rb	49	58	92	40	41	46	52	60	37
Sb	< 0.2	< 0.2	< 0.2	< 0.2	< 0.2	0.6	< 0.2	< 0.2	< 0.2
Sc	21	23	20	24	11	12	11	11	10
Sn	2	3	8	9	3	6	6	1	3
Sr	19	11	13	9	26	9	7	13	23
Ta	0.43	0.4	0.64	0.36	0.93	0.8	0.9	0.99	1.02
Th	0.73	0.7	0.86	0.63	1.99	1.92	1.95	2.13	2.08
Tl	0.2	0.24	0.42	0.23	0.16	0.21	0.24	0.31	0.16
U	0.23	0.23	0.26	0.18	0.55	0.55	0.55	0.58	0.58
V	104	138	65	191	11	11	10	9	8
W	31.6	45.9	104	32.5	112	62.7	103	114	129
Y	21.6	19.1	13.7	19.6	29.8	22.1	26.6	29.3	24.6
Zn	176	986	129	> 10000	65.9	45.6	5430	313	2610
Zr	70	65	81	57	164	160	156	167	172
La	8.26	8.19	4.43	5.74	12.2	4.87	6.91	14.4	10.4
Ce	16.7	17.4	11.3	13	26.7	9.67	16	30.4	22.9
Pr	2.03	2.13	1.49	1.72	3.28	1.35	2.04	3.93	2.87
Nd	8.73	9.02	6.82	7.52	13.9	5.83	9.08	16.5	12
Sm	2.33	2.43	1.76	2.08	3.27	1.54	2.33	4.1	3.01
Eu	0.99	0.83	0.57	0.74	0.90	0.31	0.58	1.9	1.6
Gd	3.08	2.69	1.83	2.41	3.4	1.77	2.61	4.35	3.18
Tb	0.62	0.54	0.33	0.48	0.7	0.42	0.6	0.81	0.6
Dy	3.89	3.4	2.06	3.21	4.61	3.07	4.12	4.96	3.84
Ho	0.74	0.65	0.45	0.68	0.97	0.72	0.9	1	0.83
Er	2.21	1.91	1.49	2.04	3.05	2.61	2.92	3.09	2.61
Tm	0.34	0.29	0.25	0.30	0.49	0.44	0.48	0.49	0.42
Yb	2.23	1.91	1.8	1.99	3.32	3.12	3.26	3.42	2.93
Lu	0.33	0.29	0.30	0.31	0.54	0.50	0.51	0.53	0.47

2.6. Characteristics of Mafic Xenoliths

The rhyolite cryptodome contains abundant mafic xenoliths. They are distinguished in outcrop by their granular texture and dark gray to grayish green color. The surfaces of the xenoliths are typically slightly receded in the glacially polished outcrops as the mafic material weathers more easily than the siliceous host rhyolite. The mafic xenoliths contain up to 8% pyrite, giving the xenoliths a slightly stained appearance on surface.

Based on systematic outcrop inspection using the established surface grid as a guide, 504 mafic xenoliths were identified within the six outcrops. The lengths of the long and short axes were recorded for each xenolith along with its trend. In addition, the number of xenoliths within each square meter as well as the area percent of the mafic material in each field of the grid was determined.

2.6.1. Spatial Distribution

The number of xenoliths decreases from the bottom contact of the rhyolite cryptodome towards its stratigraphic top. This can be seen in a contour map showing the relative number of xenoliths in each square meter (Fig. 2-8A).The highest number of xenoliths occurs in central part of outcrop A. The number of xenoliths decreases towards the north. Most outcrop areas contain less than 5 xenoliths per square meter.

Fig. 2-8B shows the contoured percent surface area of xenoliths in the mapped outcrops. Outcrop A shows several small zones of high percent surface area with a large irregular zone of high surface area taken up by xenoliths in the southern-central part of the outcrop. There are also several zones of high percent surface area taken up by xenoliths in Outcrop C. This is particularly the case for the NE corner of the outcrop. This area is characterized by large blocky xenoliths covering a larger portion of the surface area.

2.6.2. Size and Shape

Fig. 2-8C shows a contour map of the average long axis of the xenoliths contained within each square meter of the surface grid. Across the six outcrops, the average long axis of the

xenoliths ranges from 0 to 154 cm. The contour map demonstrates that the xenoliths are on average largest in the northern section of outcrop C. In this outcrop, the average long axis of the xenoliths contained in each square meter ranges from 20 to 60 cm. Outcrop A has two small areas in which the average long axes measurements are high. In the southernmost part of the outcrop, there is a high abundance of xenoliths with an average long axis between 40 and 80 cm.

The average aspect ratio of the xenoliths was calculated by dividing the average long axis of all xenoliths recorded in each square meter of the surface grid by the corresponding average short axis. The value calculated this way was assigned to each square of the surface grid to construct a contour map showing variations in the average aspect ratio across the coherent rhyolite outcrops (Fig. 2-8D). The results show a swath of the southernmost part of outcrop A and B that is characterized by a high aspect ratio irrespective of the overall size of the xenoliths. Three localized areas within outcrop C show a moderately high aspect ratio. The northernmost outcrops, including outcrops C, D, E, F, and G, have low average aspect ratios when compared to the other exposed parts of the rhyolite cryptodome.

The shape of the xenoliths is highly variable across the outcrops. Elongate xenoliths vary in shape from tabular to asymmetric and lens-shaped (Fig. 2-9A and B). These elongate xenoliths are frequently surrounded by smaller peanut-shaped xenoliths. The large xenoliths also sometimes possess small tails or pinched terminations, typically located on one particular side of the xenolith, notably to the east and northeast (Fig. 2-9B, C and D). Xenoliths with these attributes were most prominent within the southern outcrops. In addition, the northern outcrops contain xenoliths with highly irregular and nondescript morphologies (Fig. 2-9E). The northern portion of outcrop A contains several adjacent tabular and jagged xenoliths with long axes oriented roughly N-S in which their morphologies appear to represent one larger tabular xenolith broken into puzzle-like pieces in an E-W trend (Fig. 2-9F).

The xenoliths become increasingly blocky or irregular and less tabular from the stratigraphic bottom of the cryptodome towards its top (Fig. 2-10A). Irregularly-shaped xenoliths tend to have little to no elongation and form shapes with near-equant long and short axes.

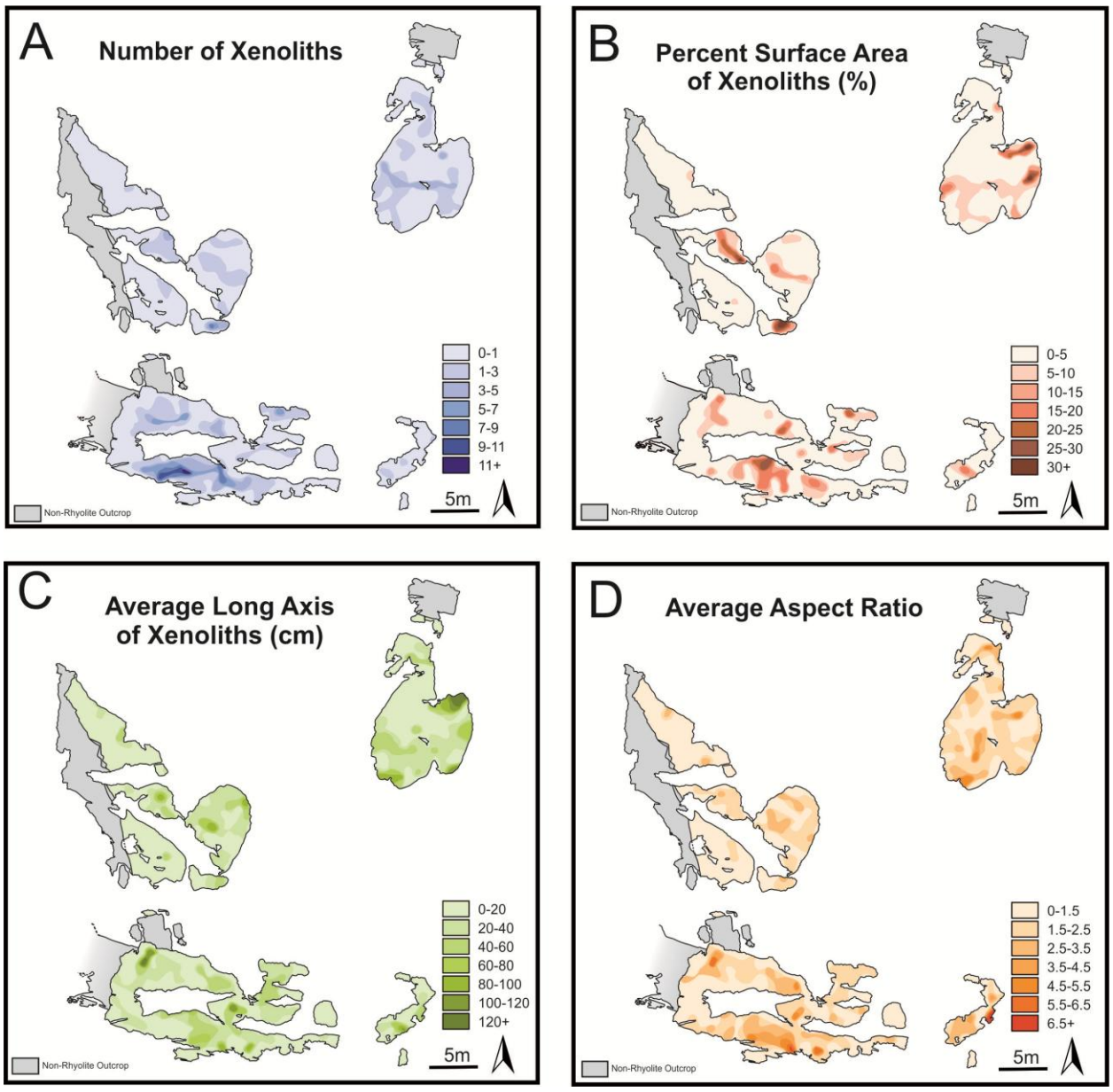

Fig. 2-8: Contour maps of the coherent rhyolite outcrops with calculated and assigned xenolith data. A. The number of xenoliths within each square meter ranging from 0-11.5. B. The percent surface area of outcrop taken up by xenoliths in two dimensions ranging from 0-55.5%. C. The average long axis of xenoliths ranging from 1-154 cm in length. D. The average aspect ratio of xenoliths ranges from 1-7.

Fig. 2-9: Photographs of principal trends in xenolith morphology, contact relationships, and textures. A. Tabular xenolith with a prominent scalloped contact (arrows) and smaller surrounding xenoliths showing interactions with asymmetric flow banding. Change in rhyolite color is visible at the contact. B. Lens-shaped xenolith with elongation of the long axis in an SW-NE trend. The xenolith has a thin tail to the NE and interaction with flow banding to the SW. C. A peanut-shaped xenolith identified by a pinched middle segment, which suggests elongation along the long axis. Xenolith is surrounded by continuous flow banding. D. A large tabular xenolith with a tail structure to the NE. E. Irregular and rounded shape of a xenolith in northern outcrop C. F. Three tabular xenoliths oriented approximately N-S that are closely adjacent and appear to fit together like puzzle pieces from E to W. Coin is 2.8 cm in diameter and the lens cap is 6 cm in diameter.

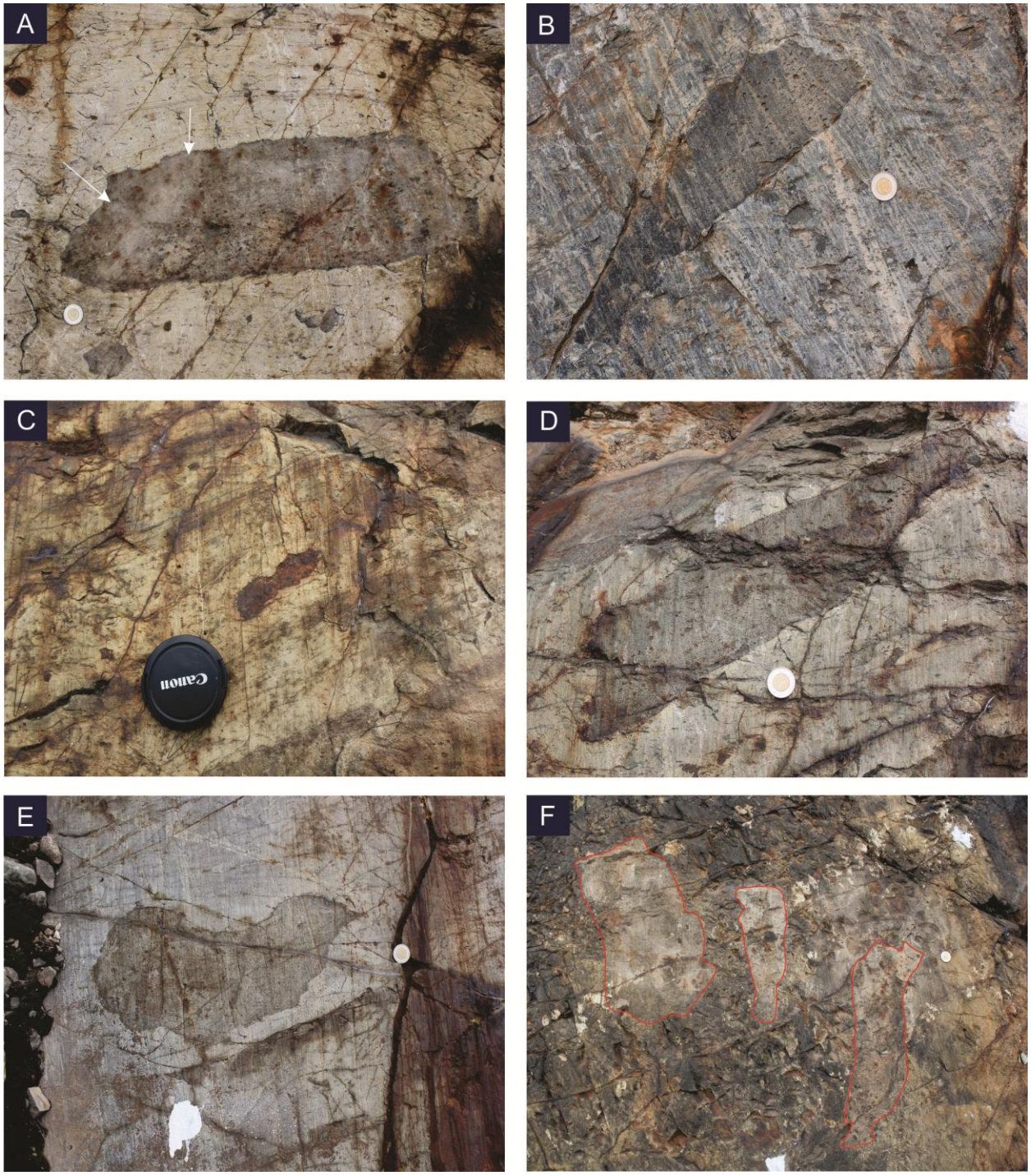
A
B
C
Canon
D
E
F

Fig. 2-10: Photos and photomicrographs showing key features found within the xenoliths at Horne West. A. A blocky xenolith within outcrop F that shows near-equant long and short axis dimensions. B. Photomicrograph of xenolith in thin section showing an angular phenocryst interpreted to be feldspar replaced by micas in PPL. C. The same section as B in XPL showing slight alignment of micas within the feldspar framework and the fine-grained subangular quartz-feldspar mosaic that composes the xenolith matrix. D. Irregular xenolith with subtle discoloration in rhyolite color at the contact. Polygonal columnar jointing is present along the northern contact of the xenolith. Fractures do not penetrate the xenolith. E. A contact between a xenolith (above) and rhyolite (below) in PPL that shows a small light rim at the contact where quartz forms larger and more coherent grains within the xenolith. F. The same image as E in XPL highlighting the contact and the grain size disparity between the two units. Coin is 2.8 cm in diameter and the camera lens is 6 cm in diameter.

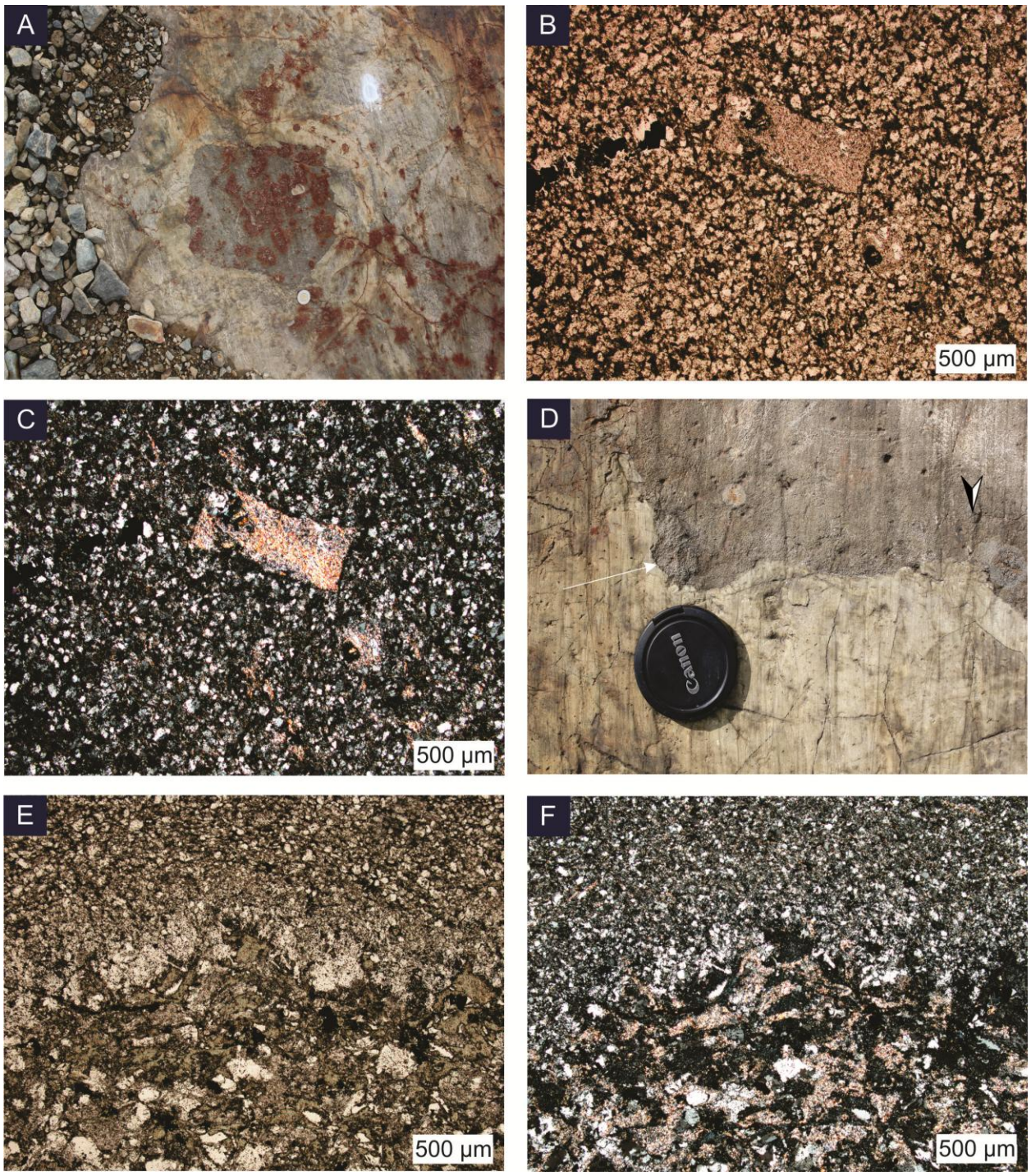
A
B
500 µm
C
500 µm
D
E
500 µm
F
500 µm

2.6.3. Trend

The trend of the long axis of each xenolith was measured to provide a quantitative assessment of the alignment between the trend of the flow-banding within the host rhyolite and the xenolith trends. The trends of xenoliths within the flow domain described above were compiled and plotted in individual rose diagrams in order to discern a predominant xenolith alignment in 2-D space (Fig. 2-11). Analysis of the rose diagrams yielded an average trend of the xenoliths in each flow domain and was used to derive a range of typical trends (Table 2-2). Using the trend of the flow banding determined from the maps, the mean difference in trend between the flow-banding and the trend of the xenoliths was determined.

Fig. 2-11: Equal-area rose diagrams projecting trend data of observed xenoliths within each flow-banding domain. Accompanying projection data can be found in Table 2-2 showing mean trend directions within each domain trending roughly E to WNW.

This analysis showed that the xenoliths are well aligned with the flow-banding in the flow domains A_1, C_1, and C (Fig. 2-4). In these domains, the difference in the average trends is less than 15 degrees. In contrast, there is a larger deviation between the trends of flow-banding

and the xenoliths in domains A_2, B, E, and G. The difference in trend exceeds 30 degrees in the flow domains E and G.

Table 2-2: Comparison between the trend of the flow-banding of the coherent rhyolite and the mafic xenoliths

Flow domain	Trend of Flow-banding	Range of typical xenolith trends	Mean trend of xenoliths	Mean Difference (in degrees)
A_1	298.0	281-290	287.4	10.6
A_2	326.0	301-310	300.3	25.7
B	301.6	281-290	280.0	21.6
C_1	290.7	281-290	296.9	6.2
C_2	265.0	271-280	278.9	13.9
E&G	341.9	321-330	305.3	36.6

2.6.4. Petrographic Characteristics

The mafic xenoliths investigated in thin section are aphanitic and some xenoliths are sparsely porphyritic. The groundmass is very fine-grained and consists of an equigranular, subangular, and subhedral mosaic of quartz and feldspar grains, with some small disseminated pyrite grains (Fig. 2-10B and C). Small white mica grains occur dispersed throughout the quartz and feldspar groundmass. The white mica locally forms small clusters around the pyrite grains, and commonly replaces feldspar. Rare euhedral feldspar phenocrysts observed in thin section of some xenoliths are entirely replaced by white mica.

The microscopic analysis shows that the xenoliths do not represent mafic volcaniclastic material entrained in the rhyolite cryptodome. The xenoliths consist of a fine-grained groundmass of interlocking subangular grains, not a matrix of rounded lithic fragments or a combination of lithic fragments and phenocrysts as would be expected for a volcaniclastic rock.

2.6.5. Contact Relationships

Contacts between the rhyolite and the xenoliths vary with the size and shape of the xenoliths but are generally sharp and well-defined. Scalloped and irregular margins are prominent throughout the outcrop seen on approximately 38% of the xenoliths (Fig. 2-9A).

Scallops commonly occur on the southern margins of tabular xenoliths and range from cm to mm scale depending on the size of the xenolith. Smaller xenoliths have smaller scallops on their margins. In addition, smaller xenoliths without scallops tend to display rounded margins and larger xenoliths show a greater tendency towards subangular and jagged margins. Several xenoliths are characterized by near-planar margins that tend to occur on the northernmost sides of the xenoliths. Within the rhyolite, the immediate rim around the xenolith is slightly lighter in color in comparison to the rhyolite further away from the contact (Fig. 2-9A and Fig. 2-10D). The discolored rim is not more than one centimeter in width.

In thin section, the contacts between the xenolith and enclosing rhyolite vary slightly from sample to sample (Fig. 2-10E and F). The contrast between the rhyolite and the mafic xenoliths is typically marked by a thin zone of aligned mica crystals (Fig. 2-12A and B). The contact is marked by a change in grain size as well as a slightly lighter rim within the xenolith at the contact presumably due to quenching at the time of emplacement. In one case, a small rhyolite inclusion occurs within the xenolith matrix, approximately 3 mm away from the contact to the surrounding rhyolite. The rhyolite inclusion has a larger grain size than the xenolith matrix. The inclusion is only 2 mm in diameter, but has irregular margins that project into the xenolith (Fig. 2-12C and D).

2.6.6. Geochemical Characteristics

Four mafic xenoliths were sampled for geochemical analysis. Three of the samples have SiO_2 contents ranging from about 50 to 56 wt.% (Table 2-1). One of the samples has an anomalously high SiO_2 content coupled with low MgO and Fe_2O_3 contents and a high K_2O value, suggesting that the major element chemistry has been modified because of hydrothermal alteration. Based on the SiO_2 content and the relatively low total alkali concentrations, the mafic xenoliths are classified as basalt to basaltic andesite.

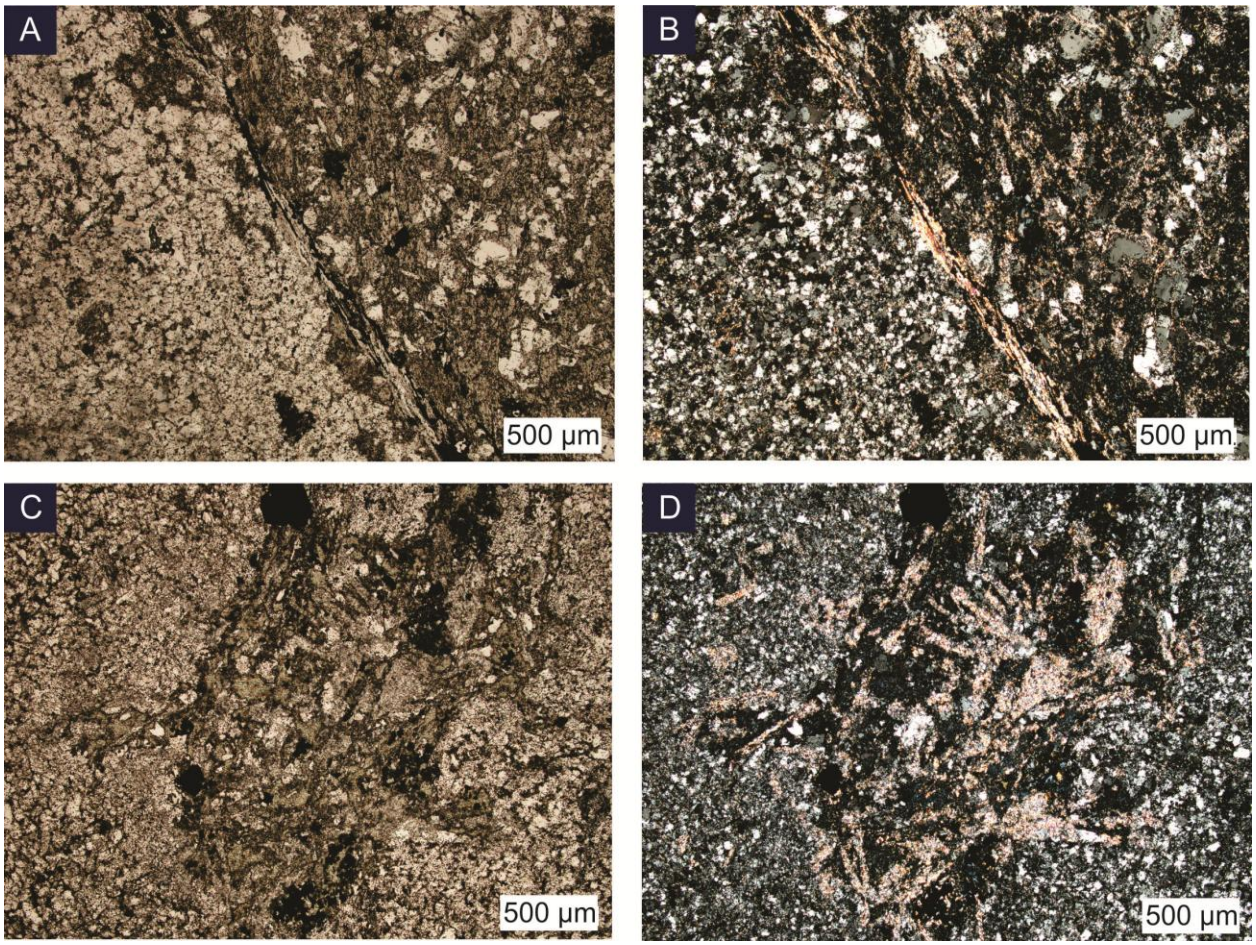

Fig. 2-12: Photomicrographs of xenolith-rhyolite contact relationships. A. The contact relationship in PPL between the xenolith (left) and the rhyolite (right) showing a clear grain size change across the contact and aligned micas that form a boundary between the two units. B. The same contact seen in A in XPL that also demonstrates the alignment of micas within the rhyolite subparallel with the xenolith-rhyolite contact. C. Inclusion of rhyolitic material within the xenolith matrix in PPL. The inclusion has irregular and projecting margins into the xenolith. D. The same rhyolite inclusion seen in C in XPL that shows the clear grains size difference in materials and the clear contact between the two units.

A basic to intermediate composition for the xenoliths is confirmed by their immobile element ratios (cf. Floyd and Winchester, 1978). In Zr/TiO_2 versus Nb/Y and P/Zr versus Ti/Zr discrimination diagrams suggested by Winchester and Floyd (1977) and Stolz (1995), the samples cluster close to the border between basalt and andesite (Fig. 2-6 and 2-7). Inspection of immobile element ratios such as Zr/Y, La/Yb, and Th/Yb further suggests that the mafic xenoliths have a tholeiitic to transitional affinity, which is consistent with previous geochemical investigations on volcanic rocks from the host stratigraphy of the Horne deposit (MacLean and Hoy, 1991; Barrett and MacLean, 1994; Barrett and MacLean, 1999).

2.7. Discussion

2.7.1. Xenolith Morphologies

Detailed field studies and petrographic analysis of the abundant xenoliths within the Horne West volcanic succession have enabled the identification of outcrop scale trends, which confirm the occurrence of magma mingling and associated synchronous emplacement of mafic and felsic magmas.

One of the most prominent outcrop scale trends is a shift of the xenolith morphology from largely tabular in the south to irregular or blocky in the north. The variation in clast shape and distribution suggests several volcanic controls including the degree of cooling that the mafic magma experienced upon incorporation into the dome, the amount of crystallization within the felsic magma, and the viscosities of both lavas upon emplacement. In general, when mafic magma is intruded into felsic magma, the magmas first come to thermal equilibrium. The resulting viscosities and crystal composition after reaching thermal equilibrium become the controlling factors on xenolith crystallization and mobility (Sparks and Marshall, 1985; Vernon, 1990). At Horne West, this controlling factor would indicate significant cooling of the mafic magma upon emplacement, which would at least quench the immediate rim in contact with the rhyolite. The mafic magma shows clear quench textures (Vernon, 1984; Vernon et al., 1988; Kuşcu and Floyd, 2001) along the xenolith-rhyolite contacts including scalloped or cuspate margins and microscopic variations in the xenolith crystallization rim where it is in contact with the rhyolite. This suggests that the xenoliths became at least partially quenched upon entrainment into the rhyolite lava. Therefore, it can be assumed that the mafic xenoliths were relatively cooled if not almost completely rigid shortly after being incorporated into the rhyolite dome.

In addition to partial quenching upon emplacement, it can also be inferred that as the xenoliths were transported further away from the mafic source zone into the rhyolite, crystallization was continuous and the xenoliths became progressively more rigid (Sparks and Marshall, 1985). The tabular xenoliths that occur in the south show a close association with the flow banding and have long axes oriented in the interpreted direction of flow. This suggests that the trend of the tabular xenoliths, at least in this area, can partially be attributed to an influence of the rhyolite flow on the alignment of the xenoliths. The elongate xenoliths with small tails to the

east were likely in part due to the rhyolite flow having the viscous force to deform small parts of the xenoliths with remaining plasticity. Because this consistent feature is not present in other outcrop areas, the xenoliths can be placed into domains, 1) a uniform flow influenced domain and 2) an irregular flow influenced domain. The main distinction between the two domains is that the former includes tabular xenoliths that were systematically aligned by the rhyolite flow with minor flow deformation features and the latter contains irregular and blocky xenoliths that were influenced by flow but produced varying morphologies in varying flow conditions. The irregular flow influenced domain contains blocky xenoliths that appear to be emplaced rigidly as well as irregular xenoliths that underwent flow-influenced deformation.

The dynamics of how the larger blocky xenoliths were transported to the northern extent of the dome are debatable. Because they are blocky and do not align themselves with the flow overall, these xenoliths are classified as belonging to the irregular flow influenced domain. Possible explanations for the occurrence of blocky xenoliths include: 1) Rigid xenoliths were formed at a different period during mafic magma emplacement compared to the tabular xenoliths, and larger batches of mafic magma were emplaced as cooler and more rigid objects, or 2) The rigid blocks were the result of cooled xenoliths that became brittle and were broken apart by the flow away from the source. The former hypothesis is favored where large xenoliths may have formed during a large initial injection of mafic magma that experienced rapid quenching and transport in a rhyolite that was slightly less viscous. Their large size likely prevented plastic deformation.

The dynamics of how the irregular xenoliths were emplaced towards the northern extent of the dome are also complex. The xenoliths coincide spatially with the blocky xenoliths but demonstrate rounded, curved, or highly irregular shapes such as a crescent or peanut. Possible explanations for the occurrence of irregular xenoliths include: 1) During an earlier pulse of mafic magma into a less viscous rhyolite flow the mafic magma was partially quenched but retained enough plasticity to be noticeably deformed by the flow, or 2) Rounded xenoliths were once rigid blocks but were emplaced within a turbulent rhyolite flow which allowed for abrasion by the rhyolite or by adjacent blocky xenoliths.

It should also be mentioned that the morphological characteristics seen cannot be explained by post-depositional deformation. At the microscopic scale, there are little to no deformation features seen with the exception of minor undulose extinction within quartz, which

can occur at very low strain (Passchier and Trouw, 1996). Angular clasts and an elongation signature that is not consistent across the outcrop for any significant distance at the Horne West outcrops also indicate a lack of strain in the two dimensions observed.

Previous interpretations of the Horne West area have suggested that the xenoliths represent wall rock fragments deposited in a laminated felsic volcaniclastic material, or a megabreccia formed near the margins of a large caldera (Daigneault and Pearson, 2006). However, the occurrence of columnar joints, monomict breccia, , classical perlite,, and variable flow-banding orientations suggest that the host of the xenoliths is a flow-banded rhyolite, not a laminated volcaniclastic rock.

2.7.2. Model of Emplacement

Based on field observations, a model of emplacement for the rhyolite cryptodome has been developed that explains the occurrence and distribution of mafic xenoliths within this unit (Fig. 2-13). The rhyolite cryptodome at Horne West represents a shallow subseafloor intrusion emplaced into a succession of stratified volcaniclastic deposits (Monecke et al., 2008). The cryptodome is thought to have breached the seafloor at least locally to allow incorporation of coarse clasts into mass-flow-derived volcaniclastic breccia stratigraphically overlying the immediate hosts to the rhyolite cryptodome. Alternatively, the presence of these clasts could be explained by the rhyolite being exposed at the seafloor through synvolcanic faulting.

Monecke et al. (2008) and Monecke and Gibson (2013) demonstrated that the Horne West succession formed within a local subsidence zone, possibly a small volcanic graben. A synvolcanic fault marking the contact between two compositionally distinct stratified volcaniclastic units and the intrusion of multiple mafic and felsic dikes in the west of the Horne West outcrop area may have represented one of the bounding faults of this small synvolcanic graben. Synvolcanic faulting is likely to have controlled emplacement of the rhyolite cryptodome described in the present study, and probably focused hydrothermal fluid flow, resulting in the formation of two zones of disseminated sulfides in the Horne West area (Monecke et al., 2008).

Because the rhyolite lava was most likely highly viscous during emplacement, the high abundance of large xenoliths in the southern outcrops may suggest proximity to their source, which is not exposed at surface. Due to their size and higher density, it is unlikely that the large

xenoliths were transported by the rhyolite lava over long distances. The xenoliths must have settled and accumulated at the base of the rhyolite cryptodome during effusive emplacement of the rhyolite lava, lateral flow of the lava, and inflation of the cryptodome. Proximity to the source is also supported by the decrease in xenoliths abundance across the outcrop to the west and up stratigraphy.

The tabular nature of the large xenoliths accumulated close to their source suggests that, in addition to alignment within the rhyolite flow, they were also likely derived from a near-tabular source. Entrainment of the xenoliths into the rhyolite and transport resulted in progressive modification of their shapes. Most notably, one outcrop area suggests that the large tabular xenoliths were dismembered during flow, resulting in the formation of smaller, blockier mafic xenoliths. Irregularly shaped xenoliths suggest early conditions that allowed for plastic bending or deformation of mafic xenoliths. Smaller and more irregularly shaped xenoliths were laterally transported further away from the source and moved higher up within the rhyolite cryptodome during inflation, explaining the observed distribution of xenoliths. During transport, the elongate xenoliths were rotated into the flow direction, explaining the general alignment of xenoliths parallel to the flow-banding. Deviations from this alignment occurred primarily where flow of the rhyolite was more turbulent, especially towards the margins of the intrusions.

The most likely source of the mafic xenoliths is a synvolcanic basaltic dike as these are characterized by similar tabular morphologies (Frost and Mahood, 1987; Foster and Hyndman, 1990; Paterson et al., 2004). This dike must have been emplaced close to the feeder of the rhyolite cryptodome or, more likely, both lavas were emplaced along the same synvolcanic fault, causing mingling to occur already along the feeder dike of the rhyolite cryptodome. Upon the intrusion of the mafic dike into or near the feeder zone of the cryptodome, the mafic material likely underwent considerable undercooling and quenching due to the significant temperature difference between rhyolite and basalt (Frost and Mahood, 1987; Sparks and Marshall, 1987; Vernon et al., 1988; Johnson and Barnes, 2006). Quenching at the rim of the basalt likely formed rigid margins that allowed the dike to break apart into smaller blocks. The plastic nature of the xenolith was presumably controlled by the size of the blocks as a larger xenolith could preserve a plastic core that was surrounded by a more rigid outer rim (Vernon, 1990).

Flow-banding within the rhyolite indicates that the lava was viscous enough to produce millimeter to centimeter wide bands that were compositionally different. The development of the

flow foliation was probably already initiated in the conduit and continued during outflow of the rhyolite lava into the cryptodome (McPhie et al., 1993). Rhyolite flow within the dome was probably sustained through continuous injection of felsic magma into the dome, which forces the lava to move outward into the volcaniclastic host and causes inflation of the dome (Ventura et al., 2006). The separation of flow bands indicates that the rhyolite was flowing from east to west. Separation of flow bands around the more tabular and elongate xenoliths with parallel flow bands adjacent to the long sides of the xenoliths indicate that the flow moved around the xenoliths. Although the xenoliths were clearly transported by the rhyolite flow, shearing along the margins of the xenoliths implies that the large xenoliths were more slowly transported than the surrounding rhyolite melt. As the xenoliths could at least initially be plastically deformed, the shapes of the xenoliths were at least in part modified by the rhyolite melt flowing around these particles. At the same time, the discoloration of the rhyolite may suggest that assimilation of the mafic material occurred during flow and continued cooling.

The final stage of xenolith emplacement includes progressive crystallization of the mafic material, causing the xenoliths to become progressively brittle and rigid. Because the rhyolite is much larger by volume and likely takes much longer to crystallize, the fully crystallized mafic xenoliths may have also undergone minor brittle deformation as the rhyolite continued to flow. This process may have produced the jigsaw-fit xenoliths that occur in the southernmost outcrop, as well as the xenoliths with more subangular and irregular morphologies.

2.7.3. Comparison to Magma Mingling in Other Environments

Previous work on magma mingling has largely focused on granitic plutons and dikes (Vernon, 1984; Frost and Mahood; 1987; Foster and Hyndman, 1990; Snyder et al., 1997; Baxter and Feely, 2002; Johnson and Barnes, 2006; Sklyarov and Fedorovskii, 2006). The textural characteristics described in these studies resemble those present in the rhyolite cryptodome at Horne West and provide support to the argument that magma mingling has occurred during the cryptodome formation. However, magma mingling in shallow intrusions such as cryptodomes has not been described in previous literature. For this reason, the present field-based study provides new information on the occurrence of magma mingling during effusive lava emplacement.

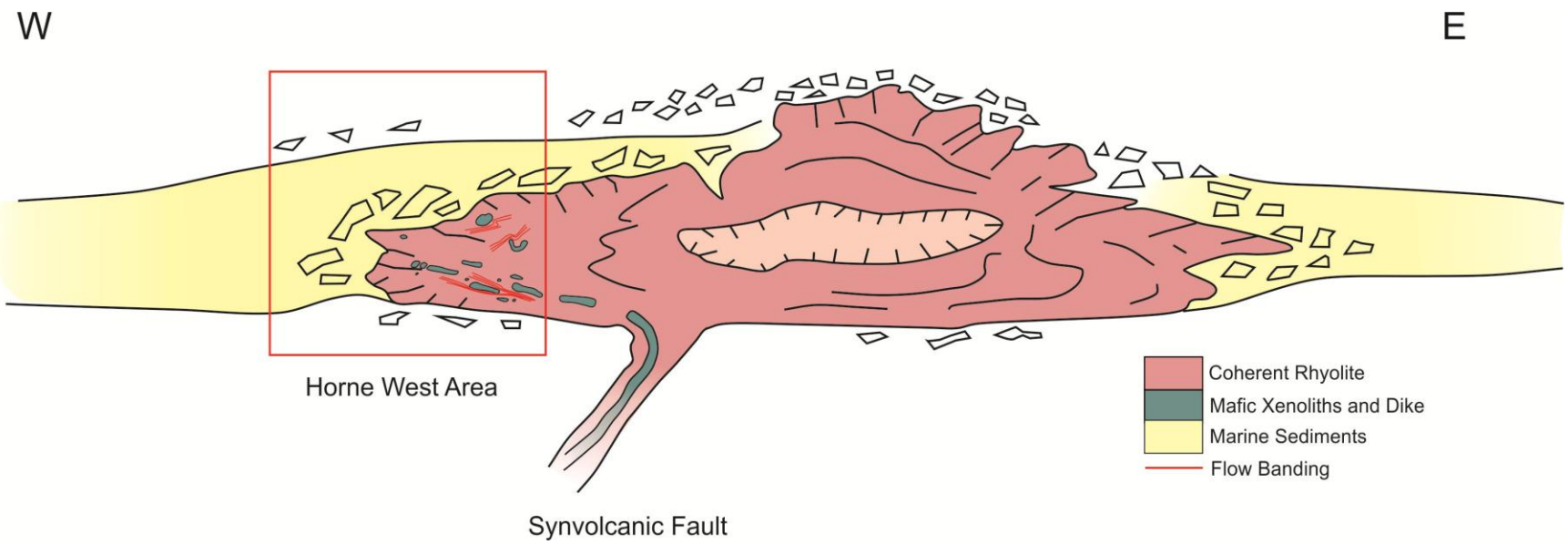

Fig. 2-13: Schematic cross section of the Horne West rhyolite cryptodome. The dome is hosted by volcaniclastic rocks that are exposed in outcrop in the north and west. Tabular xenoliths are present in the southern outcrops and make up a uniform flow-influenced domain within the rhyolite dome. The irregular flow-influenced domain comprises xenoliths that have an irregular or blocky morphology.

The xenoliths described at Horne West are similar in some aspects to enclaves described in granitoid plutons (Frost and Mahood, 1987; Vernon et al., 1988; Paterson et al., 2004). Enclaves present in host granites commonly have cuspate margins and lenticular to ellipsoid morphologies. They are typically characterized by a fine-grained texture (Vernon, 1984; Vernon et al 1988; Paterson et al., 2004; Sklyarov and Fedorovskii, 2006). In most cases, the granitic host and contained enclaves are compositionally related as the source of the enclaves has already undergone magma mixing at depth (Vernon, 1984; Vernon et al 1988). At Horne, the compositional contrast between the rhyolite host and the contained xenoliths is comparably pronounced. This may be the case because volcanism took place in a geodynamic setting where mantle-derived mafic melts could rapidly ascend into the subvolcanic environment, without undergoing much mixing, assimilation, or differentiation.

Another difference between magma mingling at Horne West and granitic plutons is related to the complexity of processes involved in magma mingling and the cooling history of the melts. In granitic plutons, the textural characteristics of enclaves can be more diverse, including not only variable compositions, but also differences in grain sizes and phenocryst populations (Vernon et al., 1988; Snyder et al., 1997; Johnson and Barnes, 2006). This is likely related to the continued influx of evolving magmas into a host magma chamber. In the case of the cryptodome at Horne West, only one magma batch appears to have supplied the lava for the intrusion of the dome. At the same time, enclaves in granitic rocks can range in shape from ductile finger-like morphologies to rounded pillows (Vernon et al., 1988; Snyder et al., 1997; Johnson and Barnes, 2006). This is probably related to the slower cooling rates of granitic plutons and the larger size of the intrusions.

2.7.4. Implications to the Geodynamic Setting

The volcanic-hosted massive sulfide deposits of the Noranda district, including the Au-rich Horne deposit, are typically associated with volcanic rocks formed in vent proximal volcanic settings such as coherent volcanic rocks and associated juvenile breccia facies. Although the host rock successions are distinctly bimodal, the majority of deposits are spatially closely related to felsic volcanic rocks such as rhyolite domes and flows (Spence and de Rosen Spence, 1975; Kerr and Gibson, 1993; Gibson and Galley, 2007). While the link between the felsic volcanic rocks

and massive sulfide deposits is mostly obvious, closely associated mafic volcanic rocks in the same areas have been more difficult to correlate to the massive sulfide deposits. At Horne, a mafic dike complex crosscuts the felsic volcanic succession, feeding into a conformably overlying mafic volcanic succession. The timing of mafic volcanism with respect to the felsic volcanic activity is poorly constrained due to the lack of indicative relationships and generally poor exposure of the volcanic units.

The present study of magma mingling at Horne West indicates that the generation of felsic and mafic melts was essentially synchronous. This suggests that deposition of the felsic-dominated succession hosting the deposits was followed only shortly after by mafic volcanism. Although the contact between both volcanic packages is not exposed, it does not appear likely that this apparently conformable contact represents a disconformity recording a period of non-deposition due to a hiatus in volcanism. The shift in composition in volcanism must have been rapid, indicating that the volcanism derived from crustal melts was succeeded quickly by the upwelling of more primitive, presumably mantle-derived melts into the subvolcanic environment.

The synchronous bimodal volcanism and the rapid shift from felsic- to mafic-dominated volcanism constrain the geodynamic environment in which the Horne deposit must have formed. As bimodal volcanism is a hallmark of modern extensional suprasubduction settings (Hannington et al., 2005), it is quite likely that the giant Horne deposit formed in a geodynamic setting broadly comparable to rifts developing in modern volcanic arcs. Such bimodal volcanism currently occurs within the eastern Manus basin, where a back-arc rift developing in preexisting arc crust is characterized by the occurrence of numerous hydrothermal vent areas, many of which produce seafloor sulfides having elevated gold grades (Moss et al,. 2001). Seafloor dredging and drilling have shown that magma mingling also occurs at this location (Kamenetsky et al., 2001; Binns, 2004).

2.8. Conclusions

Detailed mapping demonstrates that the abundant presence of mafic xenoliths within a rhyolite cryptodome located in the host rock succession of the giant Horne volcanic-hosted massive sulfide deposit was caused by the mingling of felsic and mafic melts, presumably

through synchronous emplacement along a synvolcanic fault. Incorporation of mafic xenoliths into the feeder of the rhyolite cryptodome resulted in the transport of the mafic inclusions into the effusive portion of the cryptodome. During continued lateral flow and inflation of the cryptodome, the mafic xenoliths entrained in the rhyolite were continuously dismembered. The largest tabular xenoliths accumulated at the bottom of the rhyolite cryptodome whereas irregular and blockier xenoliths were distributed throughout the dome.

The identification of textures indicative of magma mingling suggests that felsic and mafic volcanism at Horne were at least in part synchronous. The emplacement of the felsic volcanic succession hosting the orebodies and the formation of the conformably overlying package of mafic volcanic rocks were likely not separated by a significant hiatus in volcanism. Massive sulfide formation at Horne is interpreted to have coincided with a rapid shift from felsic- to mafic-dominated volcanism. The available evidence suggests that the deposit formed in a strongly extensional setting, promoting bimodal volcanism related to the upwelling of mantle-derived mafic melts into the upper crust. The geodynamic setting in which the Neoarchean Horne deposit formed was probably analogous to rifts developing in modern volcanic arcs.

CHAPTER 3
EVIDENCE FOR MAGMA MINGLING AND MIXING DURING DIKE PROPAGATION, QUEMONT HILL, ROUYN-NORANDA, QUEBEC

Manuscript to be submitted to Journal of Volcanology and Geothermal Research

Keywords: Archean, Abitibi subprovince, Blake River assemblage, Quemont deposit, volcanic-hosted massive sulfide deposits, magma mingling, magma mixing, volcanic facies mapping

3.1. Abstract

The Quemont deposit in the Abitibi greenstone belt of northern Canada represents one of the largest Au-rich volcanic-hosted massive sulfide deposits of the world. Mined between 1949 and 1971, with a short period of production in 2001, the deposit produced 13.9 Mt of ore grading 1.31% Cu and 5.38g/t Au.

The ore zones of the Quemont deposit are hosted by a 2,702 Ma felsic-dominated volcanic succession. The massive sulfides occur within a thick interval of rhyolite breccia at or near the contact with an overlying quartz-phyric coherent rhyolite. A major dike-in-dike complex located to the northwest of the deposit is interpreted to have formed through synchronous emplacement of mafic and felsic lavas along a major synvolcanic structure. Complex contact relationships indicative of magma mingling and mixing were observed along the contact between a basaltic dike and a quartz- and feldspar-phyric rhyolite intrusion.

Mingling and mixing textures observed along the contact between the dikes include the occurrence of elongate mafic xenoliths that are suspended within felsic material along the rhyolite contact, a mixed and mingled zone that is characterized by an intermediate to felsic matrix and mafic inclusions, a zone of mingling that is composed of wispy mafic xenoliths and abundant centimeter-sized mafic enclaves within a rhyolite matrix, and areas that appear macroscopically homogeneous and have intermediate compositions. These occurrences suggest effective mixing and mingling between the end-member magmas.

The results of the volcanic facies analysis indicate that the host rock succession of the Quemont massive sulfide deposit formed in a volcanic setting characterized by significant crustal

extension. Extension in an environment similar to modern arc rifts could explain the observed bimodal volcanism and the synchronous emplacement of mafic and felsic dikes at Quemont. The coincidence of crustal extension and the upwelling of mantle-derived melts into the shallow crust appear to have been instrumental in the formation of the excellent Quemont deposit.

3.2. Introduction

The Quemont volcanic-hosted massive sulfide deposit, located in Noranda district of northern Quebec, represents one of the largest gold producers of its class (Mercier-Langevin et al., 2011b). Mined between 1949 and 1971, with a short period of production in 2001, the deposit produced 13.9 Mt of ore grading 1.31% Cu, 5.5 g/t Au, and 18g/t Ag (Gibson and Galley, 2007). Despite its economic significance, comparably little is known on the geology of this important deposit and the volcanic environment in which the massive sulfides were formed.

In contrast to most other massive sulfide deposits of the Noranda district, which are hosted by a thick succession of effusive basalt and basaltic andesite flows and subordinate rhyolite flow-dome complexes (Kerr and Mason, 1990; Kerr and Gibson, 1993), the Quemont deposit is located within a felsic volcanic succession that is dominated by coherent rhyolite units and rhyolite breccia (Dimroth and Rocheleau, 1979; Lichtblau and Dimroth, 1980). The ore zones of the deposit occurred at or immediately below the contact of a thick interval of rhyolite breccia and an overlying coherent rhyolite unit. Mafic volcanic rocks are not a major component of the host rock succession of the deposit, mostly forming dikes that crosscut the felsic volcanic rocks (Weeks, 1967). As these dikes are not typically affected by hydrothermal alteration, they have previously been regarded to be late in origin and unrelated to the volcanism at Quemont (Ryznar et al., 1967).

In this paper, the geologic relationships are described for a dike-in-dike complex that is located to the northwest of the Quemont deposit. This dike complex has previously been interpreted to represent the feeder system to volcanic rocks occurring in the hanging wall of the Quemont deposit, with the dikes being emplaced along a major synvolcanic structure (Dimroth and Rocheleau, 1979; Lichtblau and Dimroth, 1980). Detailed surface mapping, coupled with textural and petrographic investigations as well as geochemical analyses, was performed to study the contact relationship between felsic and mafic dikes within this dike-in-dike complex. The

observed variations suggest that mingling and mixing of the melts of different compositions occurred along the contact of dikes of contrasting composition, suggesting that volcanism at Quemont was bimodal. Detailed textural characterization shows that different mingling and mixing textures formed, depending on the temperature and viscosity differences between the synchronously emplaced melts. As multiple melt injections occurred during dike propagation, a wide range of textural relationships can be observed. The present study demonstrates that magma mingling and mixing of felsic and mafic magmas indicates bimodal volcanism, a hallmark of extensional volcanic settings that are favorable for massive sulfide formation.

3.3. Regional Geology

The Noranda volcanic complex forms part of the Neoarchean (2,704-2,695 Ma; McNicoll et al., 2014) Blake River assemblage of the Abitibi greenstone belt, Superior Province (Fig. 3-1). The Blake River assemblage is composed of bimodal tholeiitic to calc-alkaline volcanic and volcaniclastic rocks that were deposited in a submarine setting. The rocks crop out in a 140 km long E-W trending belt from eastern Ontario into western Quebec (Dimroth et al., 1982, Goodwin, 1982). The belt is bounded by the Porcupine-Destor deformation zone in the north and the Larder Lake-Cadillac deformation zone in the south (Thurston et al., 2008).

The Noranda volcanic complex is host to 25 massive sulfide deposits that have been exploited in the past for their base and precious metal contents (Gibson and Galley, 2007; Mercier-Langevin et al., 2011a). Most of these deposits are located in the Noranda Main Camp, which comprises a thick succession of alternating packages of felsic and mafic lavas. Volcaniclastic rocks are only a minor component of the volcanic succession (Spence and de Rosen Spence, 1975; Spence, 1976; Gibson and Watkinson, 1990). U-Pb age dating of a felsic lava flow located in the upper part of the volcanic succession suggests that the host rocks of the Noranda Main Camp were essentially formed by 2,698.3 ± 1.2/-1.0 Ma (David et al., 2006, 2010).

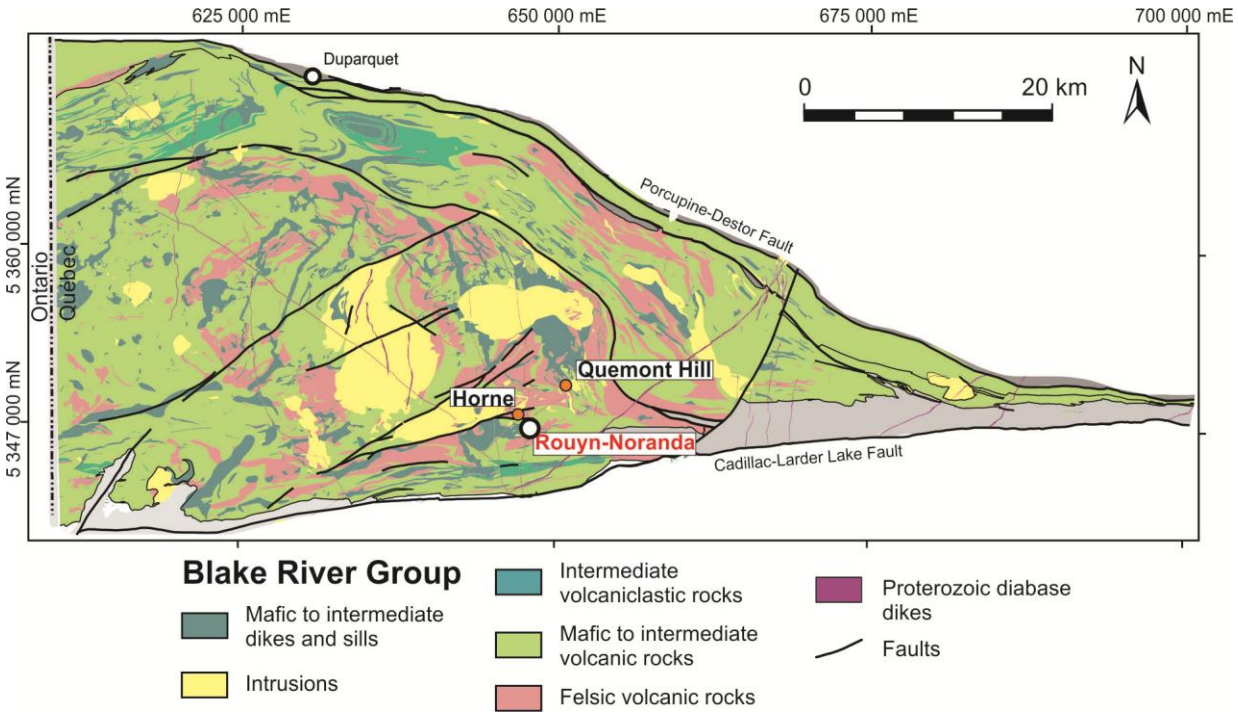

Fig. 3-1: Geological map of the eastern portion of the Archean Blake River Group with the locations of the Quemont and Horne Deposits in relation to the town of Rouyn-Noranda, Quebec (modified from Mercier-Langevin et al., 2011a).

The bimodal volcanic succession of the Noranda Main Camp has been intruded by a large number of synvolcanic diorite and gabbro dikes and sills. In addition, the synvolcanic Flavrian and Powell plutons are located in the Noranda Main Camp (Spence and de Rosen-Spence, 1975; Goldie, 1978). These plutons are composed of sill-like intrusions that are characterized by generally conformable contacts with the overlying volcanic strata. Recent dating has established that the youngest phase of the Flavrian pluton was formed 2,700.7 ± 0.6 Ma (McNicoll et al., 2014). A sample from the Powell pluton yielded an age of 2,700.1 ± 1.0 Ma (McNicoll et al., 2014). In addition to these two large plutons, the much smaller MacDonald pluton located further to the east is interpreted to be a synvolcanic intrusion. In contrast, the Lac Dufault pluton represents a younger, post-volcanic intrusion (Mortensen, 1993). It is surrounded by a pronounced contact metamorphic aureole (de Rosen-Spence, 1969; Beaty and Taylor, 1982).

The Noranda volcanic complex is subdivided into distinct fault blocks by several major faults and their extrapolations (de Rosen Spence, 1976). The Hunter block is located between the Porcupine-Destor deformation zone in the north and the Hunter Creek fault in the south. The

Hunter Creek fault and the Beauchastel fault enclose the Flavrian block that is host to the deposits of the Noranda Main Camp. The area between the Beauchastel fault and the Horne Creek fault is referred to as the Powell block. The Horne Creek fault and the Andesite fault form the boundaries of the Horne block (Fig. 3-2).

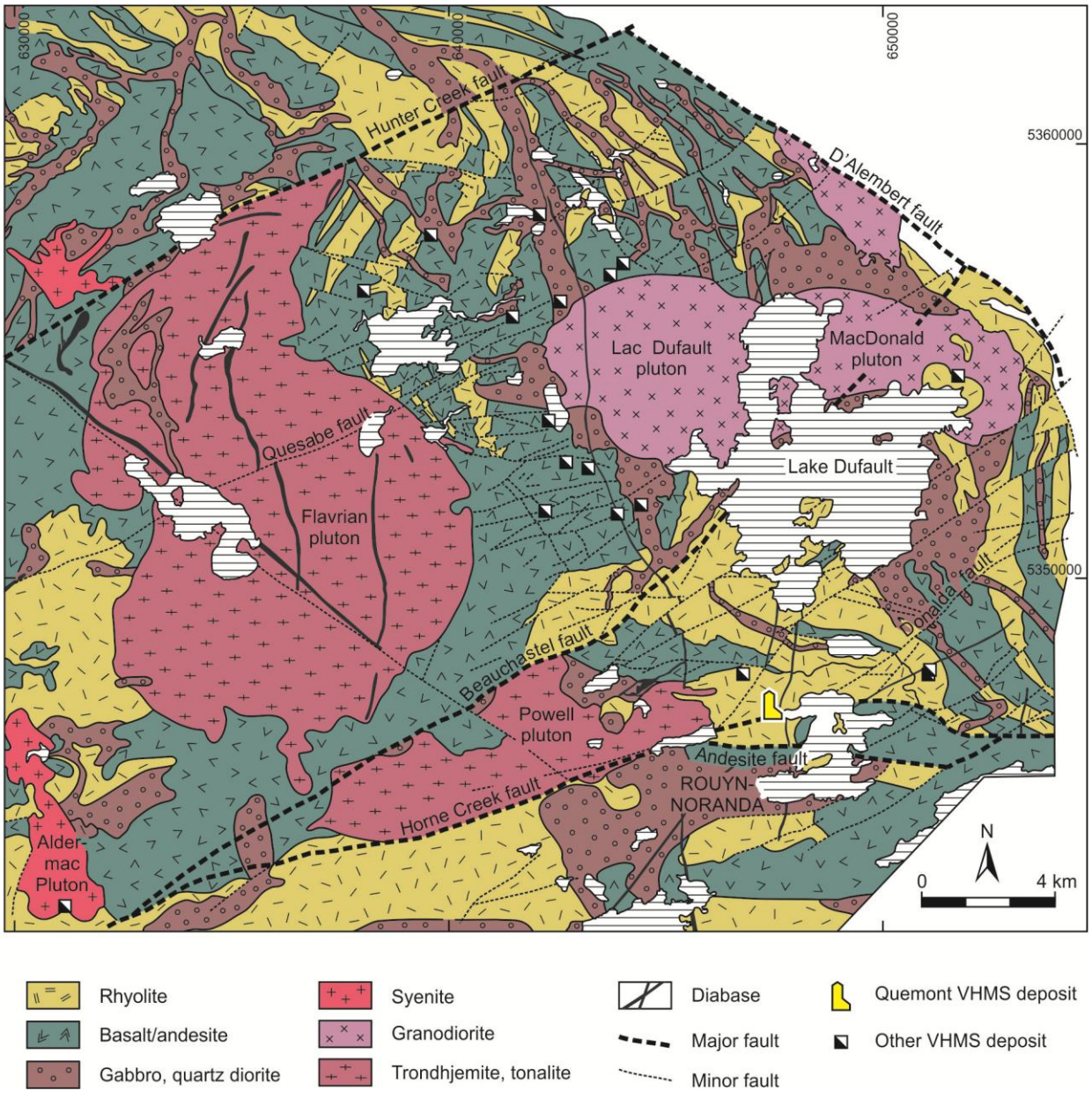

Fig. 3-2: Geological map of the Noranda volcanic complex, illustrating the distribution of major volcanic and intrusive rock units. The location of the field area near the Quemont deposit is identified (modified from Santaguida, 1999).

3.4. Geology of the Quemont Deposit

The Quemont massive sulfide deposit is located within the Powell block, north of the Horne Creek fault (Fig. 3-3). The deposit represented the second largest massive sulfide deposit within the Noranda district. The deposit was discovered in March 1945. Between 1949 and 1971, with an additional short period of production in 2001, the mine produced approximately 13.82 Mt of ore grading 1.32% Cu, 2.44 % Zn, 5.49 g/t Au, and 30.9 g/t Ag (Mercier-Langevin et al., 2011a). Due to its high Au grades, the Quemont deposit represents one of the largest gold producers of its class (Mercier-Langevin et al., 2011b).

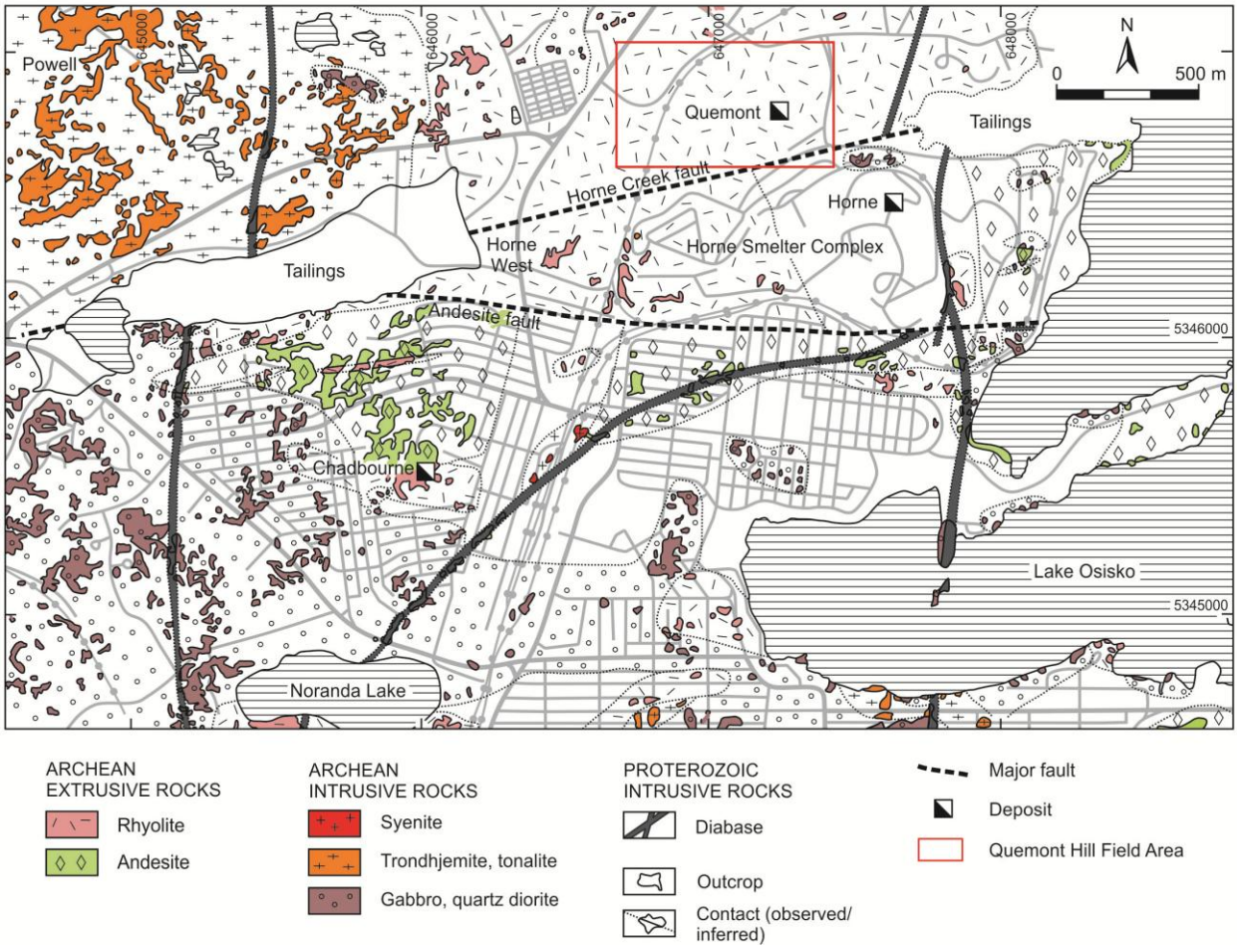

Fig. 3-3: Geological map of the Quemont and Horne deposit areas located to the north of the city of Rouyn-Noranda. The location of the field area is outlined (modified from Wilson, 1941).

Little is known on the geology of the Quemont deposit as most of the historic records collected over decades of underground production have been destroyed during a fire at the mine site (Monecke et al., 2011). Remaining mine plans suggest that the host rock succession of the deposit is composed largely of felsic volcaniclastic rocks and an overlying porphyritic rhyolite unit. The ore bodies were located mainly within the upper portion of the volcaniclastic unit (Weeks, 1963; Ryznar et al. 1967). The volcanic stratigraphy is folded into an anticline that plunges to the west, with crossfolding occurring about a N-S axis (Weeks, 1967).

As the Quemont deposit is located in a topographic low, outcrops of the immediate hosts to the deposit are limited. However, a large outcrop area informally known as Quemont Hill is located to the northwest of the deposit. The volcanic rocks exposed in this area are considered part of the Quemont host rock succession. The results of reconnaissance mapping at Quemont Hill are described by Dimroth and Rocheleau (1979).

The western portion of the approximately 400 m large outcrop area is dominated by the occurrence of a coherent rhyolite and associated breccia facies, referred to as the Joliet rhyolite. This rhyolite is in contact with a distinctly polymict breccia facies that contains rhyolite, dacite, andesite, and basalt clasts. The breccia facies is very poorly sorted and shows no sedimentary structures (Dimroth and Rocheleau, 1979). This breccia facies is stratigraphically overlain by a rhyolite breccia that is dominated by quartz-phyric rhyolite fragments (Dimroth and Rocheleau, 1979). This rhyolite breccia facies is crudely stratified and dominated by clasts that have curviplanar margins. The breccia hosts abundant rhyolite sills. The contact relationships between the rhyolite intrusions and the rhyolite breccia are highly complex and are characterized by intricate interpenetration between the lava and the breccia, suggesting that the sills were intruded into the still wet and unconsolidated rhyolite breccia (Monecke et al., 2011). To the northwest, both breccia facies recognized at Quemont Hill are crosscut by a dike complex, consisting of numerous mafic and felsic intrusions (Dimroth and Rocheleau, 1979). Preliminary mapping has established that the mafic and felsic dikes were emplaced synchronously, as suggested by the occurrence of magma mingling and mixing textures (Huthmann, 2009; Monecke et al., 2011).

Recent high-precision U-Pb analysis of a coherent quartz- and feldspar-phyric rhyolite from the Quemont host succession yielded a crystallization age of 2,702.0 Ma ± 0.8 Ma, indicating that the Quemont deposit is older than the massive sulfide deposits of the Noranda Main Camp. The obtained crystallization age is similar to an age date obtained for an aphyric

rhyolite occurring in the footwall of the Horne deposit, which is located immediately to the south of the Horne Creek fault. These results indicate that the felsic-dominated host successions of the Quemont and Horne deposit are of similar age (McNicoll et al., 2014) and probably also formed in a similar environment (Monecke et al., 2008, 2011).

3.5. Materials and Methods

To conduct detailed mapping in the 200 by 340 m large area of the dike-in-dike complex at Quemont Hill, a Magellan Pro Mark 3 differential GPS unit was used. This system uses a stationary base station GPS and a roving kinematic GPS to obtain precise GPS data points. The roving GPS was initially used to construct the precise outlines of individual outcrops. Contacts between the rock units were also mapped in the field and recorded by differential GPS. The location data were processed using the GNSS Solutions software and visualized in ArcMap 10.1. Final maps were constructed using the graphics program CorelDRAW. A final map at a scale of 1:200 was produced (Appendix)

To document the textural relationships between felsic and mafic intrusions in more detail, several areas were mapped at a scale of 1:25 (Appendix). Three 5 x 5 m large outcrops and one 4 x 3 m large outcrop were chosen for detailed mapping. This was accomplished by establishing 1 by 1 m surface grids across the outcrops. These grids were further divided into 50 x 50 cm large squares that were photographed and stitched together digitally. Volcanic features and contacts between units were mapped digitally to record detailed relationships.

Representative samples were collected across the dike-in-dike complex to determine the petrography and geochemical compositions of the mafic and felsic units. In total, 15 whole-rock samples were collected (Table 3-1). Polished thin sections were obtained for 21 rocks and representative textures and used for petrographic analysis. The major and trace element composition of 15 coherent samples showing no evidence for physical mixing between mafic and felsic melts were analyzed geochemically.

Table 3-1: Petrographic description of samples from Quemont Hill

Sample	Rock Type	Brief Description
QH-023	Aphyric Dacite	Thin section: Groundmass is completely composed of partially oriented plagioclase laths. Fine-grained seen in the thin section but not observed in hand sample, composed of plagioclase, quartz, and chlorite.
QH-024	Basalt	Thin section: Groundmass is predominantly light green chlorite. Fine-grained sample with abundant calcite, altered biotite, and hornblende. Very fine anhedral quartz that likely replaced glass. Isotropic dark mineral highly altered and unrecognizable.
QH-025	Basalt	Hand sample: Light green gray in color with mostly fine-grained equigranular matrix.
QH-026	Basalt	Hand sample: Vey fine-grained, equigranular with green, black, and minor white colors throughout.
QH-027B	QFPR-1	Thin section: Abundant quartz and feldspar phenocrysts within a mostly quartz matrix that is very fine-grained. Minor disseminated sulfides and a recrystallized quartz vein.
QH-028	QFPR-2	Hand sample: Gray, brown in color with coarse quartz phenocrysts (15%). Thin - section: Quartz phenocrysts 2-4 mm in size. Groundmass is fine-grained and is composed of a mosaic of quartz and feldspars. Minor chlorite and micas found in small veins and fractures.
QH-029	QFPR-2	Thin section: Abundant quartz phenocrysts and lesser feldspar. The groundmass is composed of fine-grained euhedral quartz. Abundant granophyric texture and micas filling in small veins or fractures that are aligned.
QH-031	QFPR-1	Rounded quartz phenocrysts (8-10%) with rims of fine-grained quartz. Abundant chlorite in groundmass, also forming veinlets. Smaller rounded radiating mica nodules surrounded by rims of quartz. Groundmass is quartz that varies in size from very fine to phenocryst (2-3 mm). No feldspars present.
QH-035	QFPR-2	Hand sample: Bluish gray (to dark grayish green in some of sample) with some oxidation occurring in small pockets. Minor sulfides in small fractures and veins. Quartz crystals vary from euhedral square crystals to more rounded, range in size up to ca. 3 mm.
QH-036	Basalt	Hand sample: Aphyric and aphanitic greenish gray in fresh color with equally distributed abundant very fine disseminated pyrite (5%). No visible phenocrysts.
QH-037	Basalt	Hand sample: Equigranular with disseminated sulfides. Greenish gray in hand sample. Thin section: Groundmass is mostly composed of chlorite with very fine anhedral quartz replacing former glass.
QH-039	QFPR-2	Quartz shows undulose extinction and has a magmatic texture. The groundmass is very fine-grained subhedral quartz and feldspar. Phenocrysts include 13-15% quartz grains that are euhedral and rounded, 2-3% highly altered feldspar. Abundant chlorite, and some micas.
QH-040	QFPR-1	Hand sample: Dark green to black in color with small 1-2 mm at most quartz phenocrysts (ca. 9-11% abundance), some small fine-grained dispersed but not disseminated pyrite.
QH-041	QFPR-1	Hand sample: Dark green to gray in fresh color with 7-9% rounded square quartz phenocrysts that are less than 2mm in size. Small blebby sulfide veins.
QH-042	Basalt	Hand sample: Aphyric and aphanitic sample that is greenish black in fresh color. Minor (<5%) disseminated sulfides.

Sample preparation for geochemical analysis initially included the removal of surface oxidation rinds from the hand specimen and any visible vein material. This was followed by crushing of the samples using a Rocklabs Boyd crusher and milling of approximately 100 g of sample material in a Rocklabs tungsten carbide ring mill. The pulps obtained were submitted for geochemical analysis to Actlabs in Ancaster, Ontario.

Major element analysis of the rocks was conducted by X-ray fluorescence analysis using standard fused disks. To minimize matrix effects, the heavy absorber fusion technique described by Norrish and Hutton (1969) was employed. The loss of ignition of the samples was determined by gravimetry following roasting of the sample powders at 1050°C for 2 hours. The total carbon and sulfur contents were determined by the Leco method, which involves combustion of the samples, followed by measurement of the carbon dioxide and total sulfur content by infrared absorption. Trace element analysis was performed by inductively coupled plasma-mass spectrometry following closed vessel digestion of the samples using a combination of hydrofluoric, hydrochloric, nitric, and perchloric acids.

Repeated analyses of sample materials and in-house and international georeference materials showed that the precision of the major and trace element analyses was typically <5% RSD for elements occurring at concentration levels significantly above their respective detection limits. Element abundances measured on international georeference materials were in close agreement with the recommended values. The deviations of the analytical results from the recommended values were found to be in the order of ±10% or below, indicating that the major and trace element analysis was highly accurate.

3.6 Quemont Hill Field Relationships

The Quemont Hill field area is characterized by an E-W trending dike swarm characterized by multiple subparallel coherent dikes with outer bounds interfingering with associated breccias (Appendix). The width of the individual dikes ranges from tens of centimeters to tens of meters. Volcanic facies present at Quemont Hill were distinguished in the field through careful mapping and identification of characteristics such as color, weathering behavior, phenocryst abundance, and contact relationships. The facies were further classified using geochemical and petrographic analyses.

3.6.1 Volcanic Facies

Coherent aphyric dacite to rhyodacite exists in the western field area as a slightly folded discontinuous unit about an E-W axis. The unit was not observed within any other portion of the dike-in-dike complex. The unit is characterized by a dark brown fresh color at the surface with orange-brown to green weathered areas. The contact between the aphyric rhyolite and the dike complex is sharp and easily recognizable. While phenocrysts were not visible in the field, closer inspection of prepared hand samples show that the unit is very fine-grained containing equigranular minerals with minor scattered quartz and feldspar phenocrysts.

Coherent quartz and feldspar phyric rhyolite (QFPR -1) is the most dominant volcanic unit found within the mapped area. The facies is most prevalent to the north and south of the dike swarm with outcrops in the mapped area ranging between 10 to 25 m in thickness. The unit is tan to brown in outcrop and ranges from green-gray to tan-green in fresh hand sample. Quartz is present as euhedral phenocrysts that range in size from 1-3 mm. The average phenocryst abundance ranges between 9-12% in most areas. This volcanic facies is flow foliated in several locations within the field area with prominent foliation textures present in the north.

The dike swarm is composed primarily of coherent mafic volcanic rocks interpreted to be basalt to basaltic andesite. The dikes are grayish-black to greenish-gray in outcrop. Basaltic dikes are characterized by a parallel, linear geometry but have curved geometries where dikes connect or bifurcate to become two individual intrusions. The average thickness of the basaltic dikes is between 2 and 5 meters. There are no visible phenocrysts in hand sample, but minor disseminated sulfides can be seen. The mafic rocks are prominent in the southeastern portion of the outcrop where the basalt is characterized by both a sill and dike geometry. The outcrops in this area contain several of the most laterally extensive mafic dikes, which connect or come in close contact. There are commonly smaller basalt dikes on the centimeter scale that occur within the larger basalt dikes in the southeast.

A second generation of quartz and feldspar phyric rhyolite (QFPR-2) is weathered yellow to brown in outcrop with abundant euhedral quartz and plagioclase phenocrysts ranging from 1-4 mm in diameter. Average phenocryst abundance observed in the field was between 17 and 24%. The color of hand samples ranges from bluish-gray, to dark greenish-gray, to gray-brown. Minor sulfides occur in small fractures and veins. The quartz and feldspar phyric rhyolite occurs in two

laterally extensive dikes, one between 5 and 15 m in thickness and another between 0.5 m and 1 m in thickness. The larger of the two dikes occurs in the middle of the mapped dike swarm and the smaller dike occurs towards the northern boundary of the complex. This unit is the primary host to the mafic xenoliths and other prominent mingling textures present in the area.

Monomict rhyolite matrix-supported breccia can be found in a limited number of locations on the periphery of the mapped dike-in-dike complex. The breccia occurs within or on the margins of the quartz and feldspar phyric rhyolite (QFPR – 1). The breccia has an irregular curved geometry as a unit and varied contact relationships with QFPR – 1. The clasts within the breccia are composed of the adjacent quartz and feldspar phyric rhyolite, are poorly sorted, curviplanar and are subangular to subrounded. Clasts range in size from 1-6 cm and are set in a fine-grained matrix.

3.6.2 Magma Mixing and Mingling

Magma mingling is prevalent along the southern contacts between the QFPR – 2 dikes and the adjacent mafic dikes. The magma mingling textures vary significantly in appearance and nature along the length of the mingling contacts from east to west, and much of the contact contains no mingling features. Magma mixing is hereby defined to indicate a homogeneous or "hybrid" composition that has resulted from the close interaction of two magmas with distinct compositions. Magma mingling refers here to magma interaction that has resulted in physically distinct magmas with heterogeneous compositions (Johnson and Barnes, 2006).

The first of the magma mingling textures occur in the stratigraphically lower part of the field area are visible at the surface as an aphyric granular mafic matrix with 1-2 mm sized quartz phenocrysts present with a non-uniform spaced distribution (Fig. 3-4A). This unit is bound to the north and the south by two small mafic dikes ranging from 10-15 cm in thickness. Upon inspection of cut samples and thin sections, the apparent homogenous mafic matrix actually contains light green-gray enclaves of volcanic material closely resembling basalt (Fig. 3-4B). The enclaves have very smooth and rounded margins that appear diffuse in some locations and dominantly appear to preserve the ductile character of the magma. These enclaves are sparse and are only centimeters in size. They tend to be elongated into small fingers including one instance of a 4 cm long sulfide enclave found within the middle of this area (Fig. 3-4C).

The magma mingling contact between the larger southern QFPR-2 dike and adjacent basalt is characterized by abundant basalt xenoliths within the quartz- and feldspar-phyric rhyolite (Fig. 3-4D). The xenoliths have long axes that are aligned and elongated parallel to the contact between the rhyolite and the basalt. The lengths of the xenolith long axes vary significantly from 1 to 96 cm. The primary xenolith morphology is lenticular to tabular. Xenoliths are characterized by sharp contacts with the enclosing rhyolite and sub angular to sub rounded margins. Xenoliths tend to be spatially removed from the rhyolite and basalt dike contact, and there are no observed xenoliths in contact with the mafic unit while intruding into the rhyolite.

The small QFPR-2 dike in the north of the dike swarm complex is characterized by a texture best explained as a basalt enclave-supported dike with surrounding rhyolite matrix that is foam-like in appearance (Fig. 3-4E and F). The texture consists of abundant centimeter-scale basalt enclaves within a rhyolite matrix. The enclaves preserve ductile and wispy textures. Basalt enclaves are brown in outcrop but green in hand sample. Large enclaves commonly have smooth sharp margins and tail-like features that appear to be a result of ductile movement of the clast during formation (Fig. 3-4E). The large enclaves range in size from 1 to 5 cm, but the unit as a whole contains abundant small (<1cm) blebs as well. The matrix is composed of coherent phenocryst-bearing rhyolite ranging from light tan to white in color.

3.6.3 Detailed Sections

Detailed map A is focused on a mafic dike that contains and mingles with the small QFPR-2 dike found in the north (Appendix). The QFPR-2 dike is characterized by a foam-like texture and several irregular xenoliths with ductile features. Larger visible enclaves range in size from the centimeter scale to tens of centimeter scale. The enclaves have curved to wispy morphologies with irregular margins that appear to have been highly viscous and "toothpaste-like" during emplacement. In the northwest corner of the grid, the foam-like texture grades into the basalt completely until QFPR-2 is indistinguishable within the basalt at the surface. The QFPR-2 reappears approximately 4 m to the east of the detailed grid. A small QFPR-1 dike appears in the central and western portion of the grid.

Fig. 3-4: Photographs showing the magma mingling textures present at Quemont Hill. A. Photograph of an aphyric granular mafic rock found in the stratigraphically lower portion of the field area with quartz phenocrysts marked by white arrows. B. Mafic enclaves in a matrix of intermediate composition. Enclaves show rounded and ductile features. C. Sample taken in the stratigraphically lower portion of the field area that contains a 3 cm long sulfide aggregate within the mafic matrix. D. Lenticular and elongate mafic xenoliths found within QFPR-2. Clasts are subangular and oriented subparallel to the mafic-QFPR-2 contact. E. Abundant mafic enclaves (larger enclaves shaded teal) and larger ductile xenoliths within a rhyolite matrix found in the smaller QFPR-2 dike. This texture has been labeled foam-like due to the high abundance of enclaves that make up the majority of the unit. F. Foam-like texture showing the margins of the small QFPR-2 dike (outlined in blue) and the rigid and bumpy texture that the mingled enclaves and rhyolite show in outcrop. The camera lens is 6 cm in diameter and the coin is 2.2 cm in diameter.

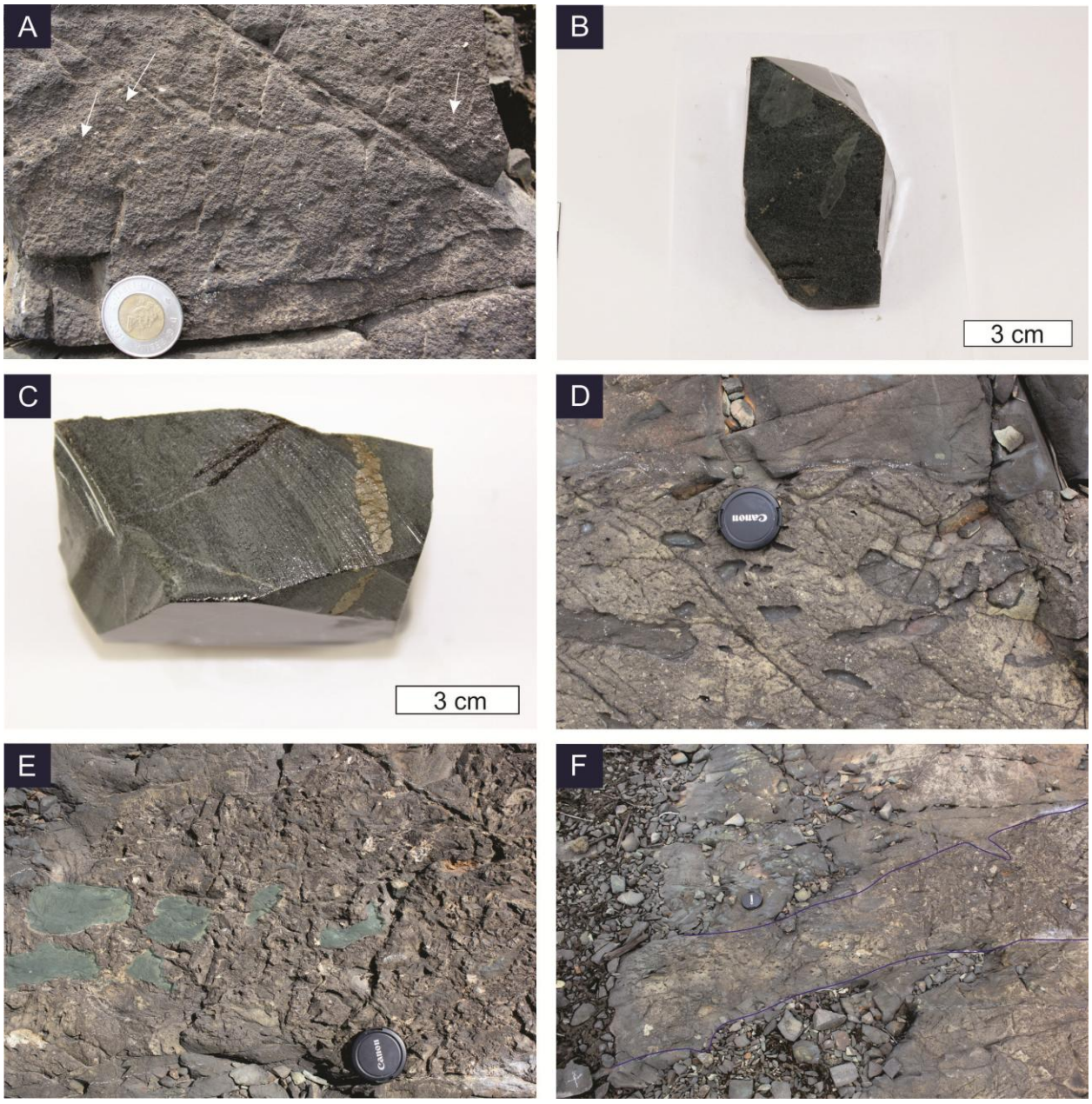
A
B
3 cm
C
3 cm
D
E
F

Detailed map B depicts a detailed section of the dike swarm closest to the source zone in which a channel sample was taken through the mingled and mixed units (Appendix). Volcanic facies within the grid have been labeled to identify and describe each unit. Unit A is a QFPR-1 with approximately 10-12% quartz phenocrysts ranging from 1-2 mm in diameter. The weathered surface is green to grayish yellow in color with very fine-grained pyrite seen in outcrop. Unit B appears to be aphyric coherent basalt in outcrop with a granular texture. Weathering in this unit varies from yellow-orange to gray and dark gray. This unit contains minor late calcite veining and forms a sharp contact with the adjacent units. In hand sample this basalt is dark green to green-black in color. Unit C was difficult to compositionally define in outcrop, because it appears to have a mafic composition, granular texture , and 1-5 mm sized quartz phenocrysts. Samples in the field from this unit showed quartz phenocrysts with a non-uniform distribution. No change in phenocryst abundance was observed from north to south within the unit and overall the rock had phenocryst abundances between 6-8% overall. Upon obtaining a fresh hand sample, it was revealed that the unit contains small green mafic enclaves that are very rounded and fluid-like in shape. The matrix containing the enclaves appears to be a composition between rhyolite and basalt but the unit as the whole is confirmed to be non-homogeneous. Unit D is very similar to Unit B but appears to have a fine granular texture in outcrop. The contact between D and E appears undulatory and slightly sheared due to volcanic processes. Unit E is also QFPR-1 with 13-15% quartz phenocrysts present.

Detailed map C is a 3x4 m grid focused on the foam-like texture found in the smaller QFPR-2 dike to the north (Appendix). The grid shows a small 40-50 cm thick quartz- and feldspar-phyric rhyolite dike that is entirely characterized by the above mentioned texture with one small featured area containing larger identifiable xenoliths. The dike is bounded to the north and the south by basalt dikes that form sharp contacts with the contained foam-like texture. The southern portion of the detailed grid is characterized by chaotic QFPR-1 discontinuous lenses that are largely broken up by the basalt unit present.

Detailed map D is a representative section of the southernmost contact between the QFPR-2 and the adjacent mafic dike (Appendix). The section also represents the westernmost extent of outcrop with visible magma mingling that was mapped in detail. The section shows abundant mafic enclaves that have long axes sub parallel to the dike contact orientations. The contact between the QFPR-2 and the mafic dike is not sharp and distinguishing a clear transition

from one composition to another is difficult. There are limited enclaves immediately adjacent to the inferred contact between the two units.

Detailed map E was mapped previously by Huthmann (2009), but the area was remapped with particular attention paid to the small scale textures, which are indicative of mixing and mingling. The detailed section shows the xenolith distribution along the QFPR-2 contact with a basalt dike immediately to the south (Appendix). The xenoliths are abundant and elongated parallel to the contact between the rhyolite and the basalt. The abundance of xenoliths decreases away from the contact but the size of the xenoliths increases. This section does not show a gradational contact between the rhyolite and basalt as seen in map D or a gap between the contact and the xenolith occurrence.

3.7 Quemont Hill Geochemistry and Petrography

The whole-rock geochemistry of the volcanic facies at Quemont Hill was determined u on samples that were representative of end-member rock compositions across the field area. The results of these geochemical analyses, including major oxides, major elements, and trace elements are reported in Table 3-2. Thin sections of the representative volcanic units in the field and of key mingling and mixing textures were analyzed and are described within the table.

3.7.1 Geochemical Characteristics

In order to determine the bulk composition of the volcanic rocks, SiO_2 versus Zr/TiO_2, P/Zr versus Ti/Zr, and Zr/TiO_2 versus Nb/Y discrimination diagrams put forth by Winchester and Floyd (1977) and Stolz (1995) were utilized (Fig.3-5, 3-6, and 3-7). The diagrams indicate similar trends for the main rock types present at Quemont Hill. Volcanic units present at Quemont display a sub-alkaline affinity with compositions ranging from basalt to rhyolite.

Based on chemical classification, mafic rocks range from basalt to andesite, depending on the composition discrimination diagram used. They are characterized by SiO_2 contents between 47 and 54 wt.%. The mafic units demonstrate increasing SiO_2 content with increasing distance from the southeastern mafic source zone. The N-S trending aphyric dacite was classified as a rhyodacite to dacite with a SiO_2 content of approximately 68 wt.%. QFPR-1 plots within the

rhyodacite-dacite field in the Zr/TiO_2 versus Nb/Y diagram but within the rhyolite to high-silica dacite field in other diagrams. The SiO_2 content of this unit ranges from 73 to 76 wt.% with decreasing concentrations up stratigraphy. QFPR - 2 has the highest average abundance of SiO_2 ranging between 77 and 80 wt.% with the slight decrease in abundance occurring up stratigraphy. The different plots consistently suggest that this unit is a rhyolite.

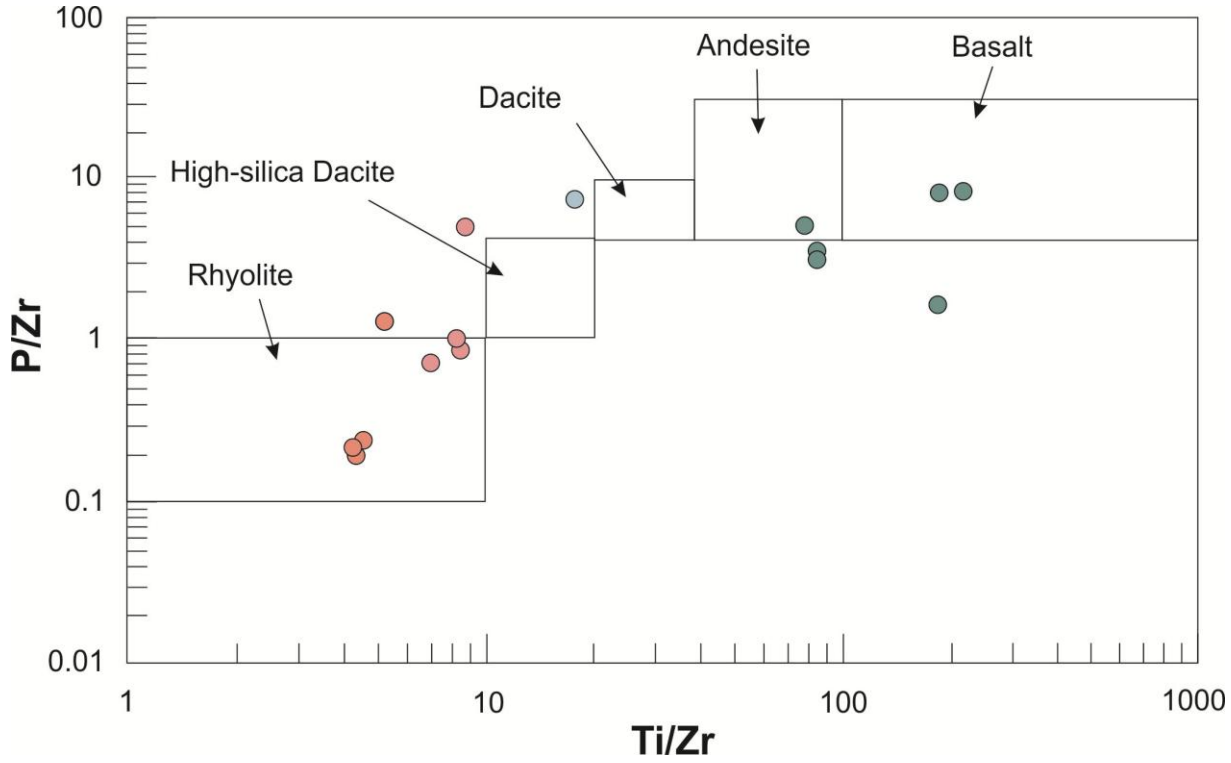

Fig. 3-5: Plot of P/Zr vs. Ti/Zr used to discriminate samples of variable compositions. QFPR-1 dikes are in pink and QFPR-3 dikes are noted in orange (diagram from Stolz, 1995)

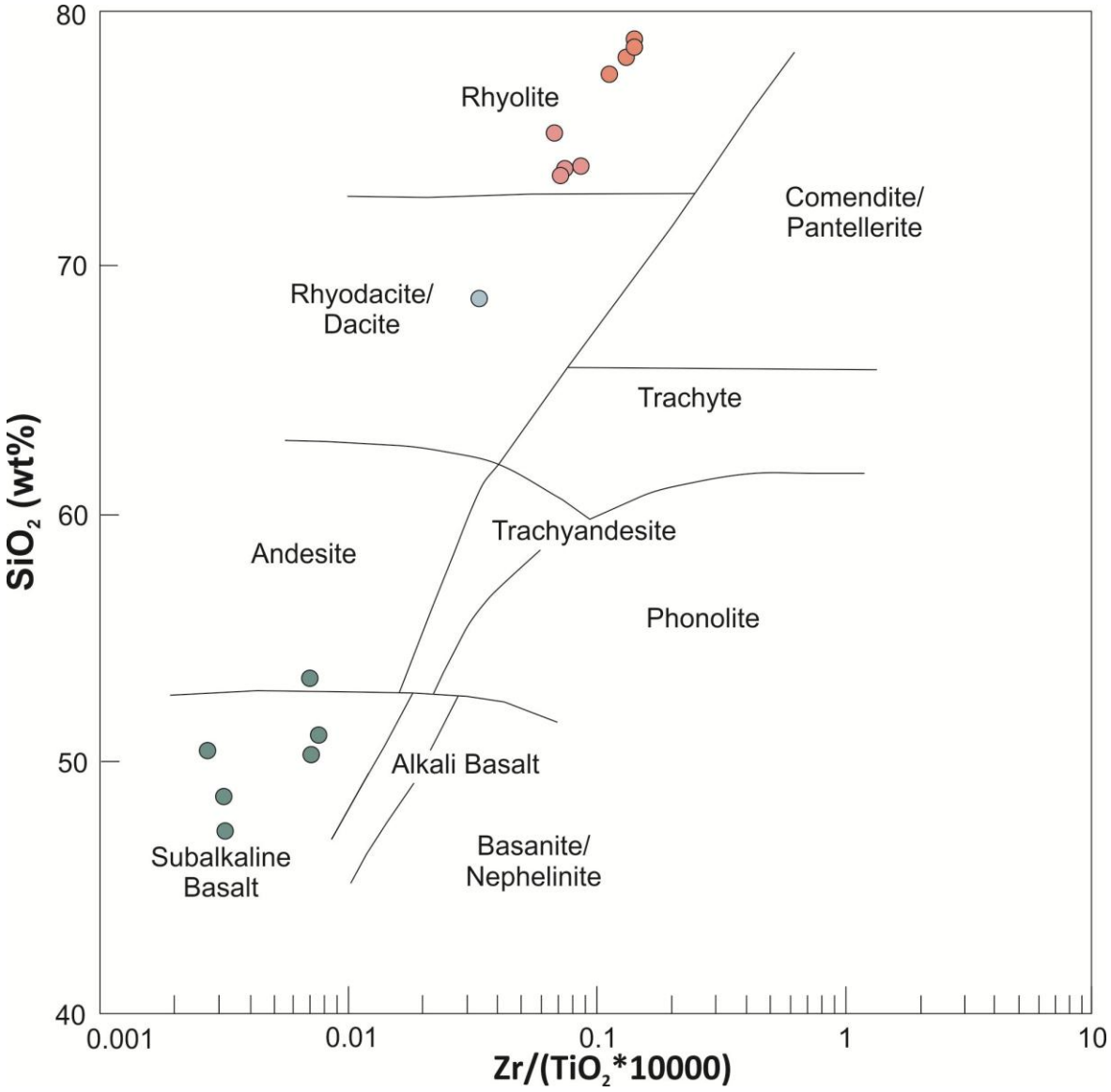

Fig. 3-6: Plot of Zr/TiO_2 vs. SiO_2 used to classify aphyric dacite (blue), basalt (teal), QFPR-1 (pink), and QFPR-2 (orange) at Quemont Hill by their immobile trace element compositions (diagram from Winchester and Floyd, 1977).

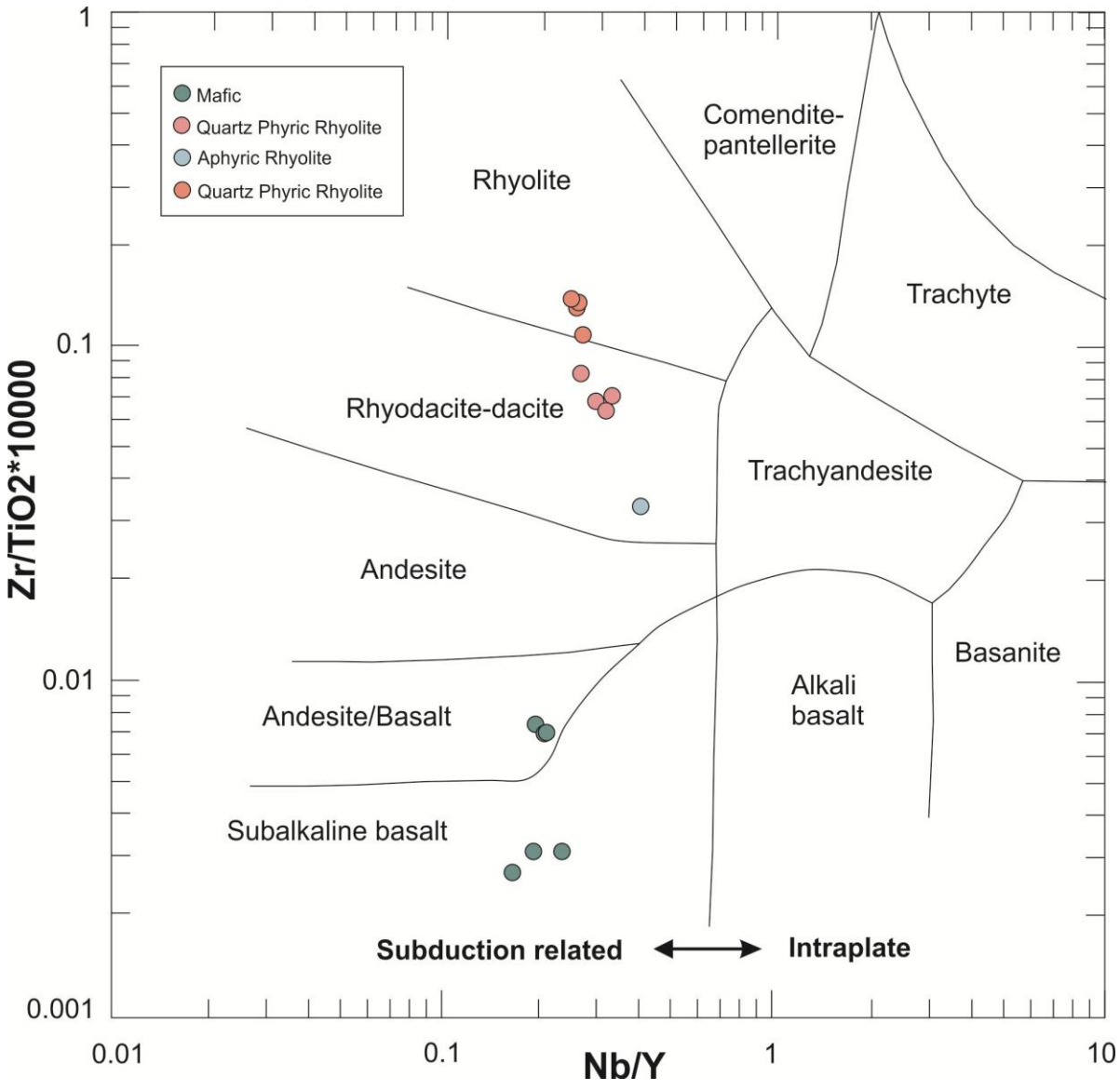

Fig. 3-7: Plot of Zr/TiO_2 vs. Nb/Y used to classify aphyric dacite (blue), basalt (teal), QFPR-1 (pink), and QFPR-2 (orange) at Quemont Hill. The whole-rock compositions demonstrate that the volcanic rocks have a subalkaline affinity (diagram from Winchester and Floyd, 1977).

Chondrite-normalized REE plots are given inFigures.3-8, 3-9,3-10, and 3-11. Mafic samples 24, 25, and 26 show near flat REE patterns with a slight enrichment of the HREE and a slightly positive Eu anomaly. Mafic samples 36, 37, and 42, collected further up stratigraphy, show negative Eu anomalies and a greater relative enrichment in LREE in comparison with the other mafic samples. The QFPR-1 samples 30, 40, and 31 have small Eu anomalies and sample 27B shows no relative anomaly in comparison with the previously mentioned samples. The QFPR-1 samples demonstrate relatively flat REE patterns with a slight enrichment in the LREE. The QFPR-2 rhyolite samples (28, 29, 35, and 39) show higher total REE concentrations in comparison with the lower silica rhyolite and dacite. All samples are characterized by a distinct negative Eu anomaly. The samples all show a relative enrichment in the LREE compared to the HREE. The aphyric dacite has normalized REE concentrations that plot between both generations of quartz phyric rhyolite and the average mafic REE concentrations. The unit shows a slight enrichment in LREE but overall has a flat REE concentration trend.

Samples QH- 036, QH- 037, and QH – 042 are identified as basalts that have negative Eu anomalies, but in addition, all three samples also plot close to or within the andesite field in all of the various discrimination diagrams used. The negative Eu anomalies also confirm a composition that is not strictly basalt for these three samples. A REE diagram was constructed by plotting an end member basalt (QH – 024) and an end member rhyolite (QH – 028) , and sample QH – 037 was used as a representative basalt/andesite unit that showed a REE trend between the two end member trends (Fig. 3-12). A REE trend was calculated to be the best fit to QH-037 using relative percentages of both rhyolite and mafic compositions. The resulting best fit line that was most similar in REE trend to QH-037 was composed of 25% rhyolite and 75% basalt. These results confirm a mixing trend between the rhyolite and basalt to produce a intermediate andesite/basalt composition.

Table 3-2: Major (wt.%) and trace element (ppm) analyses of volcanic rocks from Quemont Hill

	Aphyric Dacite	**Aphyric Basalt**					
Sample	QH - 023	QH - 024	QH - 025	QH - 026	QH - 036	QH - 037	QH - 042
SiO_2	68.52	47.21	48.62	50.49	51.04	50.3	53.32
Al_2O_3	13.93	14.76	14.52	14.07	12.42	12.38	13.39
Fe_2O_3	5.75	13.6	13.21	12.91	14.91	14.72	15.63
MnO	0.111	0.27	0.275	0.245	0.302	0.318	0.28
MgO	2.42	6.16	5.98	6.06	4.58	4.51	4.98
CaO	0.4	7.32	7.41	6.64	5.79	6.59	2.96
Na_2O	5.55	1.69	1.85	2	1.68	1.7	1.61
K_2O	0.01	0.03	0.03	0.02	0.03	0.02	0.15
TiO_2	0.53	1.157	1.141	1.244	1.493	1.486	1.71
P_2O_5	0.12	0.07	0.07	0.07	0.14	0.13	0.17
LOI	1.82	7.21	7.08	6.87	8.27	8.74	6.42
Total	99.17	99.48	100.2	100.6	100.6	100.9	100.6
Co	32	49	44	51	50	46	58
Ni	< 20	110	100	110	30	30	30
Cu	10	90	80	50	110	120	120
Zn	130	290	270	220	330	310	490
Sr	53	105	99	84	45	49	27
Y	29.4	17	15.3	16.5	37.5	37.2	37.8
Zr	180	37	36	34	113	105	120
Nb	11.8	3.9	2.9	2.7	7.2	7.6	7.7
Ag	1.2	< 0.5	< 0.5	< 0.5	0.8	0.9	1
Ba	34	43	24	12	11	10	51
La	13.8	1.92	1.39	1.47	11.5	11.2	11.7
Ce	29.1	4.65	3.69	3.86	27.5	26.5	23
Pr	3.85	0.71	0.61	0.66	3.89	3.72	3.54
Nd	16	4.13	3.49	3.76	18.3	16.9	15.9
Sm	3.72	1.76	1.7	1.61	4.98	4.9	4.37
Eu	1.04	0.875	0.722	0.678	1.17	1.13	0.919
Gd	4.06	2.55	2.27	2.33	5.5	5.42	5.38
Tb	0.7	0.47	0.44	0.44	0.96	0.96	0.98
Dy	4.56	3.02	2.84	2.98	6.28	6.13	6.14
Ho	0.99	0.63	0.58	0.6	1.34	1.29	1.31
Er	2.99	1.74	1.54	1.67	3.91	3.87	3.81
Tm	0.48	0.254	0.222	0.238	0.607	0.611	0.604
Yb	3.35	1.67	1.4	1.56	4.14	4.1	4.16
Lu	0.554	0.252	0.216	0.253	0.625	0.635	0.629
Pb	< 5	< 5	6	7	7	8	8

Table 3-2: cont'd

	Quartz/Feldspar Phyric Rhyolite (QFPR-1)				Quartz/Feldspar Phyric Rhyolite (QFPR-2)			
Sample	QH - 027	QH - 031	QH - 040	QH-041	QH-028	QH-029	QH-035	QH-039
SiO_2	75.25	73.89	73.58	73.64	79.1	78.49	78.84	77.77
Al_2O_3	11.37	10.75	11.13	10.77	11.72	11.74	11.27	12
Fe_2O_3	4.87	8.83	8.64	8.35	1.9	2.04	2.65	2.74
MnO	0.095	0.122	0.128	0.125	0.05	0.036	0.036	0.065
MgO	1.58	0.81	2.28	2.2	0.41	0.44	0.84	0.64
CaO	0.35	0.05	0.15	0.06	0.62	0.34	0.25	0.86
Na_2O	4.66	0.16	0.12	0.12	4.83	4.77	3.89	4.3
K_2O	0.02	2.28	1.72	1.73	0.77	0.79	0.87	0.62
TiO_2	0.303	0.249	0.287	0.285	0.13	0.133	0.127	0.166
P_2O_5	0.04	0.03	0.04	0.05	0.01	0.01	0.01	0.03
LOI	1.67	3.43	2.91	2.96	1.18	1.12	1.33	1.77
Total	100.2	100.6	101	100.3	100.7	99.91	100.1	101
Co	62	34	28	39	58	77	49	62
Ni	< 20	< 20	< 20	< 20	< 20	< 20	< 20	< 20
Cu	20	80	20	20	40	20	20	20
Zn	80	270	190	180	60	50	70	110
Sr	30	9	9	8	56	49	54	70
Y	47.4	57	41.6	43.2	106	100	96.5	96.7
Zr	208	216	205	210	185	181	178	191
Nb	14.9	14.8	12.3	14.1	26.5	25.4	25	25.6
Ag	1.6	1.9	1.6	2	1.4	1.4	1.1	1.4
Ba	21	850	551	556	265	253	223	263
La	15.7	14.1	9.34	11.6	48.5	45.5	25.5	65.3
Ce	34.4	31.2	22.4	28.2	92.9	72.8	60.2	87.1
Pr	4.81	4.23	3.23	3.88	13.3	12.5	7.73	17.3
Nd	20.4	18.4	14.1	17.1	55	51.4	32.2	70.8
Sm	5.47	5.24	3.88	4.59	13.2	12.1	8.21	15.8
Eu	1.71	0.755	0.629	0.709	1.29	1.2	0.945	1.61
Gd	5.95	6.86	4.75	5.42	13.8	13.1	10.7	15.9
Tb	1.13	1.39	0.98	1.01	2.54	2.43	2.18	2.54
Dy	7.58	9.19	6.89	6.9	16.6	15.4	15.1	15.6
Ho	1.69	1.94	1.52	1.49	3.54	3.37	3.23	3.3
Er	5.13	5.92	4.7	4.66	10.5	10.4	9.74	9.71
Tm	0.823	0.96	0.789	0.759	1.73	1.64	1.57	1.56
Yb	5.67	6.47	5.42	5.45	11.7	11	10.6	10.5
Lu	0.964	1.05	0.927	0.881	1.79	1.69	1.66	1.58
Pb	5	< 5	< 5	< 5	6	< 5	9	6

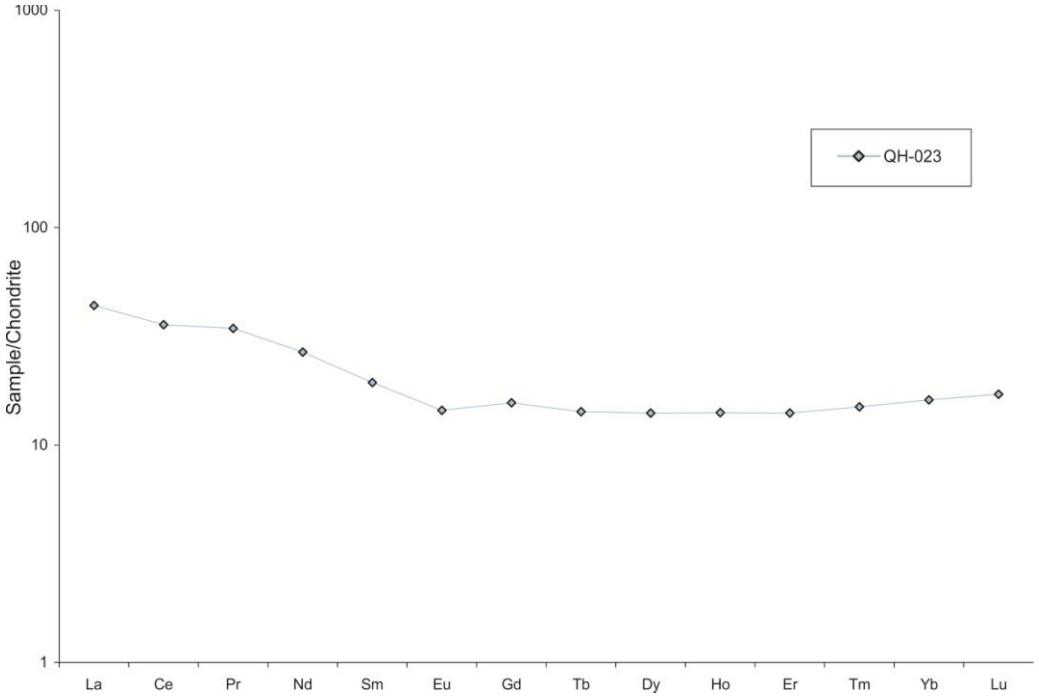

Fig. 3-8: Rare earth element plot of the aphyric dacite from Quemont Hill (chondrite data from McDonough and Sun, 1995).

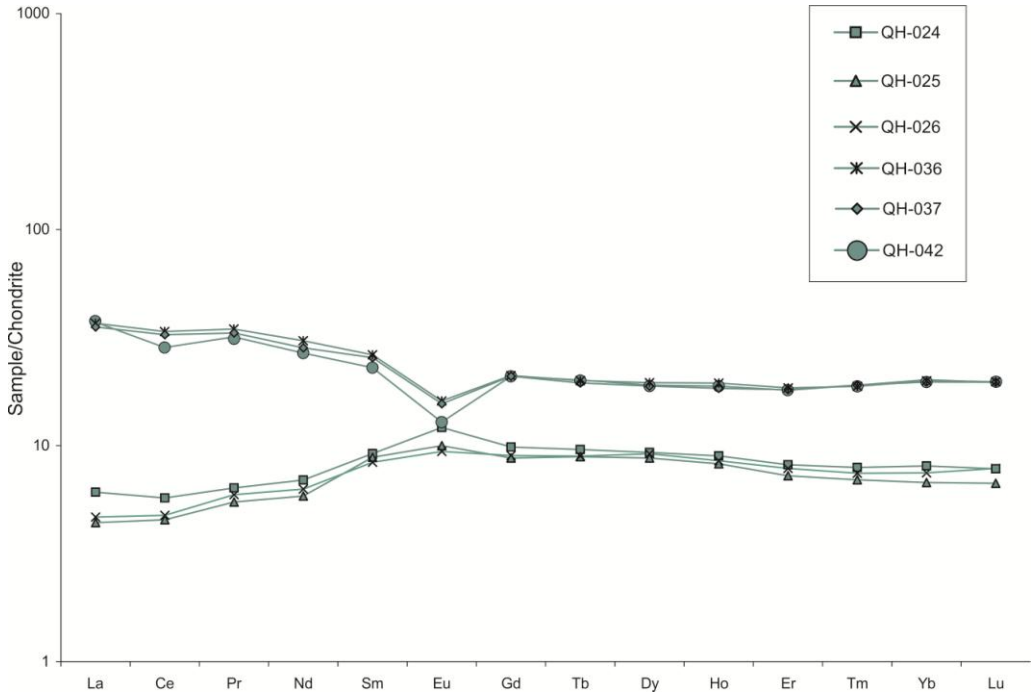

Fig. 3-9: Rare earth element plot of the basalt samples from Quemont Hill (chondrite data from McDonough and Sun, 1995)

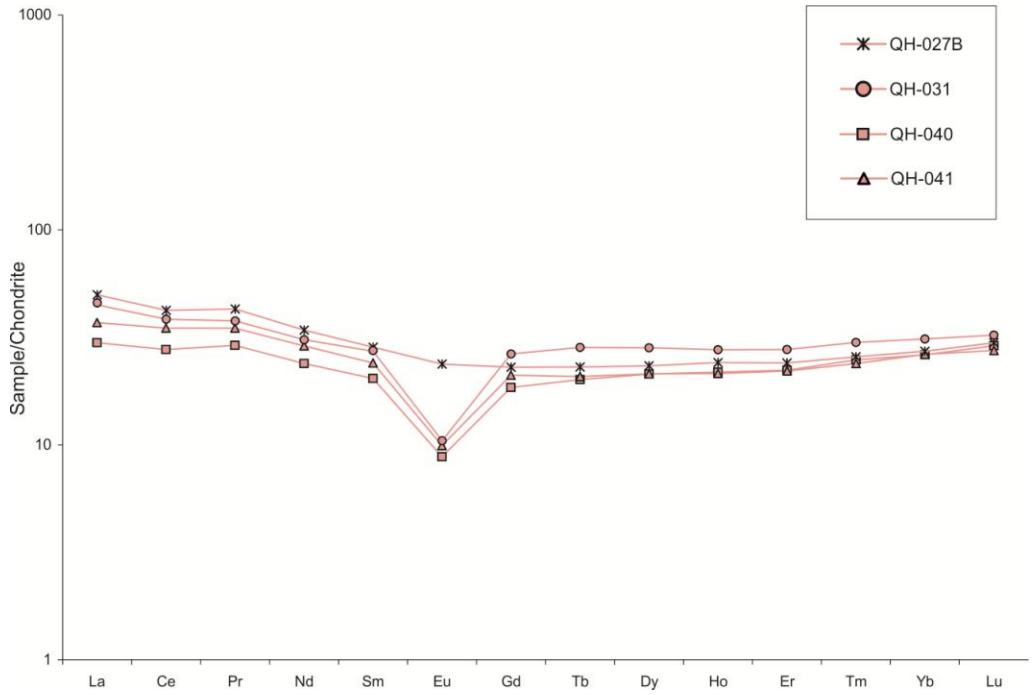

Fig. 3-10: Rare earth element plot of the quartz- and feldspar-phyric rhyolite QFPR-1 (chondrite data from McDonough and Sun, 1995).

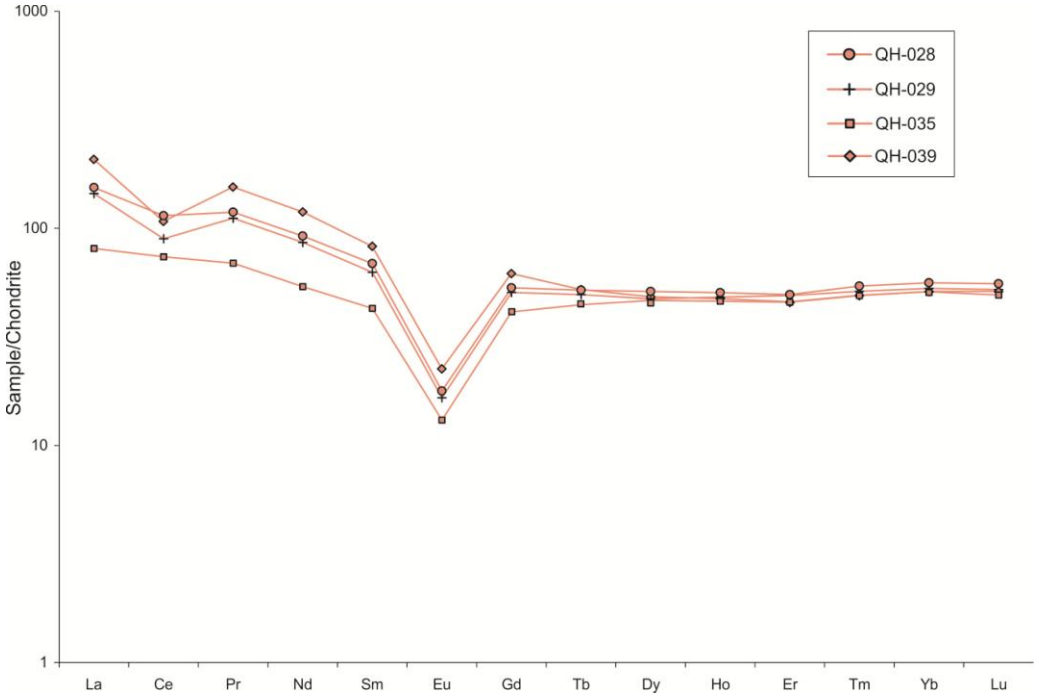

Fig. 3-11: Rare earth element plot of the quartz-and feldspar-phyric rhyolite QFPR-2 (chondrite data from McDonough and Sun, 1995).

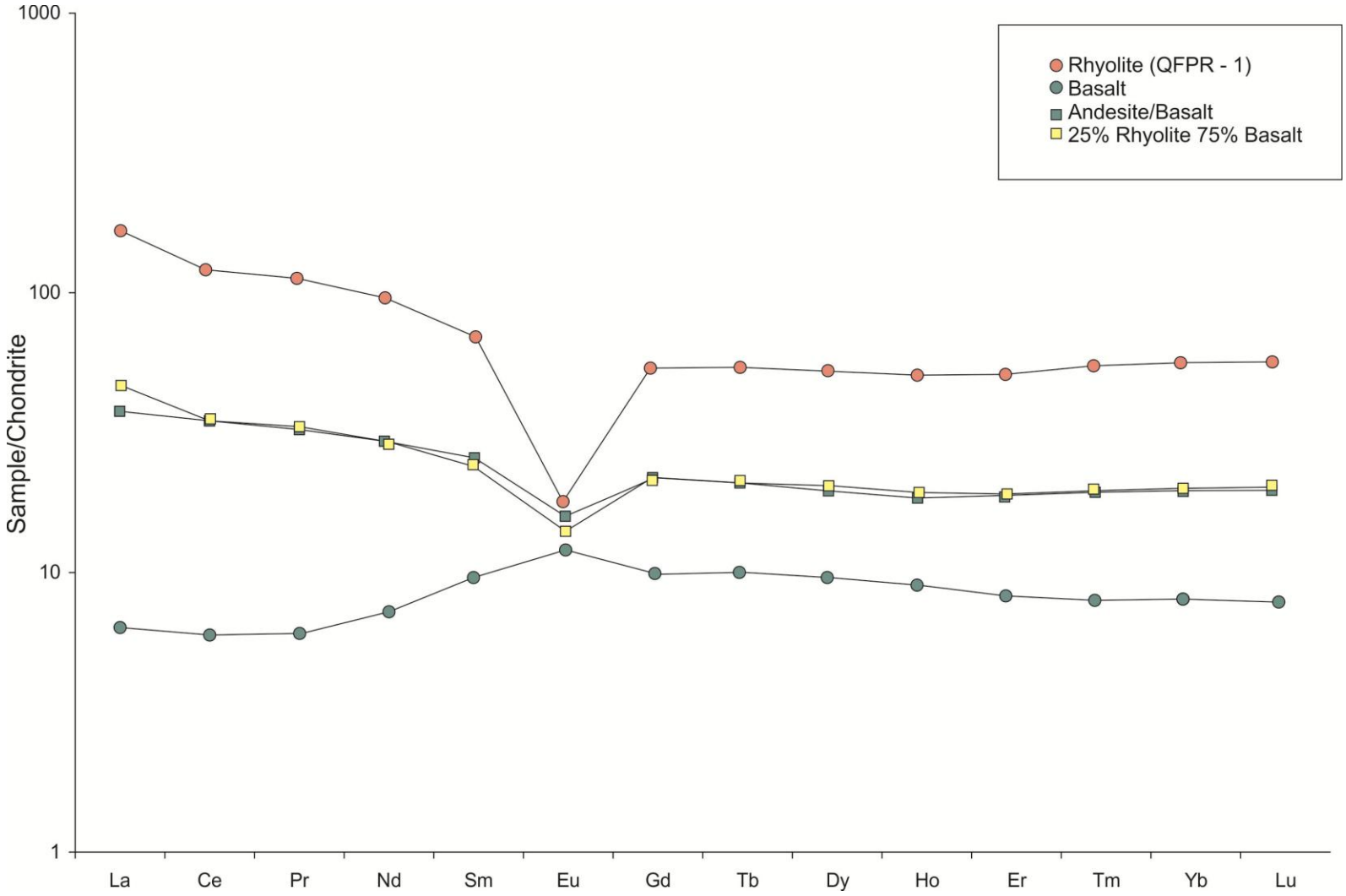

Fig. 3-12: Rare earth element plot of basalt and QFPR-2 samples taken in the lower portion of the exposed dike complex, and a basalt sample taken in the stratigraphically upper part of the study area. The sample from the stratigraphic top of the interval plots along the same REE trend as a mixed rhyolite and basalt composition of 25% and 75% respectively.

3.7.2 Petrography

The very fine groundmass of the aphyric and aphanitic dacite is composed of oriented plagioclase laths (Fig. 3-13A). Minor phenocrysts within the thin section include small clusters of plagioclase and quartz. Chlorite is prominent throughout the thin section and there is one phenocryst of plagioclase visible to the naked eye.

QFPR-1 in sample QH-031 is composed of very rounded quartz phenocrysts up to 2 mm in size, with rims of finer grained quartz around each grain (Fig. 3-13B). Smaller grains of quartz contain cores of radiating micas. The groundmass of the samples is made of quartz that shows undulose extinction and varies in grain size from very fine to small phenocryst. Sample QH -031 contained no feldspar laths or phenocrysts.

Sample QH-027B contained quartz and feldspar phenocrysts that ranged in size from 0.5-1.5 mm on average and had an abundance of 7-9% quartz and <2% feldspar (Fig. 3-13C). The groundmass is dominantly composed of subhedral quartz forming a fine-grained mosaic. Quartz shows undulose extinction and is embayed in several cases. Granophyric textures are common and composed of quartz and plagioclase.

The basalt samples contain very fine-grained minerals, most of which are altered to light green chlorite in plane polarized light (Fig. 3-13D). Some visible minerals appear to have the crystal habit of hornblende but have been altered to isotropic unrecognizable minerals (Fig. 3-13E). Anhedral quartz phenocrysts observed are interpreted to have replaced former basaltic glass. The grain size is consistent throughout the thin sections. Very fine-grained sulfides are found disseminated throughout most of the samples.

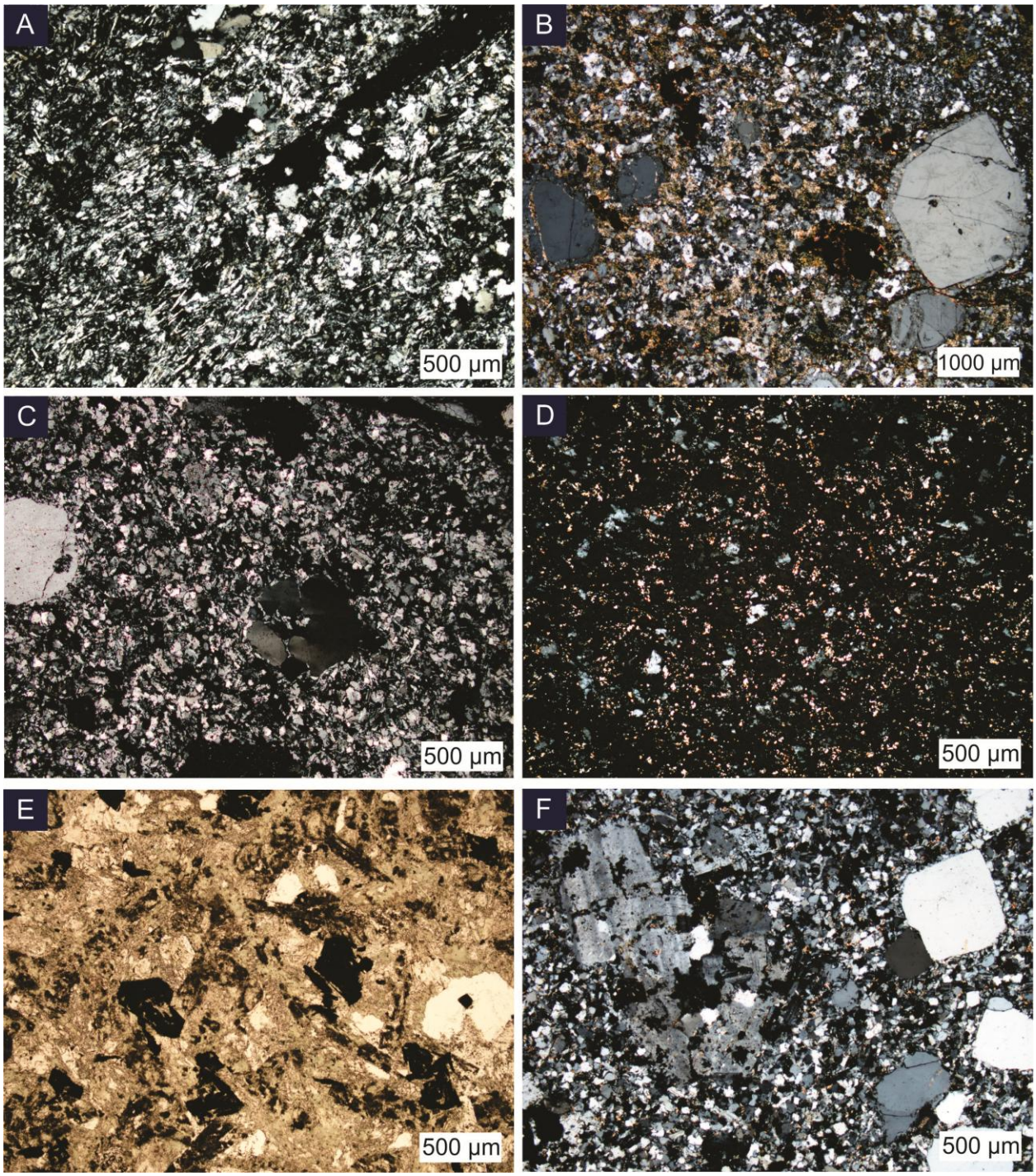

Fig. 3-13: Photomicrographs of samples from Quemont Hill. A. Aphyric dacite seen in XPL containing partially oriented plagioclase laths. B. QFPR-1 sample containing quartz rims around rounded quartz grains. C. QFPR-1 sample found in the lower portion of the field area demonstrating the typical fine-grained groundmass with rare quartz phenocrysts. D. Representative sample of basalt within the field area with very fine-grained groundmass. E. Altered prismatic minerals found within a mafic sample. F. Representative sample of QFPR-2 with abundant euhedral quartz crystals and altered and embayed plagioclase.

QFPR-2 is characterized by abundant quartz and feldspar phenocrysts within a very fine-grained euhedral to subhedral quartz and feldspar matrix (Fig. 3-13F). Thin sections show a relative abundance of 15-20% and <5% for quartz and feldspar respectively. Quartz grains show varied textures including magmatic quartz, grains that exhibit undulose extinction, and others that are euhedral but very rounded. Overall, the quartz ranges in size from 1-4 mm on average. Feldspar grains are highly altered and range in size from 0.5-1 mm on average. Thin sections also contain minor chlorite and micas. Chlorite is found as fine grains in the fine-grained groundmass and is present as sparse (<3%) clusters. Sample QH-029 shows a granophyric texture composed of quartz and plagioclase, as well as aligned micas found along veins and fractures.

Petrographic observations collected from the channel sample were compiled into a table in order to see the descriptions spatially correlated to the location of the samples (Table 3-3). The provided map shows the exact locations of the samples and approximate contacts across which the samples were taken (Fig. 3-14). Most thin sections from the channel sample show small mafic enclaves with varied contact relationships between the enclaves and the enclosing material from sharp to diffuse. Several mafic enclaves contain large quartz phenocrysts, suggesting some physical or chemical exchange between mafic and felsic units. While the dikes appear to have noticeable boundaries between mafic and mingled units in outcrop, hand samples and thin sections show no clear division between units bound within two clear QFPR-1 dikes. Corresponding channel sample photos listed in Table 3-3 are given in Figure 3-15.

The foam-like texture contains unique microscopic features in thin sections that contain mafic enclaves within an intermediate matrix. Sample QH-015 contains abundant radiating feldspar crystals within the groundmass (Fig. 3-16A). The quartz phenocrysts within the sample are rounded and in some places are embayed. The matrix contains dark blue purple chlorite in cross-polarized light. A mafic enclave within the sample contains small circular nodules of high birefringence interpreted to be micas. In addition to the radiating plagioclase nodules there are also fine prismatic radial aggregates of the same mineral directed from the enclave at the enclave-rhyolite contact (Fig. 3-16B). The contact between the enclave and the matrix is characterized by a significant grain size change and appearance of the minerals contained within each unit (Fig. 3-16C).

Table 3-3: Thin section descriptions of representative channel samples

Sample	Description
QH - 00X1	Groundmass composed of subhedral quartz, laths of feldspars, and very fine micas with 5-7% quartz phenocrysts. Plagioclase phenocrysts are highly altered and comprise <5% of the thin section. Calcite veins abundant perpendicular to sulfide veins present. Thin section contains a small green enclave that is interpreted to be mafic, which is finer-grained than the rest of the thin section. Veins of sulfides occur that are composed of cubes and striated pyrite. Contact visible between finer grained enclave and predominant groundmass, marked only by a gradual grain sixe contact over 100 µm.
QH - 00X2	Thin section is composed of mafic enclaves in a quartz and feldspar mosaic matrix. The mafic enclaves are extremely fine-grained in comparison with the groundmass. The enclaves are characterized by very undulatory and irregular margins that are projected into the groundmass like flames or trails. The groundmass contains minor sulfides and euhedral quartz phenocrysts are visible. The contact between the mafic enclave and the matrix is two-toned in color in PPL with a 200-250 µm thick rim around the entire contact (Fig. 3-15A). The contact is highly undulatory with some enclaves nearly disconnecting as rounded globules into the enclave itself (Fig. 3-15B).
QH - 00X3	The matrix is composed of mosaic quartz and feldspar with an equal proportion of plagioclase and quartz phenocrysts (2-3%). The thin section contains the contact between a mafic enclave and the surrounding matrix. The contact is very clear and marked by a significant grain size change. Although there is no rim within the xenolith found and the contact is very sharp and regular.
QH - 0002	The thin section shows a mafic enclave within a matrix composed of quartz and plagioclase phenocrysts that are equal in size (<100 µm). The mafic inclusion contains a quartz phenocryst that is 2 mm in size but the majority of phenocrysts are approximately 500 µm. The contact between the mafic enclave and the matrix is diffuse and not very clear in PPL or XPL. A slight change in grain size occurs but the mineralogy is relatively the same and there are veins of calcite that crosscut both units. Calcite is well distributed throughout the thin section and plagioclase phenocrysts are altered.
QH - 0003	Groundmass composed of very rounded phenocrysts of altered plagioclase and fragmented quartz no larger than 1 mm in diameter. Groundmass is in contact with a mafic enclave that is marked by a gradual and diffuse boundary with no large disparity in grain size change (Fig. 3-15C). The enclave is composed mainly of chlorite, minor altered plagioclase, calcite, and very fine-grained quartz and feldspar grains dispersed throughout the inclusion. The phenocrysts within the matrix are very rounded with abundant calcite found around the grains (Fig. 3-15D)
QH - 0005	The groundmass is mostly composed of very fine-grained quartz and feldspar grains and surrounding high birefringent micas. Quartz phenocrysts in the groundmass are euhedral, show undulatory extinction, and occasionally occur in a cluster with other quartz grains. Plagioclase phenocrysts are fuzzy and altered with extinction angles indicating An % compositions between 65 and 80%. Mafic enclave contained within the matrix is fine-grained and the contact between the two units is relatively sharp. The enclave contains small high birefringent micas and it appears that the contact experiences a slight accumulation of quartz.
QH - 0007	Thin section shows a uniform composition with no phenocrysts (Fig3-15E). The matrix is composed of a subangular mosaic of quartz and feldspar grains, micas, calcite, chlorite, larger broken sulfide aggregates (2-3 mm), and very altered plagioclase.
QH - 0009	The thin section is composed of a feldspar, quartz equigranular mosaic in the groundmass with dispersed calcite with <5% quartz phenocrysts and <4% very altered plagioclase grains (500-600 µm). In one corner of the thin section, there is a slightly diffuse and unclear contact between a fine-grained enclave and the predominant matrix. There are abundant disseminated very fine sulfides.
QH - 0011	Very fine groundmass of plagioclase and quartz with larger phenocrysts contained. The phenocrysts range in size from 1-2 mm and they are composed of 4-6% quartz and <3% plagioclase. Quartz phenocrysts are very rounded with several larger grains of quartz that do not go extinct in XPL (Fig. 3-15F). Thin section contains small enclaves of mostly chlorite (<3 mm) that form small pockets within the fine groundmass, and are possibly small enclaves of mafic material. Large calcite veins are present that are approximately 1 mm in width.

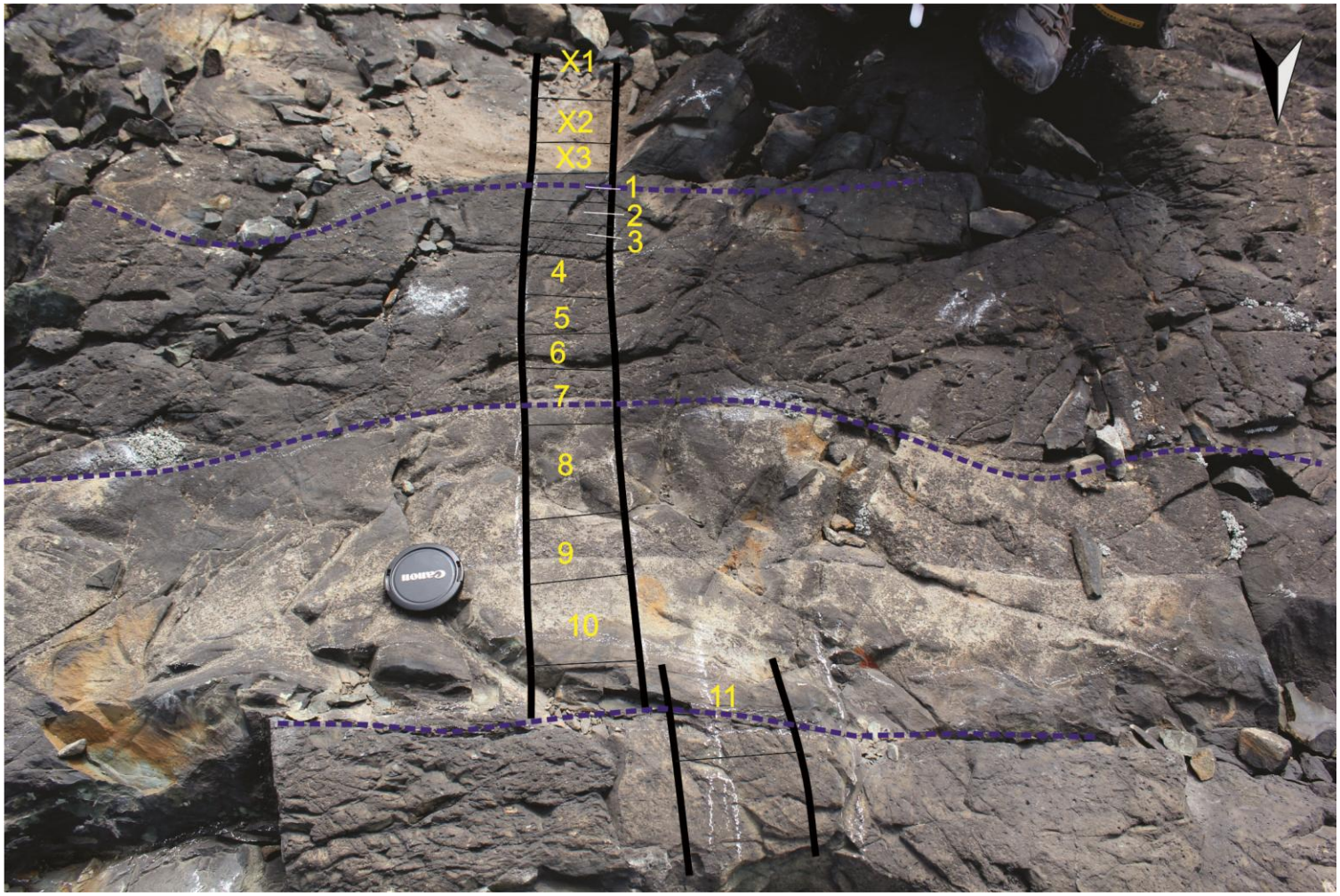

Fig. 3-14: Photograph showing the outline of the channel and samples collected for petrographic and geochemical analyses. Location of contacts is shown on the photo. The camera lens is 6 cm in diameter.

Fig. 3-15: Photomicrographs of thin sections taken from the channel samples showing the changes from south to north. A. Sample QH-00X2 that shows a small quench rim around a mafic enclave (left) at the contact with the matrix (right). B. The same contact in a different part of the enclave showing small quench enclaves within the mafic enclave (above). C. Sample QH-003 showing a very diffuse and gradual contact between the xenolith (left) and the matrix (right). D. Photo of sample QH-003 demonstrating rounded phenocrysts with small rims of fine-grained calcite. E. Sample QH-007 showing an equal proportion of fine-grained chlorite and some larger mosaic grains of quartz and feldspar. F. Sample QH-011 containing rounded quartz phenocrysts and very small enclaves of mafic material mostly altered to chlorite.

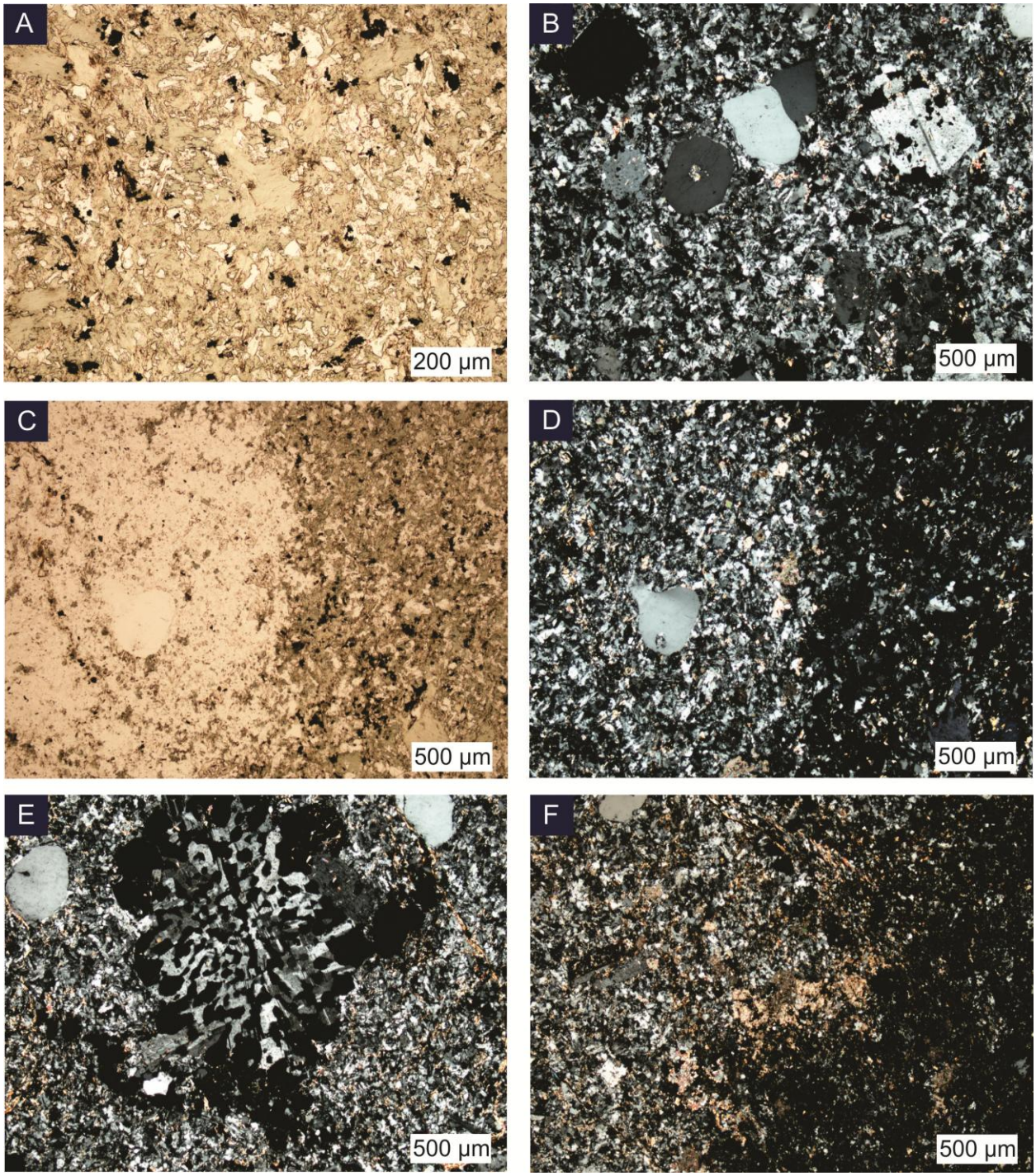
A
200 µm
B
500 µm
C
500 µm
D
500 µm
E
500 µm
F
500 µm

Fig. 3-16: Photomicrographs of textures found within the "foam-like" samples from Quemont Hill. A. Sample QH-015 showing an altered plagioclase grain with coarse calcite vein and radiating grains above and below the feldspar grain. B. Contact between an enclave of mafic material and the enclosing rhyolite marked by radiating plagioclase grains oriented away from the enclave at the contact. C. Contact relationship showing grain size change between the enclave (upper right) and the host rhyolite. D. Radiating feldspar grains seen in sample QH-013 next to a coarse-grained calcite vein. E. Magmatic quartz grains seen within the rhyolite groundmass that are rounded and anhedral. F. Mafic enclave (lower left) protruding into the rhyolite groundmass with an undulatory and irregular geometry.

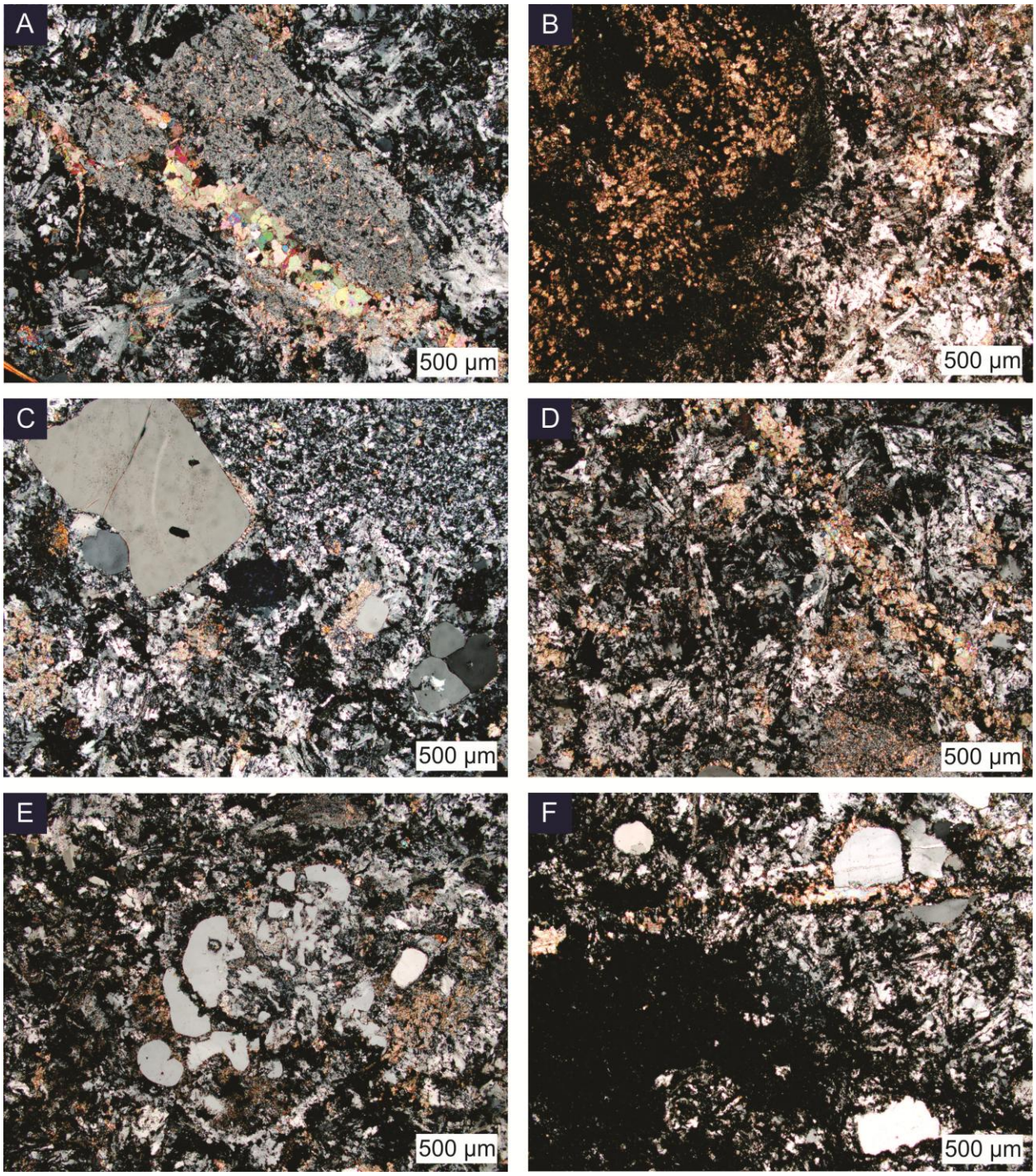
A
500 µm
B
500 µm
C
500 µm
D
500 µm
E
500 µm
F
500 µm

Sample QH-013 contains the same feldspar aggregates composed of radiating prismatic crystals within the matrix of the sample (Fig. 3-16D). There are abundant small quartz phenocrysts and minor large quartz phenocrysts (500 μm). Quartz tends to exhibit undulatory extinction (Fig. 3-16E). The enclave contained within the thin section shows no visible grains with the exception of some very fine-grained mica. The enclave protrudes into the groundmass with rounded and undulatory margins (Fig. 3-16F).

Thin sections of the xenolith texture were made across the xenolith-rhyolite contact. In sample QH-020, the xenolith is mainly composed of fine-grained chlorite, a feldspar and quartz mosaic, micas, and very fine disseminated sulfides (Fig. 3-17A). One large (2 mm) quartz phenocryst is present within the xenolith. The rhyolite contains large feldspar and quartz phenocrysts. The matrix of the rhyolite is similar in grain size to the xenolith and is composed of feldspar and quartz (Fig. 3-17B). The contact between the xenolith and the rhyolite in QH-020 is not marked by a change in grain size but does show a color change in plane- and cross-polarized light as well as a mineralogy change across the contact (Fig. 3-17C and D).

Sample QH-022 shows similar mineralogy to QH-020 in that the xenolith is very fine-grained and is composed of abundant fine-grained quartz and feldspar with chlorite and minor mica grains. Some chlorite grains are large and euhedral. The rhyolite contains feldspar and quartz phenocrysts that are generally one square millimeter with a large quartz grain that is 3 mm in diameter. Quartz is mostly euhedral with minor instances of resorbed quartz grains. There are also several examples of granophyric quartz and feldspar (Fig. 3-17E). Platy micas are aligned around the quartz and feldspar matrix and along small veins. Calcite is found along the xenolith-rhyolite contact. The contact within this sample is identical to QH-020 in that there is no grain size change, and is identified due to a shift in mineralogy and color (Fig. 3-17F).

3.8 Discussion

Extensive mapping at Quemont Hill demonstrated that the dike swarm exposed in this area represents an excellent example for the occurrence of magma mingling and mixing of synchronously emplaced mafic and felsic magmas. Evaluation of several textural features identified in outcrop and thin section allows insights into the processes controlling dike emplacement and felsic-mafic magma interaction. Identification of textural criteria indicating

Fig. 3-17: Photomicrographs of mafic xenolith mingling textures. A. Mafic xenolith showing abundant chlorite that is very fine-grained. No phenocrysts are observed. B. Rhyolite (QFPR-2) showing the quartz and feldspar phenocrysts within a fine-grained groundmass. C. Contact between the rhyolite (left) and the xenolith (right). D. The same contact seen in C in XPL showing very little grain size change across the contact. E. Granophyric texture seen within the rhyolite. F Another diffuse contact between the xenolith (right) and the rhyolite (left) marked by a change in mineralogy only.

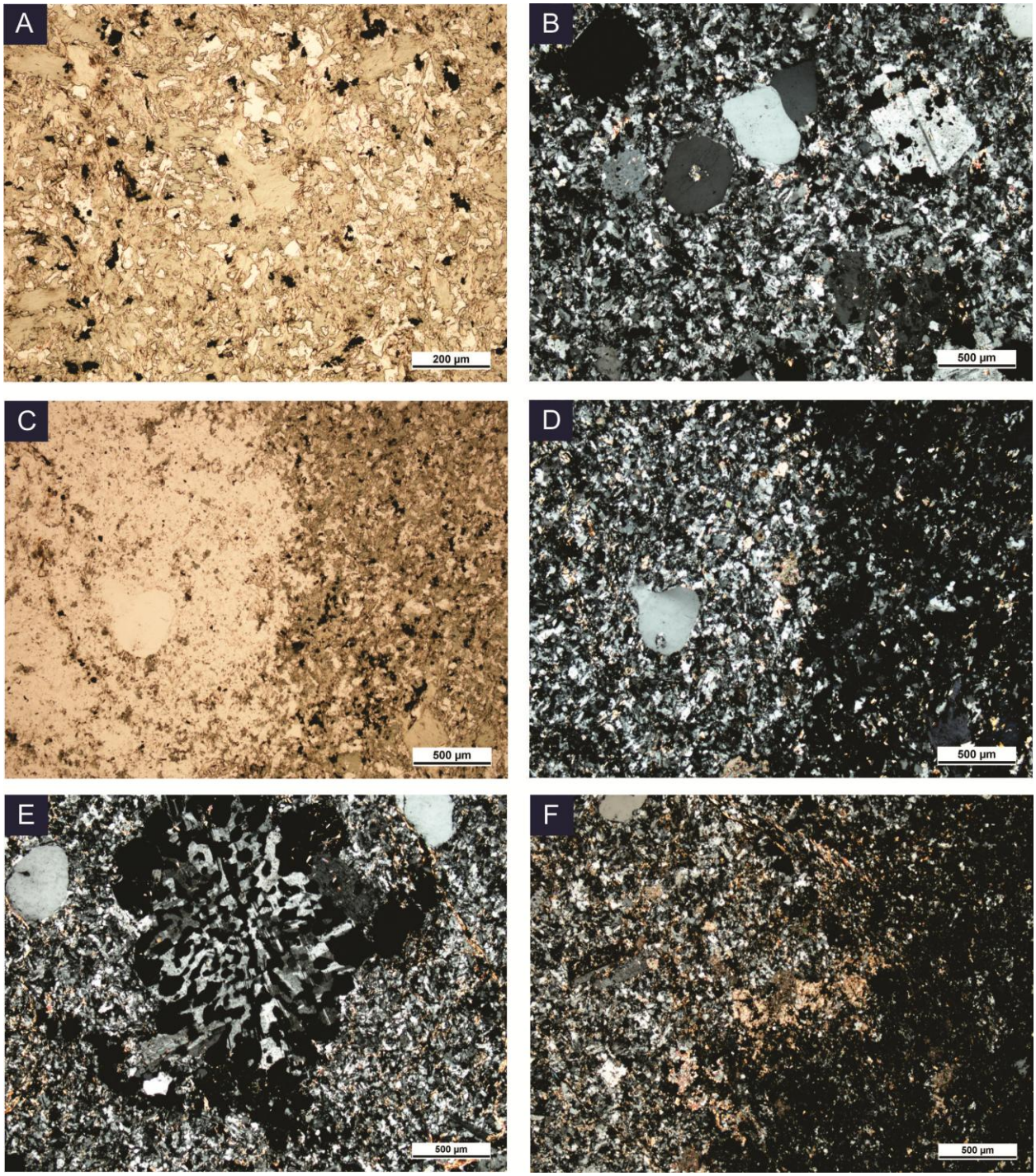
A
200 µm
B
500 µm
C
500 µm
D
500 µm
E
500 µm
F
500 µm

that the felsic and mafic units were emplaced synchronously has implications to the setting in which the giant Quemont massive sulfide deposit formed.

3.8.1 Magma Mingling and Mixing

The occurrence of magma mingling between mafic and felsic magmas at Quemont Hill resulted in the widespread formation of mafic xenoliths and enclaves in the felsic dikes.

The formation of xenoliths is interpreted to have occurred by emplacement of basalt into the QFPR-2 dike in the southern portion of the exposed section. The ratio of felsic magma to mafic magma in this area is high and it is likely that the mafic magma was quenched upon interaction with the cooler felsic melt. Small xenoliths were formed in a semi-plastic to semi-rigid state, which allowed them to break apart as they cooled. They were then transported within the rhyolite as the dike was emplaced. The elongation of xenoliths likely indicates a plastic nature, allowing them to deform along the direction of dike emplacement. Previous mapping by Huthmann (2009) indicated evidence of xenoliths with irregular shapes that appear to be the result of two xenoliths fused together. It is thought that this geometry also formed due to remaining plasticity of the xenoliths (Huthmann, 2009).

The sharp contact between the rhyolite and the basalt in the southern portion of the outcrop area indicates that the basalt is not the source of the mafic xenoliths. This is likely the reason why xenoliths are not in contact with the adjacent basalt and why the xenoliths are located distally from the contact (see detailed map D). It is interpreted that a mafic unit was intruded earlier in the complex formation history and was entrained into the rhyolite. The mafic enclaves were quenched against the cooler rhyolite and were then transported by the felsic melt. After the unit was mostly cooled, a second pulse of mafic magma intruded the dike complex along the observed QFPR-2-basalt contact, resulting in the formation of the sharp contact seen in the field. It was also previously observed in a small mapping project that a small basalt apophysis intruded into the QFPR-2 dike in the opposite orientation of the interpreted flow direction, indicating that it intruded after the QFPR-2 dike had cooled and stopped flowing (Huthmann, 2009).

The small QFPR-2 dike in the north is distinguished from the larger QFPR-2 dike in the south based on its size and the degree of interaction between felsic and mafic magmas. It

contains three separate mixing and mingling features along the strike of the dike, but magma mingling and mixing is not observed over long distances in these areas.

Within the easternmost portion of the small QFPR-2 dike in the north (detailed map A), both magma mixing and mingling occurs. Thin section observations suggest that the dike displays a felsic to intermediate interior that grades outwards towards more mafic compositions. However, surface mapping appears to display a more well-defined contact between the exterior and interior. The groundmass of the interior dike contains round and partially embayed quartz and plagioclase within a fine-grained chlorite-rich matrix, which appears to be the resulting composition due to incomplete mixing between the bounding basalt dikes and felsic magma. The unit does contain mafic enclaves, which is indicative of non-homogenous incorporation of mafic material that is distinct from the remainder of the dike matrix. It is difficult to prove the intermediate character of the matrix without geochemical evidence, although the mineralogy of the channel sample taken through the unit appears to confirm this interpretation. The description of this dike is similar in many ways to composite dike descriptions by Snyder et al. (2007). These authors described a mafic dike that has been intruded by a more felsic dike. Textural features included: (1) contacts between the mafic and felsic dike that appear more planar in the field than compositional evidence would suggest, (2) xenocrysts that are found within the basic members, (3) enclaves of a more mafic affinity present within the more silicic zone of the composite dike, and (4) chemical mixing between the two end-member compositions (Snyder et al., 1997).

The textural evidence is consistent with the early intrusion of a mafic magma, followed shortly by the intrusion of the felsic QFPR-2 magma. It is likely that the magmas were emplaced rapidly with sustained injection due to the proximity to the source. Due to the extensive nature of the dike complex, the source area likely saw continuous emplacement of the magmas, which could produce turbulence and maintain high heat flow. The sustained turbulence and heat flow could facilitate mixing within this area by keeping the magmas from undergoing crystallization. The dynamics and extent of mixing require that the equilibrium temperature of the two magmas was high enough to maintain a liquid state that would enable chemical exchange and ductile movement of the remaining basalt enclaves (Sparks and Marshall, 1985). It is possible that the basalt enclaves were incorporated as a smaller second pulse of mafic magma and were able to be

partially quenched within the intermediate matrix so that they could not be incorporated completely.

The foam-like texture occurs near the middle of the outcropping section. QFPR-2 rhyolite that lacks textural evidence for mingling and mixing occurs on either side of the foam-like zone to the east and west. It is interpreted that this texture formed during a pause in rhyolite emplacement or movement when the dike was not propagating upwards substantially. This would allow any mafic unit in the area the opportunity to mingle with the rhyolite.

The radiating feldspar grains within the felsic matrix likely formed by one of three possible ways including: (1) slight undercooling of the rhyolite after interaction with the mafic melt, (2) superheating of the rhyolite from the interaction with the mafic melt, or (3) mingling of rhyolite and mafic material which separated out enclaves of rhyolite and enclaves of mafic material, in which the rhyolite was later undercooled (Lofgren, 1980, Lofgren, 1983; Fowler et al., 2002; Johnson and Barnes, 2006). The radiating sperulites are composed of feldspar crystals that formed due to undercooling of the rhyolite. The grains are large and according to Fowler et al. (2002), the fiber width of a spherulite increases with decreasing undercooling, indicating that the undercooling did not have to be by a significant amount (Fowler et al., 2002). Superheating of the rhyolite magma by the basalt could destroy nuclei within the rhyolite (Lofgren, 1983). This would cause nucleation from fewer points throughout the rhyolite melt upon cooling which may form a spherulite-like set of crystals to form. Finally, if the mingling of magmas involved small enclaves of both felsic and mafic material, the felsic material could have been undercooled along with the mafic material in smaller batches of liquid material (Fowler et al., 2002). The existence of enclaves within the matrix that have clear and sharp contacts with the surrounding material suggests that while the mafic unit was able to superheat the rhyolite, the basalt was still significantly under-cooled, preventing mixing with the rhyolite. This would suggest that the temperature of the magma upon mingling was above 800°C but well below 1100°C. This hypothesis also supports the disappearance of the rhyolite unit into the basalt (see detailed map C). The rhyolite likely paused at this location, found a pathway that directed the dike elsewhere in three dimensional space, and then the dike continued along the same original trend several meters away vertically.

Mixing of the magmas in the upper portion of the exposed section is demonstrated by the REE plots. The REE patterns indicate the occurrence of magma mixing at a ratio of

approximately 25% rhyolite and 75% basalt. This indicates that at the locations the samples were taken, the rhyolite and basalt were able to come to equilibrium that allowed chemical exchange. Since there are no phenocrysts within the basalt, it is assumed that the basalt mainly incorporated chemical components from the rhyolite melt. It is suggested that at this distance from the source, the magma emplacement and movement slowed, facilitating exchange of chemical components to form an intermediate composition. The temperature at which this process occurred must have been high enough to prevent the basalt from undergoing any amount of crystallization and ensure chemical mixing which would likely be closer to 1100°C, or the crystallization temperature of the basalt (Neves and Vauchez, 1995). The mechanism by which the basalt maintained this temperature without quenching at such a distance from the source is unclear at present.

3.8.2 Volcanic Processes

Extensive mapping and detailed facies analysis allows the development of a model explaining the distribution of volcanic facies at Quemont Hill and the generation of the observed textures of magma mingling and mixing.

Dike emplacement, most likely along a preexisting synvolcanic structure, commenced with the intrusion of the QFPR-1 rhyolite that is exposed throughout the entire outcrop area. The rhyolite intruded into at least partially wet and unconsolidated breccia, as evidenced by the occurrence of sediment-matrix monomict rhyolite breccia at the margins of the unit that are interpreted to represent peperite (cf. Skilling et al., 2002).

Petrographic evidence suggests that the melt forming the QFPR-1 rhyolite dike was rapidly evolving and cooling. This is indicated by the round and embayed nature of the quartz phenocrysts contained in QFPR-1 rhyolite samples in the southeast of the outcrop area. Rounding and embayment of the quartz phenocrysts results from resorption of the quartz in the magma due to changes in magma composition. Resorption releases some of the SiO_2 back into the melt surrounding the phenocrysts, but as diffusion is slow, homogenization of the melt away from the grain boundary was unlikely to occur. Upon cooling, the SiO_2 within the melt recrystallized around the preexisting quartz phenocrysts. This is similar to the processes put forth by Streck (2008) in which dissolution and resorption leads to dissolution of crystallized material back into the melt in addition to later processes that occur when the melt is in disequilibrium and

crystallizes new minerals, preferentially around partially resorbed crystals that act as nuclei. As this texture was only seen in the distal southeastern outcrops of the QFPR-1 rhyolite, the dike may be composed of multiple magma batches that evolved slightly differently, but were emplaced along the same synvolcanic structure.

The aphyric dacite found in the western field area is cross-cut by all other units in the field with the exception of the QFPR-1 rhyolite. The aphyric dacite was emplaced after the formation of the QFPR-1 rhyolite dike. It is unclear at present whether the aphyric dacite represents a sill or dike. The curved geometry observed in the mapped area could be the result of post-depositional folding. However, as little evidence for deformation is observed in the case of the northeast-striking dikes, this would imply that the fold axis is parallel to the strike of the dike-in-dike complex. This is consistent with other observations in the Quemont Hill area (T. Monecke, personal communication).

The relationship between emplacement of QFPR-2 and the basalt dikes can be established unequivocally. The QFPR-2 dikes and basalt dikes both cross-cut the QFPR-1 dikes and the aphyric dacite. The entrainment of mafic enclaves and xenoliths into the QFPR-2 dikes as well as the occurrence of mixing in the upper part of the exposed dike complex indicate that the QFPR-2 magma and the mafic magma were synchronously emplaced within a period that would allow the units to coexist as two non-solid magmas. It is interpreted that the two QFPR-2 dikes were emplaced synchronously as well and that the difference in textures seen in the dikes is a function of the volume of magma emplaced as well as the rate at emplacement.

The basalt dikes were emplaced initially during a period of time when the QFPR-2 dikes were still plastic. However, there is evidence that the mafic volcanism outlasted the emplacement of QFPR-2. This is indicated by the cross-cutting dike and sill-like geometry that occurs to the south at the stratigraphic bottom of the exposed section, the clear and sharp contact along the QFPR-2 dike to the south, and the fact that multiple small basalt dikes occur within larger basalt dikes. The dike- and sill-like basalt in the south-east truncates the QFPR-2 dike in the east as well as all other units, indicating that after the mixing and mingling had occurred between the basalt and rhyolite, there was emplacement of a larger batch of basalt that cross-cut those units. The QFPR-2 dike to the south contains mafic xenoliths but there is no connectivity between the xenoliths and the adjacent basalt. The southern contact of the QFPR-2 dike is sharp and shows no evidence for mingling. The sharp contact indicates that the basalt along the southern contact

was likely emplaced after the formation of the QFPR-2 dike that must have already contained the enclosed xenoliths. There is also indication of at least one additional pulse of mafic magma, which exists in the form of small cm-scale dikes that are intruding and locally quenched within the larger mafic dikes, especially within the southern portion of the outcrop.

3.8.3 Comparison to other Occurrences of Magma Mingling and Mixing

While textures indicative for magma mingling and mixing similar to those found at Quemont Hill have been previously documented, diversity of textural relationships in similarly small field areas is rarely encountered. The dike-in-dike complex at Quemont Hill displays a heterogeneous style of magma interaction with characteristics previously described from dikes, sills, lava flows, and plutons (Snyder et al., 1997; Paterson et al., 2004; Johnson and Barnes, 2006).

For example, Snyder et al. (1997) described composite dikes from the Isle of Skye and the magmatic province near the Maine coast displaying textures of magma mingling not unlike those occurring in the southeastern portion of the northern QFPR-2 dike. However, these textures do not occur throughout the entire Quemont Hill complex, or even throughout the entire QFPR-2 dike.

The xenoliths within the southern QFPR-2 dike are similar to xenoliths in plutons and in dikes described in previous research by Frost and Mahood (1987), Vernon et al. (1988), and Paterson et al. (2004). The xenoliths observed at Quemont Hill are similar to the xenoliths and enclaves described by previous authors in that they have subangular margins, are lenticular to ellipsoid in morphology, are more mafic than their host rock, and have a fine-grained texture in comparison to their host rock (Vernon, 1984; Sparks and Marshall, 1985; Vernon et al 1988; Paterson et al., 2004; Sklyarov and Fedorovskii, 2006). The similarities confirm that characteristic textures form during magma mingling in both the volcanic and plutonic environments.

Neves and Vauchez (1995) and Johnson and Barnes (2006) described the dynamics of magma mixing and the physical characteristics of two magmas that underwent chemical exchange. However, these descriptions refer to plutons where magma mixing near the magma source results in intermediate magma compositions. At Quemont Hill, magma mixing occurred

at a much smaller scale than in plutons and did not involve mixing of approximately equal proportions of mafic and felsic melt. Magma mixing is not widespread throughout the outcrop area, but restricted to the upper portion of the exposed section.

Comparison of the textural evidence documented at Quemont Hill with descriptions in the literature confirms that the rhyolitic and basaltic magmas were synchronously emplaced. The coexistence of these magmas over such a long distance along a single conduit is, however, unusual. The compositions of the magmas undergoing magma mingling at Quemont Hill are also uncommon as most previous research documented examples of mingling between magmas of felsic and intermediate compositions (Vernon, 1984; Neves and Vauchez, 1995; Kuşcu and Floyd, 2001).

3.8.4 Geodynamic Setting

The majority of volcanic-hosted massive sulfide deposits in the Noranda district are located within the Noranda Main Camp. The host rocks of these deposits are dominantly effusive basalt and basaltic andesite flows with subordinate rhyolite flow-dome complexes (Gibson and Galley, 2007). The mafic-dominated volcanic succession of the Noranda Main Camp was deposited rapidly within a large subsidence structure (Gibson and Watkinson, 1990) between approximately 2,701 and 2,698 Ma (David et al., 2006, 2010; McNicoll et al., 2014).

In contrast to the massive sulfide deposits of the Noranda Main Camp, the two largest deposits of the district, Quemont and Horne, are located to the south of the Beauchastel fault within volcanic successions dominated by felsic volcanic rocks (Kerr and Gibson, 1993). Recent dating has shown that these felsic-dominated volcanic successions formed at approximately 2,702 Ma, suggesting that the Quemont and Horne deposits are older than those of the Noranda Main Camp. The new geochronological constraints contradict earlier inferences that the Quemont and Horne deposits formed at the margin of the subsidence structure of the Noranda Main Camp (Lichtblau and Dimroth, 1980). Quemont and Horne clearly formed in a volcanologically distinct environment in a geodynamic setting that may have been differed from that of the younger volcanism in the Noranda Main Camp.

So far, the importance of mafic volcanic rocks in the felsic-dominated host rock successions of the Quemont and Horne deposits has not been discussed in much detail. As

described above, mafic volcanic rocks do not represent a major component of the volcanic host rock succession of the Quemont deposit although the felsic volcanic rocks are crosscut by mafic dikes. Within the dike-in-dike complex of Quemont Hill, mafic intrusions clearly represent an important component. It is current unknown whether the mafic dikes at Quemont Hill represent the feeders to a distinct mafic volcanic succession in the hanging wall of the Quemont deposit or not.

Analogous to Quemont, the felsic-dominated host rock succession of the giant Horne deposit is also crosscut by a mafic dike complex. Within the deposit area, these dikes are very abundant. The dikes commonly show chilled margins with the surrounding felsic volcanic rocks and generally do not show evidence for hydrothermal alteration, implying that they were emplaced largely after waning of the hydrothermal activity. The mafic dikes feed into a thick succession of mafic rocks that overlies the felsic host rock succession of the Horne deposit (Kerr and Mason, 1990; Monecke et al., 2008). The contact between the felsic volcanic rocks and the overlying mafic volcanic rocks appears to be conformable although the mafic volcanic succession has been variably interpreted to represent effusive lavas or intrusions (Price, 1934; Monecke et al., 2008).

The results of the present detailed volcanic facies analysis at Quemont Hill establish for the first time that felsic and mafic volcanism at Quemont must have been synchronous and that mafic melts that were presumably mantle-derived were emplaced in the shallow crust at Quemont at approximately 2,702 Ma. The observed magma mingling and mixing along the contact between a felsic and a mafic dike indicates bimodal volcanism, which is a hallmark of strongly extensional settings (cf. Hannington et al., 2005). Crustal extension provides access to mantle-derived mafic melts that are emplaced into shallow crustal levels and felsic melts are generated at the same time through magmatic differentiation or partial melting of the crust (Piercey, 2011). The high heat flow associated with synvolcanic intrusions provides an important prerequisite for the formation of long-lived hydrothermal systems that form volcanic-hosted massive sulfide deposits (Franklin et al., 2005).

The Quemont deposit was likely formed within a zone of rapid subsidence such as a rift or half-graben. The dike-in-dike complex at Quemont Hill was clearly emplaced within a major synvolcanic structure (Lichtblau and Dimroth, 1980), perhaps one bounded by faults formed in such a zone of rapid subsidence. Subsidence occurred within a volcanic environment dominated

by felsic volcanism, involving the emplacement of large flow domes such as the Joliet rhyolite and thick breccia piles that were intruded by felsic lavas (Monecke et al., 2011). The Quemont deposit probably formed in a geodynamic environment comparable to incipient rift zones in modern volcanic arcs that are commonly dominated by felsic volcanism. In these marine extensional basins, mafic-dominated volcanism is typically related to peak extension (Stolz, 1995).

3.9 Conclusion

Detailed volcanic facies analysis provided evidence for the occurrence of magma mingling and mixing during dike emplacement in the volcanic host rock succession of the world-class Quemont deposit in the Neoarchean Abitibi greenstone belt. The volcanic textures identified along a contact between a rhyolite and basalt dike indicate that magma mingling and mixing occurred contemporaneously to dike emplacement and propagation. The relationships between both intrusions vary along strike of the dike and include the presence of abundant mafic enclaves in the quartz- and feldspar-phyric dike, the occurrence of mafic xenoliths, and chemical mixing of mafic and felsic material. Continued injection of magma during dike propagation created a rapidly evolving system allowing heterogeneous mingling and mixing along the entire length of the dike.

The results of the new research demonstrate that the Quemont deposit was formed in an extensional volcanic environment. Dike emplacement occurred along a major synvolcanic structure located proximal to the site of massive sulfide formation. Although the immediate host rock succession of the Quemont deposit is dominated by felsic volcanic rocks, felsic volcanism must have occurred contemporaneously to the emplacement of mantle-derived melts in the upper crust. The Quemont deposit likely formed in a geodynamic setting that was not unlike rifts developing in modern volcanic arcs.

CHAPTER 4
CONCLUSION

4.1. Goals of Study at Horne West and Quemont Hill

The present study aimed to describe and interpret textural relationships formed through the synchronous emplacement of felsic and mafic melts during the formation of the host rock successions of the world-class Horne and Quemont deposits in the Neoarchean Abitibi greenstone belt. Individual goals for the study included:

1) Defining and characterizing volcanic textures that are produced through the mixing and mingling of lavas of contrasting compositions. This included the detailed analysis in the field as well as the petrographic analyses of thin sections.

2) Reconstructing the volcanic processes that resulted in the incorporation of mafic xenoliths into the rhyolite cryptodome at Horne West and the synchronous emplacement of mafic and felsic melts along a dike-in-dike complex at Quemont Hill.

3) Contributing to the body of knowledge regarding the volcanic environment in which VHMS deposits form and potential geodynamic setting of the Neoarchean Horne and Quemont deposits, which represent two of the largest gold producers of their class.

4.2. Results of Study at Horne West

Volcanic facies analysis indicates that the abundant mafic xenoliths contained in the rhyolite cryptodome at Horne West were incorporated into the felsic lava through a process of magma mingling. It is suggested that mingling with the mafic lava occurred along the feeder of the cryptodome, allowing entrainment of mafic material into the rhyolite. The relatively rigid mafic xenoliths incorporated into the felsic lava were dismembered during continued flow.

The volcanic facies relationships suggest synchronous intrusion of both mafic and felsic lavas controlled by synvolcanic faulting. The faulting is interpreted to be related to local crustal extension, resembling rift zones in modern arcs. The field observations further indicate that the shift from felsic-dominated volcanism at Horne to mafic-dominated intrusive and extrusive volcanism must have occurred over a short time span. Rapid crustal extension could have promoted rapid upwelling of mantle-derived melts into the shallow crust.

4.3. Results of Quemont Hill Study

The field area at Quemont Hill represents an excellent example for the occurrence of heterogeneous mixing and mingling along the contacts of a basalt and a quartz- and feldspar-phyric rhyolite dike. Analysis of the textural relationships along the strike of the dikes is suggestive of a dynamic emplacement scenario that involved the emplacement of multiple pulses of mafic and felsic magma along propagating dikes. Due to variations in viscosity differences over short distances, a variety of textural relationships could be observed, ranging from magma mixing to different types of mingling.

The synchronous emplacement of felsic and mafic melts clearly occurred along a major synvolcanic structure. Extension must have been fairly dramatic and continuous throughout the formation of the host rock succession of the Quemont deposit. This is suggested by the occurrence of several mafic dikes that were emplaced into each other, forming a dike-in-dike complex. The observations of the present study highlight that the Quemont deposit must have formed in a strongly extensional setting. Although the relative volume of mafic volcanic rocks in the host rock succession is small, the observed occurrence of magma mingling and mixing at Quemont Hill demonstrates that volcanism at the time of massive sulfide formation was bimodal in nature.

4.4. Comparison of Quemont Hill and Horne West

Comparison of the volcanic environments in which the Horne and Quemont deposits formed provides some insights into geodynamic settings favorable for the formation of world-

class massive sulfide deposits during the Neoarchean. The following similarities have been identified:

1) The host rock successions of both world-class deposits are dominated by felsic volcanic rocks. Despite the dominance of felsic volcanic rocks, there is clear evidence for the occurrence of contemporaneous mafic volcanic activity. At least locally, felsic and mafic units have been synchronously emplaced within the host rock successions of the Horne and Quemont deposits, as suggested by the observed textural evidence for magma mingling and mixing.

2) Magma mingling and mixing occurred along the margins of felsic and mafic intrusions that were emplaced along the same synvolcanic structures. This indicates that bimodal volcanism occurred contemporaneously to synvolcanic faulting caused by crustal extension.

3) Recent high-precision U-Pb zircon dating (McNicoll et al., 2014) indicates that the volcanic successions hosting the Horne and Quemont deposits are older than the bimodal volcanic succession hosting the massive sulfide deposits of the Noranda Main Camp. The occurrence of magma mingling within the Old Waite dike swarm (Gibson, 1990) suggests that similar processes described in this research also occurred during emplacement of the volcanic rocks of Noranda Main Camp. This suggests that the same favorable environment characterized by coincidence of crustal extension and bimodal volcanism was created twice over a period of approximately 2 Ma in the Noranda area. However, mafic volcanism in the Noranda Main Camp was more voluminous, possibly suggesting that upwelling of mantle-derived material was more pronounced during this stage of formation of the Noranda volcanic complex.

4) Overall, the volcanic environment and geodynamic setting envisaged here for the formation of the Au-rich Horne and Quemont massive sulfide deposits are not unlike those observed in modern environments. Although there is no consensus of whether plate

tectonics were active in the Neoarchean, similar relationships between crustal extension, bimodal volcanism, and hydrothermal activity exist in modern arc environments.

4.5. Recommendations for Future Research

The results and findings of the present study provide the basis for future research focusing on the setting of the world-class Horne and Quemont deposits and comparisons between the deposits of the Noranda South and Main Camps. In particular, the following research directions are suggested:

1) Further volcanic facies mapping should be conducted at Quemont Hill. This should include mapping of the areas of the Joliet rhyolite and the overlying breccia facies. New mapping in these areas would provide important information on the setting of the Quemont deposit and the mechanisms of breccia formation and emplacement at Quemont. Mapping could also extend towards the northeast along the dike-in-dike complex. Although historic maps indicate the occurrence of a fault to the east of Quemont Hill, whether the dike-in-dike complex feeds into discrete volcanic units should be tested; these units would presumably be located in the stratigraphic hanging wall of the Quemont deposits.

2) Additional mapping in the area is also proposed to resolve the structural relationships between the Quemont Hill area and adjacent outcrop areas. In particular, the relationships between the host rock successions of the Quemont and Horne deposits remain enigmatic. More detailed mapping along both sides of the Horne Creek fault may contribute to a better understanding of the volcanic setting of both deposits and establish possible lithological correlations across the fault.

3) Modeling of the volcanic processes described within this study would be beneficial to constrain the viscosities and temperatures at which mingling and mixing of mafic and felsic lavas must have occurred. This could be completed with experimental investigations to attempt to create textures resembling those observed in the field.

4) A larger regional study focusing on magma mingling and mixing throughout the Noranda district would be beneficial to further understand magmatic controls on the formation of massive sulfide deposits. Establishing the role of bimodal volcanism in the formation of the younger deposits of the Noranda Main Camp could provide new insides into regional setting of massive sulfide formation during the deposition of the Blake River assemblage.

REFERENCES CITED

Allen, R.L., Weihed, P., Blundell, D.J., Crawford, T., Davidson, G., Galley, A., Gibson, H., Hannington, M., Herrington, R., Herzig, P., Large, R., Lentz, D., Maslennikov, V., McCutcheon, S., Peter, J., Tornos, F., 2002. Global comparison of volcanic-associated massive sulphide districts, in: Blundell, D.J., Neubauer, F., Von Quadt, A. (Eds.), The timing and Location of Major Ore Deposits in an Evolving Orogen. Geological Society, London, Special Publications 204, p. 13-37.

Appel, P.W.U., 1979. Stratabound copper sulfides in a banded iron-formation and in basaltic tuffs in the Early Precambrian Isua supracrustal belt, West Greenland. Econ. Geol. 74, p. 45-52.

Barrett, T.J., MacLean, W.H., 1994. Mass changes in hydrothermal alteration zones associated with VMS deposits of the Noranda area. Explor. Mining Geol. 3, p. 131-160.

Barrett, T.J., MacLean, W.H., 1999. Volcanic sequences, lithogeochemistry, and hydrothermal alteration in some bimodal volcanic-associated massive sulfide systems, in: Barrie, C.T., Hannington, M.D. (Eds.), Volcanic-Associated Volcanic Massive Sulfide Systems: Processes and Examples in Modern and Ancient Settings. Reviews in Economic Geology 8, p. 101-131.

Barrie, C.T., Hannington, M.D., 1999. Classification of volcanic-associated massive sulfide deposits based on host-rock composition, in: Barrie, C.T., Hannington, M.D. (Eds.), Volcanic-Associated Volcanic Massive Sulfide Systems: Processes and Examples in Modern and Ancient Settings. Reviews in Economic Geology 8, p. 1-11.

Baxter, S., Feely, M., 2002. Magma mixing and mingling textures in granitoids: Examples from the Galway granite, Connemara, Ireland. Mineral. Petrol. 76, p. 63-74.

Beaty, D.W., Taylor, H.P., 1982. Some petrologic and oxygen isotopic relationships in the Amulet Mine, Noranda, Quebec, and their bearing on the origin of Archean massive sulfide deposits. Econ. Geol. 77, p. 95-108.

Binns, R.A., 2004. Data report: Spinifex-textured basalt xenoliths at Pacmanus, Papua New Guinea, in: Barriga, F.J.A.S., Binns, R.A., Miller, D.J., Herzig, P.M. (Eds.), Proc. ODP Sci. Res. Ocean Drilling Program, College Station, Texas, 19 p.

Clift, P.D., 1995. Volcaniclastic sedimentation and volcanism during the rifting of western Pacific backarc basins, in: Taylor, B., Natland, J. (Eds.), Active Margins and Marginal Basins of the Western Pacific. American Geophysical Union, Washington, p. 67–98.

Daigneault,R., Pearson, V., 2006. Physical volcanology of the Blake River caldera complex: a new interpretation of an old structure, in: Mueller, W.U., Daigneault, R., Pearson, V., Houlé, M., Dostal, J., Pilote, P. (Eds.), The Komatiite-Komatiitic Basalt-Basalt Association in Oceanic Plateaus and Calderas: Physical Volcanology and Textures of Subaqueous Archean Flow Fields in the Abitibi Greenstone Belt. Geological Association of Canada-Mineralogical Association of Canada Joint Annual Meeting Montreal, Quebec, Field Trip A3, Guidebook, p. 62-72.

David, J., Dion, C., Goutier, J., Roy, P., Bandyayera, D., Legault, M., Rhéaume, P., 2006, Datations U-Pb effectuées dans la Sous-province de l'Abitibi à la suite des travaux de 2004-2005. Ministère des Ressources naturelles et de la Faune, Québec, report RP 2006-04, 22 p.

David, J., Vaillancourt, D., Bandyayera, D., Simard, M., Dion, C., Goutier, J., Dion, C., Barbe, P., 2010. Datations U-Pb effectuées dans les sousprovinces d'Ashuanipi, de La Grande, d'Opinaca et d'Abitibi en 2008−2009. Ministère des Ressources naturelles et de la Faune, Québec, report RP 2010-11, 37 p.

de Rosen-Spence, A., 1969. Genèse des roches à cordiérite-anthophyllite des gisements cupro-zincifères de la région de Rouyn-Noranda, Québec, Canada. Can. J. Earth Sci., p. 1339-1345.

de Rosen-Spence, A.F., 1976. Stratigraphy, development and petrogenesis of the central Noranda volcanic pile, Noranda, Quebec. Ph.D. thesis, University of Toronto, Toronto, Ontario, 166 p.

Dimroth, E., Rocheleau, M., 1979. Volcanology and sedimentology of Rouyn-Noranda area, Quebec. Field trip A-1. Geological Association of Canada, Quebec, 205 p.

Dimroth, E., Imreh, L., Rocheleau, M., Goulet, N., 1982. Evolution of the south-central part of the Archean Abitibi belt, Quebec. Part I: Stratigraphy and paleogeographic model. Can. J. Earth Sci. 19, p.1729-1758.

Fisher, D.F., 1974. A volcanic origin of the No. 5 Zone of the Horne mine, Noranda, Quebec. Econ. Geol. 69, p. 1352-1353.

Floyd, P.A., Winchester, J.A., 1978. Identification and discrimination of altered and metamorphosed volcanic rocks using immobile elements. Chem. Geol. 21, p. 291-306.

Foster, D.A., Hyndman, D.W., 1990. Magma mixing and mingling between synplutonic mafic dikes and granite in the Idaho-Bitterroot batholiths, in: Anderson, J.L. (Ed.), The Nature and Origin of Cordilleran Magmatism. Geol. Soc. Amer. Mem. 174, p. 347-358.

Fowler, A.D., Berger, B., Shore, M., Jones, M.I., Ropchan, J., 2002. Supercooled rocks: development and significance of varioles, spherulites, dendrites and spinifex in Archean volcanic rocks, Abitibi greenstone belt, Canada. Precambrian Res. 115, p. 311-328.

Franklin, J.M., Gibson, H.L., Jonasson, I.R., Galley, A.G., 2005. Volcanogenic massive sulfide deposits, in: Hedenquist, J.W., Thompson, J.F.H., Goldfarb, R.J., Richards, J.P. (Eds.), Economic Geology 100th Anniversary Volume. Society of Economic Geologists, Littleton, p. 523-560.

Frost, T.P. Mahood, G.A., 1987. Field, chemical, and physical constraints on mafic-felsic magma interaction in the Lamarck granodiorite, Sierra Nevada, California. Geol. Soc. Amer. Bull. 9, p. 272-291.

Fryer, P., Taylor, B., Langmuir, C.H., Hochstaedter, A.G., 1990, Petrology and geochemistry of lavas from the Sumisu and Torishima backarc rifts. Earth Planet. Sci. Lett. 100, 161-178.

Gibson, H.L., 1990. The Mine Sequence of the Central Noranda Volcanic Complex: geology, alteration, massive sulphide deposits and volcanological reconstruction. Ph.D. thesis, Carleton University, Ottawa, Ontario, 715 p.

Gibson, H.L., Watkinson, D.H., 1990. Volcanogenic massive sulphide deposits of the Noranda Cauldron and Shield Volcano, Quebec. Canadian Institute of Mining Metallurgy Special Volume 43, p. 119-132.

Gibson, H., Galley, A., 2007. Volcanogenic massive sulphide deposits of the Archean, Noranda District, Quebec, in: Goodfellow, W.D. (Ed.), Mineral Deposits of Canada: A Synthesis of Major Deposit-Types, District Metallogeny, the Evolution of Geological Provinces, and Exploration Methods: Mineral Deposits Division, Geological Association of Canada, Special Publication, p. 533-552.

Gibson, H.L., Morton, R.L., Hudak, G.J., 1999. Submarine volcanic processes, deposits, and environments favorable for the location of volcanic-associated massive sulfide deposits, in: Barrie, C.T., Hannington, M.D. (Eds.), Volcanic-Associated Volcanic Massive Sulfide

Systems: Processes and Examples in Modern and Ancient Settings. Reviews in Economic Geology 8, p. 13-51.

Gibson, H.L., Kerr, D.J., Cattalani, S., 2000. The Horne mine: geology, history, influence on genetic models, and a comparison to the Kidd Creek mine. Explor. Mining Geol. 9, 91-111.

Gill, J.B., Hiscott, R.N., Vidal, P., 1994. Turbidite geochemistry and evolution of the Izu-Bonin arc and continents. Lithos 33, 135-168.

Goldie, R., 1978. Magma mixing in the Flavrian pluton, Noranda area, Quebec. Can. J. Earth Sci. 15, p. 132-144.

Goodwin, A.M., 1982. Archean volcanoes in southwestern Abitibi belt, Ontario and Quebec: form, composition, and development. Can. J. Earth Sci. 19, p. 1140-1155.

Hannington, M.D., de Ronde, C.E.J. and Petersen, S., 2005. Sea-floor tectonics and submarine hydrothermal systems, in: Hedenquist, J.W., Thompson, J.F.H., Goldfarb, R.J., Richards, J.P. (Eds.), Economic Geology 100th Anniversary Volume. Society of Economic Geologists, Littleton, p. 111-141.

Hochstaedter, A.G., Gill, J.B., Morris, J.D., 1990. Volcanism in the Sumisu Rift: II. Subduction and non-subduction related components. Earth Planet. Sci. Lett. 100, 195-209.

Hodge, H.J., 1967. Horne mine, in: Abel, M.K. (Ed.), CIMM Centennial Field Excursion Northwestern Quebec - Northern Ontario. Canadian Institute of Mining and Metallurgy, Montreal, p. 40-45.

Huthmann, F., 2009, Volcanic setting of the Quemont massive sulphide deposit, Rouyn-Noranda, Quebec. B.Sc. thesis, TU Bergakademie Freiberg, Germany, 40 p.

Johnson, K., Barnes, C.G., 2006, Magma mixing and mingling in the Grayback pluton, Klamath Mountains, Oregon, in: Snoke, A.W., Barnes, C.G. (Eds.), Geological Studies in the Klamath Mountains Province, California and Oregon: A Volume in Honor of William P. Irwin. Geol. Soc. Amer. Spec. Pap. 410, p. 247-267.

Kamenetsky, V.S., Binns, R.A., Gemmell, J.B., Crawford, A.J., Mernagh, T.P., Maas, R., Steele, D., 2001. Parental basaltic melts and fluids in eastern Manus backarc basin: implications for hydrothermal mineralisation. Earth Planet. Sci. Lett 184, p. 685-702.

Kerr, D.J., Gibson, H.L., 1993. A comparison of the Horne volcanogenic massive sulfide deposit and intracauldron deposits of the Mine Sequence, Noranda, Quebec. Econ. Geol. 88, p. 1419-1442.

Kerr, D.L., Mason, R., 1990. A re-appraisal of the geology and ore deposits of the Horne mine complex at Rouyn-Noranda, Quebec, in: Rive, M., Verpaelst, P., Gagnon, Y., Lulin, J.M., Riverin, G., Simard, A. (Eds.), The Northwestern Quebec Polymetallic Belt: A Summary of 60 Years of Mining Exploration. The Canadian Institute of Mining and Metallurgy, Special Volume 43, Montreal, p. 153-165.

Kuşcu, G.G., Floyd, P.A., 2001. Mineral compositional and textural evidence for magma mingling in the Saraykent volcanic. Lithos 50, p. 207-230.

Lichtblau, A.P., Dimroth, E., 1980. Stratigraphy and facies at the south margin of the Archean Noranda caldera, Noranda, Québec. Geological Survey of Canada, Paper 80-1A, p. 69-76.

Lofgren, G.E., 1980. Experimental studies on the dynamic crystallization of silicate melts, in: Hargraves, R.B. (Ed.), Physics of Magmatic Processes. Princeton University Press, Princeton, NJ, p. 488-551.

Lofgren, G.E., 1983. Effects of heterogeneous nucleation on basaltic textures: a dynamic crystallization study. J. Petrol. 24, p. 229-255.

McDonough, W.F. and Sun, S.S., 1995. The composition of the earth. Chem. Geol. 120, p. 223-253.

McNicoll, V., Goutier, J., Dubé, B., Mercier-Langevin, P., Ross, P.S., Dion, C., Monecke, T., Legault, M., Percival, J., Gibson, H., 2014. New U-Pb geochronology from the Blake River Group, Abitibi greenstone belt, Quebec, and implications for base metal exploration. Econ. Geol. 109, 27-59.

McLean, W.H., Hoy, L.D., 1991. Geochemistry of hydrothermally altered rocks at the Horne mine, Noranda, Quebec. Econ. Geol. 86, p. 506-528.

McPhie, J., Doyle, M., Allen, R., 1993. Volcanic Textures: A Guide to the Interpretation of Textures in Volcanic Rocks. Centre for Ore Deposit and Exploration Studies, University of Tasmania, 198 p.

Mercier-Langevin, P., Goutier, J., Ross, P.-S., McNicoll, V., Monecke, T., Dion, C., Dubé, B., Thurston, P., Bécu, V., Gibson, H., Hannington, M., Galley, A., 2011a. The Blake River

group of the Abitibi greenstone belt and its unique VMS and gold-rich VMS endowment. Geological Survey of Canada Open File 6869, 61 p.

Mercier-Langevin, P., Hannington, M.D., Dube, B., Becu, V., 2011b. The gold content of volcongenic massive sulfide deposits. Miner. Deposita 46, p. 509-539.

Monecke, T., Gibson, H., 2013. Surface geology of the giant Horne volcanic-hosted massive sulphide deposit, Rouyn-Noranda, Quebec. Geological Survey of Canada, Open File 7412, 6 maps and 3 p.

Monecke, T., Gibson, H., Dubé, B., Laurin, J., Hannington, M.D., Martin, L., 2008. Geology and volcanic setting of the Horne deposit, Rouyn-Noranda, Québec: Initial results of a new research project. Geological Survey of Canada, Current Research 2008-9: 16 p.

Monecke, T., Gibson, H., Hannington, M., McNicoll, V., 2011. Felsic host-rock successions of the VMS deposits in the Noranda Camp, in: Mercier-Langevin, P., Goutier, J., Ross, P.S., McNicoll, V., Monecke, T., Dion, C., Dubé, B., Thurston, P., Bécu, V., Gibson, H., Hannington, M., Galley A. (Eds.), The Blake River Group of the Abitibi Greenstone Belt and its Unique VMS and Gold-rich VMS Endowment. Geological Survey of Canada Open File 6869, p. 27-39.

Mortensen, J.K., 1993. U-Pb geochronology of the eastern Abitibi subprovince. Part 2: Noranda-Kirkland Lake area. Can. J. Earth Sci. 30, p. 29-41.

Moss, R., Scott, S.D., Binns, R.A., 2001. Gold content of eastern Manus basin volcanic rocks: Implications for enrichment in associated hydrothermal precipitates. Econ. Geol. 96, p. 91-107.

Neves, S.P., Vauchez, A., 1995. Successive mixing and mingling of magmas in a plutonic complex of northeast Brazil. Lithos 34, p. 275-299.

Norrish, K., Hutton, J.T., 1969. An accurate X-ray spectrographic method for the analysis of a wide range of geological samples. Geochim. Cosmochim. Acta 33, p. 431-453.

Paterson, S.R., Pignotta, G.S., Vernon, R.H., 2004. The significance of microgranitoid enclave shapes and orientations. J. Struct. Geol. 26, p. 1465-1481.

Passchier, C.W., Trouw, R. A., 1996. Microtectonics. Springer, Berlin, 289 p.

Péloquin, A.S., Potvin, R., Paradis, S., Laflèche, M.R., Verpaelst, P., Gibson, H.L., 1990. The Blake River group, Rouyn-Noranda area, Quebec: a stratigraphic synthesis, in: Rive, M., Verpaelst, P., Gagnon, Y., Lulin, J.M., Riverin, G., Simard, A. (Eds.), The Northwestern

Quebec Polymetallic Belt: A Summary of 60 Years of Mining Exploration. The Canadian Institute of Mining and Metallurgy, Special Volume 43, Montreal, p. 107-118.

Piercey, S.J., 2011. The setting, style, and role of magmatism in the formation of volcanogenic massive sulfide deposits. Miner. Deposita 46, 449-471.

Powell, W.G., Carmichael, D.M., Hodgson, C.J., 1995. Conditions and timing of metamorphism in the southern Abitibi greenstone belt, Quebec. Can. J. Earth Sci. 32, p. 787-805.

Price, P., 1934. The geology and ore deposits of the Horne mine, Noranda, Quebec. Transactions of the Canadian Institute of Mining and Metallurgy and of the Mining Society of Nova Scotia 37, 108-140.

Ryznar, G., Campbell, F.A., Krouse, H.R., 1967. Sulfur isotopes and the origin of the Quemont ore body. Econ. Geol. 62, p. 664-678.

Santaguida, F., 1999. The paragenetic relationships of epidote-quartz hydrothermal alteration within the Noranda Volcanic Complex, Quebec. Ph.D. thesis, Carleton University, Ottawa, Ontario, 302 p.

Shinjo, R., Kato, Y., 2000. Geochemical constraints on the origin of bimodal magmatism at the Okinawa Trough, and incipient back-arc basin. Lithos 54, 117-137.

Sinclair, W.D., 1971. A volcanic origin for the No. 5 Zone of the Horne mine, Noranda, Quebec. Econ. Geol. 66, 1225-1231.

Skilling, L.P., White, J.D.L., McPhie, J., 2002. Peperite: a review of magma-sediment mingling; J. Volcanol. Geotherm. Res. 114, p. 1-17.

Sklyarov, E.V., Fedorovskii, V.S., 2006. Magma mingling: Tectonic and geodynamic implications. Geotectonics 40, p. 120-134.

Snyder, D., Crambles, C., Tait, S., Wiebe, R.A., 1997. Magma mingling in dikes and sills. J. Geol. 105, p. 75-86.

Sparks, R.S.J., Marshall, L.A., 1985. Thermal and mechanical constraints on mixing between mafic and silicic magmas. J. Volcanol. Geotherm. Res. 29, p. 99-124.

Spence, A.F., 1976. Stratigraphy, development and petrogenesis of the central Noranda volcanic pile, Noranda, Quebec. Ph.D. thesis, University of Toronto, Toronto, Ontario, 166 p.

Spence, C.D., de Rosen-Spence, A.F., 1975. The place of sulfide mineralization in the volcanic sequence at Noranda, Quebec. Econ. Geol. 70, p. 90-101.

Stolz, A.J., 1995. Geochemistry of the Mount Windsor volcanics: implications for the tectonic setting of Cambro-Ordovician volcanic-hosted massive sulfide mineralization in northeastern Australia. Econ. Geol. 90, p. 1080-1097.

Streck, M.J., 2008. Mineral textures and zoning as evidence for open system processes.. Rev. Mineral. Geochem. 69, p. 595-622.

Thurston, P. C., Ayer, J. A., Goutier, J., Hamilton, M. A., 2008. Depositional gaps in Abitibi Greenstone belt stratigraphy: a key to exploration for syngenetic mineralization. Econ. Geol. 103, p. 1097-1134.

Ventura, G., Del Gaudio, P., Iezzi, G., 2006. Enclaves provide new insights on the dynamics of magma mingling: A case study from Salina Island (Southern Tyrrhenian Sea, Italy). Earth Planet. Sci. Lett. 243, p. 128-140.

Vernon, R.H., 1984. Microgranitoid enclaves in granites; globules of hybrid magma quenched in a plutonic environment. Nature 309, p. 438-439.

Vernon, R.H., 1990. Crystallization and hybridism in microgranitoid enclave magmas: Microstructural evidence. J. Geophys. Res. 95, p. 17,849-17,859.

Vernon., R.H., Etheridge, M.A., Wall, V.J., 1988. Shape and microstructure of microgranitoid enclaves: Indicators of magma mingling and flow. Lithos 22, p. 1-11.

Weeks, R., 1967. Quemont Mining Corporation, Limited, in: M.K. Abel (Ed.), CIMM Centennial Field Excursion Northwestern Quebec - Northern Ontario. Canadian Institute of Mining and Metallurgy, Montreal, p. 46-51.

Wilson, M.E., 1941. Noranda district, Quebec. Geological Survey of Canada Memoir 229, 162 p.

Winchester, J.A., Floyd, P.A., 1977. Geochemical discrimination of different magma series and their differentiation products using immobile elements. Chem. Geol. 20, p. 325-343.

APPENDIX A
SUPPLEMENTAL ELECTRONIC FILES

The following data files contain supplemental data in support of the thesis work at Horne West and Quemont Hill. The files include the large final map produced of the Quemont Hill dike swarm in addition to five smaller detailed maps focusing on textures. Additional data files include the full collection of geochemistry data collected at both Horne West and Quemont Hill for reference.

AppendixA_QuemontHillMap.pdf	This file contains the map of the Quemont Hill dike swarm using collected digitized GPS data points.
AppendixB1_MapA_Quemont.pdf	This file contains a detailed digitized map of location A in the Quemont Hill field area.
AppendixB2_MapB_Quemont.pdf	This file contains a detailed digitized map of location B in the Quemont Hill field area.
AppendixB3_MapC_Quemont.pdf	This file contains a detailed digitized map of location C in the Quemont Hill field area.
AppendixB4_MapD_Quemont.pdf	This file contains a detailed digitized map of location D in the Quemont Hill field area.
AppendixB5_MapE_Quemont.pdf	This file contains a detailed digitized map of location E in the Quemont Hill field area.
AppendixC_HorneWest_Geochem.xls	The file contains whole rock geochemistry for samples collected at Horne West. Data is organized by rock type.
AppendixD_QuemontHill_Geochem.xls	The file contains whole rock geochemistry for the samples collected at Quemont Hill. Data is organized by sample number.